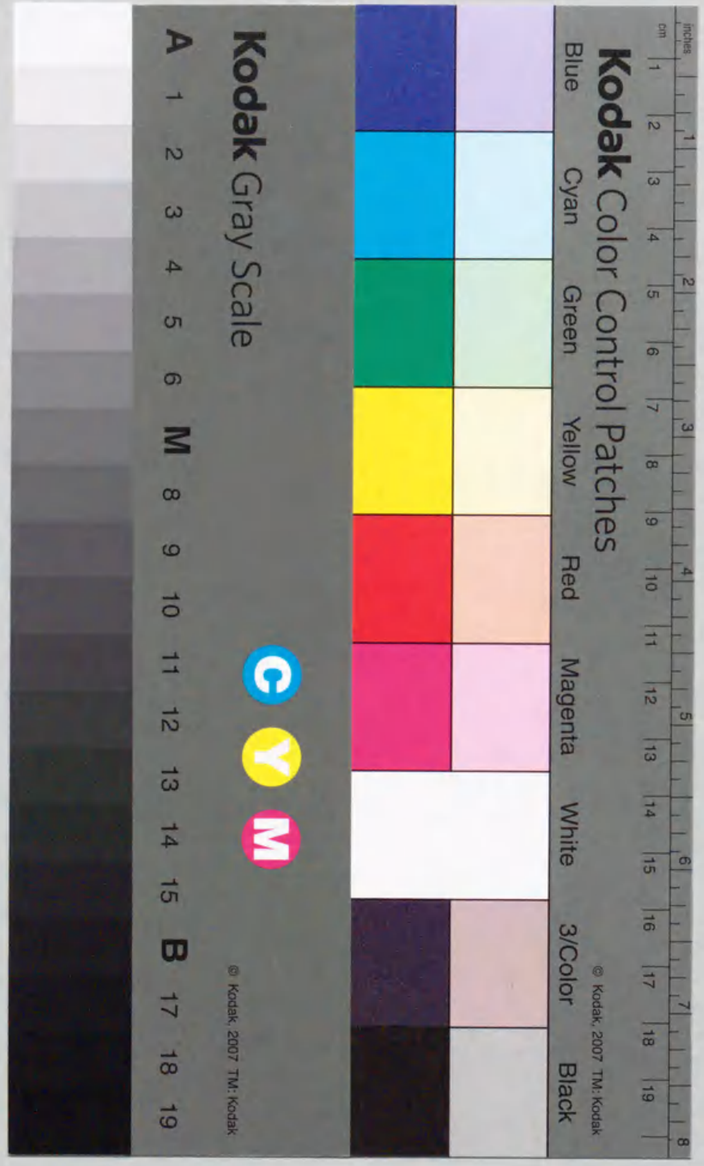

学位論文

Production and characterization of novel carbon nanostructures by high-temperature laser-vaporization and arc-discharge

高温レーザー蒸発およびアーク放電による
新規炭素ナノ集合体の生成とキャラクタリゼーション

名古屋大学大学院 理学研究科 物質理学専攻

小塩 明

本 論 文

(1)

Production and characterization of novel carbon nanostructures by high-temperature laser-vaporization and arc-discharge

by

Akira Koshio

Division of Material Science, Graduate School of Science
Nagoya University

2000

Contents

Chapter 1

General Introduction

Until quite recently, diamond and graphite were the only known carbon allotropes. However, the discovery of fullerenes in 1985 and of carbon nanotubes in 1991 has expanded the investigation of carbon allotropes dramatically in a number of disciplines, including physics and chemistry.

1.1 Fullerenes

1.1.1 Fullerenes: The Third Carbon Allotrope

In 1985, Kroto and Smalley discovered the "soccer ball molecule", fullerene C_{60}, with its beautiful structure [1.1]. They observed a very strong signal corresponding to C_{60} in the mass spectrum of the carbon clusters produced by a laser-vaporization cluster-beam mass spectrometer in He gas. A signal corresponding to C_{70} was the next strongest after C_{60}. In their first paper, they hypothesized that these carbon clusters had no dangling bonds and a cage-like molecular structure. They also predicted that the structure of the magic carbon cluster, C_{60}, was a very stable, specific carbon cluster due to its truncated icosahedron structure (a soccer ball structure), consisting of 20 hexagons and 12 pentagons. However, its molecular structure was not proved until Krätschmer and Huffman achieved bulk production of C_{60}.

For five years from the discovery of C_{60} fullerene, "the soccer ball hypothesis" was not confirmed in spite of many experiments because their experiments were performed by using the mass spectrometry of rarefied ion beam. In 1990, Krätschmer and Huffman succeeded in the bulk production of fullerenes by a resistance heating of a graphite rod in He [1.2]. They also succeeded in the extraction of a series of fullerenes (C_{60}, C_{70}, C_{76}, C_{78} .....).

High-temperature laser-vaporization and DC arc-discharge are well known methods of producing fullerenes and carbon nanotubes, in addition to the Krätschmer and Huffman resistance heating method. Smalley *et al.* reported [1.3] that fullerenes were effectively produced by laser-vaporization (Nd:YAG) at high-temperature (more than 1,000 °C) in flowing Ar (a high-temperature laser-vaporization (laser-furnace) method). Endohedral metallofullerenes and single-wall carbon nanotubes (SWNTs) are also produced by the laser-furnace method effectively, but this method is not suited to bulk production. On the contrary, a DC arc-discharge between two graphite

electrodes can produce grams of fullerene soot, as the anode is vaporized in the high-temperature plasma arc. The carbon soot deposited on the chamber wall contains fullerenes and the cathode deposit contains multi-wall carbon nanotubes (MWNTs). When metal-doped graphite anodes are used, metallofullerenes and SWNTs are produced in the carbon soot, as described latter in this chapter.

1.1.2 Endohedral Metallofullerenes

Smalley *et al.* imprisoned metals in the fullerene cage shortly after the discovery of C_{60} [1.4]. They produced LaC_n ($44 \leq n \leq 80$, n: even number) from La-doped graphite by the laser-vaporization cluster beam method, and suggested that a La atom was imprisoned in the fullerene cage; however, this was not proven by mass spectrometry. After the discovery of the C_{60} bulk production method, Smalley *et al.* produced and extracted La@C_{82} using the laser-furnace method with a La-doped graphite target rod in a high-temperature Ar flow (1,200 °C, 250 Torr) [1.5].

After the report of the La metallofullerene produced by the laser-furnace method, production and isolation of various metallofullerenes were achieved through the DC arc-discharge with metal-doped graphite electrodes. III group transition metals such as Sc, Y and La are easily imprisoned in the fullerene cage. Lanthanide atoms such as Ce, Pr, Nd, Gd, Er, Tb and Tm can be imprisoned easily [1.6]. In addition to the series of rare earth elements, the group II metals such as Ca can be imprisoned the fullerene cage [1.7].

Various endohedral metallofullerenes are generally produced by the DC arc-discharge method, mainly because a large amount of carbon soot containing endohedral metallofullerenes can be produced effectively. The obtained endohedral metallofullerenes can be separated and isolated by high performance liquid chromatography (HPLC) method. However, the purification of endohedral metallofullerenes is difficult, mainly because that the content of the metallofullerenes in the extract is very limited and, furthermore, the solubility in normal HPLC solvents is even lower than that of various higher fullerenes. It took almost two years for metallofullerenes to be completely isolated by HPLC since the first extraction of La@C_{82} by Smalley and co-workers. The success of the purification has been a big breakthrough for a further progress on metallofullerene studies.

Structural and electronic properties of endohedral metallofullerenes have been

proved by many experiments. In 1995 Shinohara and co-workers reported that Synchrotron X-ray study of Y@C_{82} with maximum entropy method (MEM) can give us a direct structural evidence that the yttrium atom is encapsulated within the C_{82} cage [1.8].

1.1.3 Heterofullerenes

Heterofullerenes containing atoms such as B and N as part of the carbon cage have been produced. Heterofullerenes are expected to form nanostructures with physical and chemical properties different from those of fullerenes.

It has been reported that $C_{59}B$ and $C_{69}B$ were produced by DC arc-discharge or laser-furnace method with B-doped graphite rod [1.5, 1.9, 1.10]. Muhr *et al.* have reported that $C_{59}B$ and $C_{69}B$ were extracted by pyridine from the obtained soot [1.10].

Carbon arc-discharge in N_2 or NH_3 is believed to produce $C_{59}N$ [1.11, 1.12]; however, the reproducibility is poor. Mass spectrometry of the products of C_{60} fulleride reacted with an organic molecular has observed fragments such as $C_{59}N^+$ and $C_{59}NH^+$. This suggests the existence of $C_{59}N$ heterofullerene under cluster beam conditions [1.13, 1.14]. After the cluster beam experiment the dimer $C_{59}N$ and $C_{59}HN$ were produced by Wudl *et al.* [1.13, 1.15].

1.2 Carbon Nanotubes

Carbon nanotubes are composed of graphene sheets rolled into seamless hollow cylinders with diameters ranging from 1 nm to about 50 nm. Two kinds of carbon nanotubes, multi-wall carbon nanotubes (MWNTs) and single-wall carbon nanotubes (SWNTs), are produced mainly by DC arc-discharge. MWNTs were discovered by Iijima in 1991 within a carbonaceous deposit, which was left on a cathode after the recovery of fullerene soot produced by arc-discharge [1.16]. SWNTs were discovered in 1993 during the course of synthesizing carbon nanocapsules filled with magnetic fine metal particles (Fe, Co, Ni) [1.17–1.19].

1.2.1 Multi-Wall Carbon Nanotubes (MWNTs)

For the production of MWNTs, pure carbon is evaporated mainly in He gas. Hydrogen can also be employed as working gas for producing MWNTs [1.20, 1.21]. In the latter case, clean MWNTs samples (i.e., MWNTs with less byproducts such as carbon nanoparticles) are produced, though the total amount of grown MWNTs are less than that obtained in He.

A DC arc-discharge for the production of MWNTs in He gas is carried out at gas pressure of at least 200 Torr, below which MWNTs are hardly formed. MWNTs grow inside a cylindrical hard deposit on the tip of a cathode, which consists of two regions: an inner fibrous black core and an outer gray hard shell.

An end of a MWNTs is capped by graphitic layers, and the number of layers at the tips is same as that at the side wall. The caps have polyhedral shapes with sharp corners, at which pentagons (five-membered rings) are believed to be located. As for fullerenes, pentagons have to be introduced into the hexagonal network for the graphene sheet to form a closure. Curvatures of a graphene sheet concentrate around the pentagons, so the locations where a pentagon exists extrude like corners of a polyhedron, whereas other places without pentagons are flat. Tips of MWNTs show various shapes depending on how the six pentagons are introduced into the hexagonal network.

Recently it has been reported that the smallest carbon nanotube occurring at the central core of a MWNTs which was prepared by arc-discharge evaporation of pure graphite in Ar gas [1.22]. The tubule is about 0.5 nm in diameter, which presumably

corresponds to (5,5) tube. According to band calculations, tubules with around 0.4 nm diameter become metallic regardless of chirality unlike conventional SWNTs with diameter of larger than 0.7 nm. The tubule is capped at the one end possibly with a half of a dodecahedron carbon cage. which violates the "isolated pentagon rule (IPR)" for fullerene structure.

MWNTs are being investigated for several applications including cold field electron emmiters [1.23], gas storage materials [1.24], and electrode materials of secondary batteries and capasitors [1.25].

1.2.2 Single-Wall Carbon Nanotubes (SWNTs)

The diameter of SWNTs ranges from 0.7 nm to about 3 nm. The smallest diameter corresponds to that of C_{60} molecules. Metal catalysts are necessary to synthesize SWNTs for both DC arc-discharge and high-temperature laser-vaporization. The yield of SWNTs depends strongly on the catalyst used as well as working gas and its pressure. The catalytic activities of various metals have been confirmed, in particular the catalytic activities of Co, Ni, La, Ce, Y etc. are the most active. It has been reported that when iron alone was used as catalyst, no SWNTs were produced if the working gas was pure He or mixture of CH_4/He. However, in CH_4/Ar mixture, growth of SWNTs was observed, though the density was very low [1.17].

The yield of SWNTs is markedly improved by using a mixture of two metals even though each metal shows no or very little catalytic activity when used alone. Typical examples of such an effect are encountered in Fe/Ni, Rh/Pt and Ni/Y (Ni/Co is also a good catalyst). The Ni/Y binary system is one of the most effectual catalysts for forming abundant SWNTs by the arc-discharge, being comparable to or more effective than the Fe/Ni and Rh/Pt alloy. For the production of SWNTs by laser-furnace method the most effectual catalyst is Ni/Co, not Ni/Y.

SWNTs grow in both cathode and chamber soot, though the density of SWNTs in the respective soot depends on the composition of Ni/Y mixture. When Ni-rich mixture are used, the highest density of SWNTs is obtained in the cathode soot, especially in "collar"-like soot around the root of a cylindrical hard deposit. Using a Ni-rich mixture, Journet *et al.* reported that the highest yield ($\sim$ 90 %) of SWNTs was obtained [1.26].

The density and purity of SWNTs can be increased by the catalytic activities of

metals to a certain extent, however, a lot of impurities, such as amorphous carbon particles, metal particles and carbon nanocapsules, are produced together with SWNTs. Though some methods for purification of SWNTs have been reported [1.27–1.31], high-quality carbon nanotubes have to be produced in order to study detailed bulk properties of carbon nanotubes and to be applied to the application.

It has been well known that a large amount (gram order) of high purity-MWNTs is produced by chemical vapor deposition (CVD) method with metal catalysts [1.32, 1.33]. Recently Nagy and co-workers have reported large-scale synthesis of SWNTs by catalytic chemical vapor deposition (CCVD) method [1.34]. However, a sample of 100 % SWNTs has not been obtained yet.

1.3 Novel Carbon Nanostructures: Fullerene and Carbon Nanotube Related Materials

The discovery of C_{60}, C_{70} and higher fullerenes production method in a macroscopic quantity by Krätschmer and co-workers in 1990 [1.2] has made possible the exhaustive investigation of fullerene chemistry, physics and material science. Since then various types of fullerenes, such as endohedral metallofullerenes [1.35] and heterofullerenes [1.10, 1.36] have been produced and isolated, and the structures have been revealed to data.

Particularly C_{60} has been considered as the smallest fullerene having the cage-structure that can be produced, separated and isolated in macroscopic quantity. This is largely because of the fact that C_{60} is the smallest fullerene which satisfies the so-called isolated pentagon rule (IPR) [1.37]. Some smaller fullerenes than C_{60}, such as C_{20}, C_{28} and M@C_{28} (M = U, Ti etc.), have been expected to be stable on cluster-beam experiments [1.38] and theoretical calculations [1.39–1.42], however, the bulk production and the isolation have not been succeeded and the intensive investigation have not been done.

Fullerene-like carbon clusters containing titanium atoms, such as Met-Cars (metallocarbohedrenes) [1.43–1.51], are predicted to have unique structural and electronic properties. However, bulk production has not succeeded, and there are no detailed investigation of such clusters.

As for carbon nanotube related materials, several materials have been reported. Attempts have been made to fill carbon nanotubes with metals or metallic compounds to obtain nanocomposite materials. Several nanocomposite structures of metal- (or metallic compounds-) filled carbon nanotubes have been reported [1.52–1.55]. Moreover recently Luzzi and co-workers reported that C_{60} molecules were enter the tubes in the gas phase (bucky-peapods) [1.30].

Fullerenes and carbon nanotubes will likely prove important materials in the 21st century. In addition to the known fullerenes an carbon nanotubes mentioned above, more novel, fascinating and interesting carbon nanostructures are likely hidden in the carbon soot produced by the arc-discharge and laser-vaporization of a graphite, particularly metal-doped graphite. This paper investigates the production and characterization of novel carbon nanostructures (materials related to fullerenes and carbon

nanotubes) by high-temperature laser and arc-discharge vaporization.

Bibliography

[1.1] H. W. Kroto, J. R. Heath, S. C. O'Brien, R. F. Curl, and R. E. Smalley, *Nature* **318**, 162 (1985).

[1.2] W. Krätschmer, L. D. Lamb, K. Fostiropoulos, and D. R. Huffman, *Nature* **347**, 354 (1990).

[1.3] R. E. Haufler, Y. Chai, L. P. F. Chibante, J. Conceicao, C. Jin, L. S. Wang, S. Maruyama, and R. E. Smalley, *Mat. Res. Soc. Symp. Proc.* **206**, 627 (1990).

[1.4] J. R. Heath, S. C. O'Brien, Q. Zhang, Y. Liu, R. F. Curl, H. W. Kroto, F. K. tittel, and R. E. Smalley, *J. Am. Chem. Soc.* **107**, 7779 (1985).

[1.5] Y. Chai, T. Guo, C. Jin, R. E. Haufler, L. P. F. Chibante, J. Fure, L. Wang, J. M. Alford, and R. E. Smalley, *J. Phys. Chem.* **95**, 7564 (1991).

[1.6] H. Shinohara, M. Takata, M. Sakata, T. Hashizume, and T. Sakurai, *Materials Science Forum* **232**, 207 (1996).

[1.7] Z. Xu, T. Nakane, and H. Shinohara, *J. Am. Chem. Soc.* **118**, 11309 (1996).

[1.8] M. Takata, B. Umeda, E. Nishibori, M. Sakata, Y. Saito, M. Ohno, and H. Shinohara, *Nature* **377**, 46 (1995).

[1.9] T. Guo, C. Jin, and R. E. Smalley, *J. Phys. Chem.* **95**, 4984 (1991).

[1.10] H. J. Muhr, R. Nesper, B. Schnyder, and R. Kötz, *Chem. Phys. Lett.* **249**, 399 (1996).

[1.11] T. Pradeep, V. Vijayakrishnan, A. K. Santra, and C. N. R. Rao, *J. Phys. Chem.* **95**, 10564 (1991).

[1.12] R. Yu *et al.*, *J. Phys. Chem.* **99**, 1818 (1995).

[1.13] J. C. Hummelen, B. knight, J. Pavlovich, R. González, and F. Wudl, *Science* **269**, 1554 (1995).

[1.14] J. Averdung, H. Luftmann, I. Schlachter, and J. Mattay, *Tetrahedron* **51**, 6977 (1995).

[1.15] M. Keshavarz-K *et al.*, *Nature* **383**, 147 (1996).

[1.16] S. Iijima, *Nature* **354**, 56 (1991).

[1.17] S. Iijima and T. Ichihashi, *Nature* **363**, 603 (1993).

[1.18] D. S. Bethune, C. H. Kiang, M. S. de Vries, G. Gorman, R. Savoy, J. Vazquez, and R. Beyers, *Nature* **363**, 605 (1993).

[1.19] Y. Saito, T. Yoshikawa, M. Okuda, N. Fujimoto, K. Sumiyama, K. Suzuki, A. Kasuya, and Y. Nishina, *J. Phys. Chem. Solid* **54**, 1849 (1993).

[1.20] X. K. Wang, X. W. Lin, V. P. Dravid, J. B. Ketterson, and R. P. H. Chang, *Appl. Phys. Lett.* **66**, 2430 (1995).

[1.21] Y. Ando, X. Zhao, and M. Ohkohchi, *Carbon* **35**, 153 (1997).

[1.22] S. Iijima, in *Advanced Materials 2000: Proceedings of the 7th NIRIM international symposium on advanced materials (ISAM 2000)*, edited by Y. Bando, Y. Matsui, M. Mitome, K. Kimoto, K. Tajima, and N. Aida (National Institute for Research in Inorganic Materials, Japan, 2000), p. 1.

[1.23] Y. Saito, S. Uemura, and K. Hamaguchi, *Jpn. J. Appl. Phys.* **37**, L346 (1998).

[1.24] A. C. Dillon, K. M. Jones, T. A. Bekkedahl, C. H. Kiang, D. S. Bethune, and M. J. Haben, *Nature* **386**, 377 (1997).

[1.25] C. Niu, E. K. Sichel, R. Hoch, D. Moy, and H. Tennent, *Appl. Phys. Lett.* **70**, 1480 (1997).

[1.26] C. Journet, W. K. Maser, P. Bernier, A. Loiseau, M. L. de la Chapelle, S. Lefrant, P. Deniard, R. Lee, and J. E. Fischer, *Nature* **388**, 756 (1997).

[1.27] K. Tohji, T. Goto, H. Takahashi, Y. Shinoda, N. Shimizu, B. Jeyadevan, I. Matsuoka, Y. Saito, A. Kasuya, T. Ohsuna, K. Hiraga, and Y. Nishina, *Nature* **383**, 679 (1996).

[1.28] S. Bandow, A. M. Rao, K. A. Williams, A. Thess, R. E. Smalley, and P. C. Eklund, *J. Phys. Chem. B* **101**, 8839 (1997).

[1.29] K. B. Shelimov, R. O. Esenaliev, A. G. Rinzler, C. B. Huffman, and R. E. Smalley, *Chem. Phys. Lett.* **282**, 429 (1998).

[1.30] B. W. Smith and D. E. Luzzi, *Chem. Phys. Lett.* **321**, 169 (2000).

[1.31] E. Mizoguti, F. Nihey, M. Yudasaka, S. Iijima, T. Ichihashi, and K. Nakamura, *Chem. Phys. Lett.* **321**, 297 (2000).

[1.32] K. Mukhopadhyay, A. Koshio, N. Tanaka, and H. Shinohara, *Jpn. J. Appl. Phys.* **37**, L1257 (1998).

[1.33] K. Mukhopadhyay, A. Koshio, T. Sugai, N. Tanaka, H. Shinohara, Z. Konya, and J. B. Nagy, *Chem. Phys. Lett.* **303**, 117 (1999).

[1.34] J. F. Colomer, C. Stephan, S. Lefrant, G. Van Tendeloo, I. Willems, Z. Kónya, A. Fonseca, Ch. Laurent, and J. B. Nagy, *Chem. Phys. Lett.* **317**, 83 (2000).

[1.35] H. Shinohara, *Advances in Metal and semiconductor Clusters* **4**, 205 (1998).

[1.36] Z. C. Ying, R. L. Hettich, R. N. Compton, and R. E. Haufler, *J. Phys. B: At. Mol. Opt. Phys.* **29**, 4935 (1996).

[1.37] H. W. Kroto, *Nature* **329**, 529 (1987).

[1.38] T. Guo, M. D. Diener, Y. Chai, M. J. Alford, R. E. Haufler, S. M. McClure, T. Ohno, J. H. Weaver, G. E. Scuseria, and R. E. Smalley, *Science* **257**, 1661 (1992).

[1.39] M. Feyereisen, M. Gutowski, J. Simons, and J. Almlöf, *J. Chem. Phys.* **96**, 2926 (1992).

[1.40] T. Guo, R. E. Smalley, and G. E. Scuseria, *J. Chem. Phys.* **99**, 352 (1993).

[1.41] E. J. Bylaska, P. R. Talor, R. Kawai, and J. H. Weare, *J. Phys. Chem.* **100**, 6966 (1996).

[1.42] S. Portmann, J. M. Galbraith, H. F. Schaefer, G. E. Scuseria, and H. P. Lüthi, *Chem. Phys. Lett.* **301**, 98 (1999).

[1.43] B. C. Guo, K. P. Kerns, and A. W. Castleman, Jr., *Science* **255**, 1411 (1992).

[1.44] S. Wei, B. C. Guo, J. Purnell, S. Buzza, and A. W. Castleman, Jr., *J. Phys. Chem.* **96**, 4166 (1992).

[1.45] B. C. Guo, S. Wei, J. Purnell, S. Buzza, and A. W. Castleman, Jr., *Science* **256**, 515 (1992).

[1.46] S. F. Cartier, Z. Y. Chen, G. J. Walder, C. R. Sleppy, and A. W. Castleman, Jr., *Science* **260**, 195 (1993).

[1.47] S. Wei, B. C. Guo, J. Purnell, S. Buzza, and A. W. Castleman, Jr., *Science* **256**, 818 (1992).

[1.48] Z. Y. Chen, G. J. Walder, and A. W. Castleman, Jr., *J. Phys. Chem.* **96**, 9581 (1992).

[1.49] S. Wei, B. C. Guo, J. Purnell, S. A. Buzza, and A. W. Castleman, Jr., *J. Phys. Chem.* **97**, 9559 (1993).

[1.50] B. C. Guo, K. P. Kerns, and A. W. Castleman, Jr., *J. Am. Chem. Soc.* **115**, 7415 (1993).

[1.51] S. Wei, B. C. Guo, H. T. Deng, K. Kerns, J. Purnell, S. A. Buzza, and A. W. Castleman, Jr., *J. Am. Chem. Soc.* **116**, 4475 (1994).

[1.52] P. M. Ajayan and S. Iijima, *Nature* **361**, 333 (1993).

[1.53] C. G. Piécourt, Y. Le Bouar, A. Loiseau, and H. Pascard, *Nature* **372**, 761 (1994).

[1.54] P. M. Ajayan, O. Stephan, Ph. Redlich, and C. Colliex, *Nature* **375**, 564 (1995).

[1.55] J. Sloan, J. Cook, J. R. Heesom, M. L. H. Green, and J. H. Hutchison, *J. Cryst. Growth* **173**, 81 (1997).

Chapter 2

Production and Characterization of C_{36} Related Materials

2.1 Introduction

The discovery of C_{60}, C_{70} and higher fullerenes production method in a macroscopic quantity by Krätschmer and co-workers in 1990 [2.1] has made possible the exhaustive investigation of fullerene chemistry, physics and material science. Since then various types of fullerenes, such as endohedral metallofullerenes [2.2] and heterofullerenes [2.3, 2.4] have been produced and isolated, and the structures have been revealed to data. Particularly C_{60} has been considered as the smallest fullerene having the cage-structure that can be produced, separated and isolated in macroscopic quantity. This is largely because of the fact that C_{60} is the smallest fullerene which satisfies the so-called isolated pentagon rule (IPR) [2.5]. Some smaller fullerenes than C_{60}, such as C_{20}, C_{28} and M@C_{28} (M = U, Ti etc.), have been expected to be stable on cluster-beam experiments [2.6] and theoretical calculations [2.7–2.10], however, the bulk production and the isolation have not been succeeded and the intensive investigation have not been done.

C_{36} has also been predicted as one of the smaller fullerenes, and its production in a macroscopic quantity has not been succeeded. The C_{36} and the other carbon clusters, $C_{2n}(2 \leq 2n \leq 100)$, have been observed experimentally in a study of the jet-cooled cluster beam experiments by Cox and co-workers [2.11] and Smalley and co-workers [2.12]. The structures of C_{36} and other carbon clusters have been investigated by gas-phase mobility measurements by ion chromatography [2.13–2.15], however, after their experiments, the prominent study of the C_{36} bulk production has not been done, and also the detailed structure and properties of C_{36} have not yet been clarified.

In fact, it was not until quite recently that the first smaller fullerene than C_{60}, C_{36}, has been produced by the electric DC arc-discharge method by Zettl and co-workers [2.16]. They have reported that a solid C_{36} was produced in macroscopic quantity by the DC arc-discharge with a graphite electrode in 400 Torr helium, and separated by a sublimation method. They have also reported that the separated sample contained $C_{36}H_6$ which has been six-hydrogenated per C_{36} molecule, because C_{36} was a fairy reactive material, more than C_{60} or C_{70}. Their study of the solid ^{13}C NMR and some theoretical calculations [2.17–2.27] suggest that a fullerene-like caged C_{36}, which consist of twelve pentagons and six hexagons, exists as a covalently-bonded cluster-assembled material in the solid state. And their data also suggest D_{6h} symmetry for the C_{36} molecule. Some calculations of structures and energies suggest that C_{36} form stronger inter-cage bonds than larger fullerenes, and various types of C_{36}-based oligomers for solid-state structures, such as linear polymer and superbenzene structure, have been predicted. The stability of C_{36}^{-} and C_{36}^{2-} was also studied theoretically [2.28]. Jeffrey *et al.* have calculated electron-phonon interaction potential in solid C_{36} and have predicted the possibility of larger superconducting transition temperature than alkali-doped C_{60} solids [2.29, 2.30].

Zettl's experimental studies and many theoretical studies have predicted have predicted that C_{36}-based materials have interesting functions. Unfortunately, attempts to reproduce the production of C_{36} by DC arc-discharge have not been successful, probably because the optimum arc-discharge and sublimation conditions for the production and purification of C_{36} are still not known. I reported the preparative scale synthesis of C_{36} by the high-temperature laser-vaporization (laser-furnace) method, and the purification and identification of C_{36} hydrides and oxyhydrides ($C_{36}H_6$ and $C_{36}H_6O$ respectively) [2.31]. In a previous study, I observed a signal corresponding to $C_{36}H_4$ by LD TOF-MS (laser desorption and ionization time-of-flight mass spectroscopy) in soot produced by the laser-furnace method with graphite rods containing binary metal catalysts, such as Ni/Co and Ni/Y. These metals are known to enhance the production of single-wall carbon nanotubes (SWNTs). I found that metal catalysts also enhanced the production of C_{36} related materials, and that purified C_{36} materials exist as a cluster-assembled material in the solid state, not in molecular form like C_{60}.

Here, I describe the first successful production of C_{36}-related materials ($C_{36}H_4$, $C_{36}H_4O$, $C_{36}H_6$ and $C_{36}H_6O$) via the laser-furnace method using metal-doped graphite rods and a new laser-furnace LD TOF-MS. In addition, in this chapter, I describe the production of $C_{36}H_6$ via DC arc-discharge with metal-doped graphite electrodes, and its purification and isolation by high-performance liquid chromatography (HPLC). Moreover, I discuss my experiments with matrix-assisted laser desorption and ionization (MALDI) TOF mass spectrometry, which suggest the existence C_{36} cluster-assembled materials. The conditions for producing C_{36}-related materials are consistent with those of SWNTs. I also discuss the possible structures of C_{36}-related material based on spectroscopic characterization.

2.2 Experimental

2.2.1 High-Temperature Laser-Vaporization (Laser-Furnace) Method

Smalley and co-workers developed the high-temperature laser-vaporization (laser-furnace) method to produce empty fullerenes and metallofullerenes [2.32]. The laser-furnace method using a binary metal-doped graphite composite rod, such as Ni/Co/C and Ni/Y/C, is now known to be one of the most effective methods for producing SWNTs in high yield and purity [2.33]. However, the laser-furnace products have not been thoroughly investigated to date. From a carbon cluster perspective, investigations of SWNTs intermediates and its precursors in the growth of SWNTs is of particular interest.

I developed a new apparatus to produce and analyze products containing C_{36} materials produced by the laser-furnace method. Figure 2.1 shows a image of the high-temperature laser-vaporization (laser-furnace) LD TOF mass spectrometer, and Figure 2.2 shows the schematic diagram. It consists of three parts: a electric furnace (heated region, 300mm) with a target rod in a quartz tube (inner diameter, 28 mm), a chamber for transferring of a sample plate (15mm × 15 mm) which the product deposited on, and the LD TOF mass spectrometer. Ni/Co- or Ni/Y- doped graphite composite rods [Ni(0.6 atomic %)/Co(0.6%) or Ni(4.2%)/Y(1.0%); Toyo Tanso Co.Ltd., 5 mm × 5 mm × 20 mm] were used.

The second-harmonic output of a Nd:YAG laser (wavelength, 532 nm; frequency, 10 Hz; pulse width, 6-7 ns; power, 600 mJ/pulse; diameter of the laser spot, ca. 1 mm; GCR-250, Spectra-Physics Laser, Inc.) was used to vaporize the metal-doped graphite composite rods at a temperature, which set between a room temperature and 1000°C, in an Ar flow. A focusing lens controlled automatically to change the laser shot position was employed in order that the laser shot should irradiated a fresh graphite plane. The Ar pressure was set between 1 and 760 Torr and the flow rate was 300 ml/min.

The soot containing various fullerenes, SWNTs and C_{36} species were collected on a water cooled nickel plate. The plate was anaerobically transferred to the acceleration region of ion lenses in the LD TOF mass spectrometer. The mass analysis was done in the LD TOF MS chamber pressure of 10^{-7} Torr. The linear reflectron-type

LD TOF mass spectrometer employs vertical laser desorption. The third-harmonic output of the other Nd:YAG laser (wavelength, 355 nm; frequency, 2 Hz; pulse width, ; MINI LIGHT II, HOYA Continuum) for desorption and ionization directly irradiated the collected products on the plate. The pulse sequence, such as the delayed time and the acceleration time of ions, were controlled by the pulse generator (DG535, STANFORD RESEARCH SYSTEMS, INC.). The acceleration voltage was typically set at 2400 V. The time-of-flight signals were analyzed by a transient digitizer (LeCroy 9400 A). The conversion from time to mass scale and the analysis of the TOF spectra were performed on a personal computer (NEC PC9801-VX).

The new apparatus enabled to observe *in situ* laser-furnace products for the first time.

2.2.2 DC Arc-Discharge Method

Arc discharge was performed by a conventional electrical DC arc-discharge. The same Ni/Y- or Ni/Co-doped graphite rod as those used for laser-furnace experiments was used as the anode. The gap of the anode (15 mm square) and the cathode (a carbon block) was set to 1 mm. The arc was sparked at 300 A in a He of 400 Torr static atmosphere. The soot containing C_{36} species, fullerenes and SWNTs was collected and extracted by solvents such as toluene and CS_2. The extracts were analyzed by the homemade LD-TOF mass spectrometer system and the other one (KOMPACT MALDI IV SHIMADZU). The later system has a N_2 laser at a wavelength of 337 nm for desorption and ionization. The soot containing SWNTs was characterized by a scanning electron microscope (SEM) (JEOL JSM-6340F).

2.2.3 Separation and Purification of C_{36} Species by a High Performance Liquid Chromatography (HPLC)

The separation of C_{36} species from fullerenes and purification was done by a high performance liquid chromatography (HPLC) (detection, UV 280 nm: PU-987, UV-970, JASCO Corp.) with a 5PBB column (20 mm × 250 mm, nacalai tesque) with 100% CS_2 eluent. It is the reason why CS_2 can much more solve C_{36} species than any other solvents. The coarse separation and purification were done at 10 ml/min. and at 5 ml/min. flow rate respectively.

2.2.4 ^{13}C NMR

^{13}C NMR measurements of the purified samples were performed using 500 MHz JEOL JNM-LA500 FT NMR system at a room temperature in CS_2 solvent.

Chromium(III) acetylacetonate ($Cr(acac)_3$) and $CDCl_3$ were used as a relaxant and a locking solvent, respectively. $CDCl_3$ is the most suitable relaxant for the C_{36} related materials because its ^{13}C signals (77.0 ppm) do not overlap the signal region of the C_{36} related materials, and also the solubility for $CDCl_3$ is good. To obtain an NMR spectra with good S/N ratios, continuous averaging as long as 2-3 days was required.

2.2.5 Transmission Electron Energy Loss Spectroscopy (T-EELS)

A few droplets of solution were put on a holey carbon micro-grid and then heated in vacuum for 30 min. to remove the solvent molecules. EELS analysis were performed with a Gatan spectrometer (GIF, Gatan Imaging Filter) in an electron microscope (JEOL 2010F) operated at 120 kV. When using a typical manometer probe ($\sim$ 2 mm), the convergence and collective angles for the transmission EELS analysis are set to 7.5 and 10 mrad, respectively.

2.3 Results and Discussion

2.3.1 Observation of C_{36} species via the laser-furnace method

Figure 2.3 shows *in situ* LD TOF-positive mass spectra of soot produced by the laser-furnace method. The spectra in (a), (b) and (c) were obtained using pure graphite, Ni/Co-doped graphite (Ar 100 Torr), and Ni/Co-doped graphite (Ar 500 Torr), respectively. The temperature of the furnace was set at 1000°C. Under these production conditions (Figs. 2.3(a) and (b)), signals corresponding to C_{60}, C_{70}, and other higher fullerenes were observed, but no prominent signals. Of note, the weak signals seen at 436 and 452 amu with pure graphite at 500 Torr Ar and Ni/Co/C at 100 Torr Ar were enhanced dramatically using a Ni/Co/C composite rod at a pressure of 500 Torr Ar. In particular, the $C_{36}H_4$ (436 amu) signal was more intense than that of C_{60}. Presumably, the signal at 452 amu is the oxide of $C_{36}H_4$, $C_{36}H_4O$, because the difference in the mass number is 16 amu, and no intermediate signal was detected.

The intact C_{36} was not observed and only the hydrides and oxyhydrides. C_{36} must be quite reactive so that, immediately after its formation, C_{36} incorporates four hydrogen atoms on the reactive sites even though only a trace amount of hydrogen sources is present in the entire laser-furnace LD TOF-MS combined system.

Figure 2.4(a) shows a high-resolution mass spectrum in the range of the C_{36} species in Fig. 2.3(c). In general, a distribution of carbon species is characterized by combinations of the carbon isotope abundance ($^{12}C = 98.9\%$, $^{13}C = 1.1\%$). The observed ion intensity distribution of $C_{36}H_4$ is consistent with that of the corresponding calculated theoretical distribution as shown in the insert. $C_{36}H_4$ and $C_{36}H_4O$ in the as-produced soot converted entirely to $C_{36}H_6$ and $C_{36}H_6O$, respectively, upon CS_2 solvent extraction (Fig. 2.4(b)). The result for the solvent extraction of $C_{36}H_6$, rather than the intact C_{36} or $C_{36}H_4$, is consistent with a previous report by Piskoti *et al.* [2.16]. The peak intensity of the oxide species, $C_{36}H_6O$, has decreased after the extraction. It is likely that the solubility of the oxide species for CS_2 is much less than that of $C_{36}H_6$ species.

The observed transformation from the four hydrogenated species, $C_{36}H_4$, to the six hydrogenated species, $C_{36}H_6$, on the extraction suggests that two reactive sites were newly formed on $C_{36}H_4$, favorable to incorporate two additional hydrogen atoms.

This may be due to bond-breaking of the solid composed of $C_{36}H_4$ upon CS_2 extraction, which may lead to the formation of a molecular $C_{36}H_6$ species in solution. The C_{36} species are soluble in CS_2 as reported previously [2.16].

A Similar enhancement has been observed for Ni/Y-doped graphite rod but was not observed for Fe- and Ti-doped graphite rods. Namely, the formation of C_{36} species is efficiently catalyzed by exactly the same metal catalysts as in those for SWNTs. Thus the laser-furnace conditions (metal catalysts in the graphite target rod, Ar pressure, furnace temperature) that C_{36} species are observed in were consistent with those of SWNTs [2.33].

2.3.2 Large Scale Production of C_{36} Species by DC Arc-Discharge and Separation by HPLC

I have found that the C_{36} species had been efficiently produced by the laser-furnace method and that the dramatic enhancement of C_{36} species' signals had been detected by LD TOF-MS, however, a small quantity of products (the production rate of the soot, ca.1 mg/h) made difficult to be separated and isolated, and to be characterized by bulk measurements in detail. In contrast, a DC arc-discharge is difficult to control the condition, such as a temperature around the carbon arc plasma, but in general it can produce the soot containing fullerenes and SWNTs in a gram quantity. Similarly the C_{36} species can also be produced by the arc-discharge of a metal-doped graphite electrode which is the same as that enhanced the production of C_{36} species for the laser-furnace method.

Figure 2.5 shows the LD TOF mass spectrum of a CS_2 extract of soot produced by the arc-discharge of Ni/Y/C composite electrodes in a constant 400 Torr He atmosphere. Signals corresponding to fullerenes, such as C_{60}, C_{70} and C_{84}, were detected in the fullerene region, and a strong peak smaller than that of C_{60} was also observed. The signal stronger than that of C_{60} corresponds to $C_{36}H_6$ (438 amu), which has the same mass number as the strong signal observed by the laser-furnace method. As with the CS_2 extract of laser-furnace products, no signal was observed in the mass range between the "C_{36} species region" (ca.450 amu) and C_{60}. In contrast to the laser-furnace products, no signal of the oxide species $C_{36}H_6O$ was observed in the extract of the arc-discharge products. This suggests that the arc-discharge of

Ni/Y/C composite electrode only produces hydride species ($C_{36}H_6$) more efficiently than the laser-furnace method. The mass spectrum of the extract also indicates that the $C_{36}H_6$ molecule has specific structural and electronic stability.

The DC arc-discharge conditions that significantly enhance the production of C_{36} species are consistent with the arc-discharge conditions that efficiently produce SWNTs [2.34]. In general, a soot containing SWNTs is deposited in sheets or webs on the arc-chamber wall. The soot containing the C_{36} species observed in this experiment formed a web-like deposit. Figures 2.6(a) and (b) show SEM images of the as-produced and purified soot, respectively, used to obtain the mass spectrum in Fig. 2.5. It is obvious that the soot contains a high density of SWNTs. The SEM image (Fig. 2.6(b)) shows that the bundles of SWNTs have diameters of ca. 10 nm, and there are thicker bundles with diameters of ca.100 nm. The thicker bundles condensed after extraction and purification.

Figure 2.7 shows an HPLC chromatogram of the CS_2 extract that gives the mass spectrum in Fig. 2.5. The HPLC chromatogram was obtained at a flow rate of 10 ml/min. The peak due to C_{36} species (shaded area called fraction 1) appears ca. 6 min. earlier than C_{60} and C_{70}. In this first separation, C_{36} fraction 1 was roughly separated from C_{60}, C_{70}, and the other higher fullerenes. In general, the HPLC resolution of fullerene species with a PBB column for a 100% CS_2 eluent is no better than with other columns and eluents. In spite of its low HPLC resolution, CS_2 has the best solubility for C_{36} species compared to other solvents, such as toluene and pyridine. A second separation of the C_{36} species fraction was done with a PBB column with CS_2 eluent at a flow rate of 5 ml/min. (Fig. 2.8). The HPLC peak of C_{36} species appears to consist of at least overlapping peaks. I separated the fraction 1, obtained by the first separation, into three HPLC fractions, called fractions 1-1, 1-2, and 1-3, as shown in Fig. 2.8.

Figures 2.9(a), (b) and (c) show MALDI TOF mass spectra of fractions 1-1, 1-2 and 1-3, respectively, using cobalt ultra fine particles (Co-UFP) as a matrix. Without the matrix, TOF mass signals of the separated C_{36} species fractions were not observed. Details of the MALDI TOF mass spectrometry of the separated and purified C_{36} species are discussed in the next section.

The abundant species in the fraction 1-1, with an earlier retention time than that of $C_{36}H_6$, had a mass of 524 amu (Fig. 2.9(a)). Many weak LD TOF signals

corresponding to various hydrocarbon species were also observed in fraction 1-1. This fraction has the earliest retention time, and might be expected to include residual hydrocarbon species in the extract. Clearly, fraction 1-2 only contains $C_{36}H_6$ (Fig. 2.9(b)). Fraction 1-3 contains only one species, with a mass number of 219 amu (Figure 2.9(c)). Interestingly, the mass numbers of the species contained in each successive fraction were successively smaller.

Figures 2.10 (a), (b) and (c) show the UV-Vis-near IR absorption spectra of fractions 1-1, 1-2, and 1-3, respectively. The three spectra have no common characteristic features. Two spectra of fractions 1-1 and 1-3 are similar, and characterized by an onset at about 2,000 nm. Presumably, fraction 1-1 consists of several hydrocarbons, because several signals are observed in the mass spectrum (Fig. 2.9(a)) and the HPLC retention time is the shortest. The obtained UV-Vis-near IR spectra of fractions 1-2 ($C_{36}H_6$ fraction) and 1-3 suggest the existence of isomers or the formation of oligomers by reactive molecules. The UV-Vis-near IR absorption spectrum of the $C_{36}H_6$ fraction is characterized by an onset at about 1,800 nm.

A $C_{36}H_6$ signal was also observed in the C_{76} fraction (produced by arc-discharge using Sc/C-doped graphite [2.35]) separated by the multi-step HPLC separation technique, as shown in Fig. 2.11. Figure 2.12 shows an HPLC chromatogram of the C_{76} fraction. The shaded area is the C_{36} species fraction having the same retention time as the "Co/Ni sample".

2.3.3 A Cluster-Assembled C_{36} Species and Its MALDI TOF Mass Spectrometry

As mentioned above, MALDI TOF MS detected the purified C_{36} species produced by the laser-furnace method [2.31]. Like the separated C_{36} species prepared by the DC arc-discharge method, they were difficult to detect with LD TOF mass spectrometry without a matrix. In particular, no $C_{36}H_6$ signal was observed in samples separated and purified from fullerenes. Figure 2.13(a) shows a LD TOF mass spectrum of the C_{36} species fraction shown as the shaded area in Fig. 2.7 without a matrix. The laser power for desorption and ionization used to obtain this mass spectrum was close to the threshold, and it did not depend on the distribution of the obtained mass signals. In spite of the fact that some signals were detected in the mass range from 200 to 500

amu (Fig. 2.5), only a signal at 219 amu was observed in the C_{36} species fraction. The species at 219 amu detected without a matrix should correspond to the species in the fraction 1-3, because the mass spectrum of the C_{36} species fraction without a matrix is consistent with that of fraction 1-3 (Fig. 2.9(c)).

One possibility is that the $C_{36}H_6$ material is a thermally unstable involatile that is difficult to desorb and ionize. In Fig. 2.13(a), only the signal at 219 amu was observed, indicating that $C_{36}H_6$ dissociates almost completely to give the 219 amu species. The 219 amu species is $C_{18}H_3$, half of $C_{36}H_6$. Obviously, $C_{36}H_6$ is fragile during desorption/ionization. Consequently, I used a MALDI technique to detect $C_{36}H_6$ with cobalt ultra fine powder (Co-UFP) as a matrix. Co-UFP has been used to analyze various compounds [2.36]. Simple spectra are obtained for low-mass samples, because Co-UFP itself generates only positive Co ions, while organic matrices produce complicated spectra below 500 amu. This is why Co-UFP is suitable for detecting $C_{36}H_6$ (438 amu) and was used in this study.

Figure 2.13(b) shows the MALDI TOF mass spectrum of the C_{36} fraction with Co-UFP. The N_2 laser used for desorption and ionization was used at a power close to the threshold for observing a signal. An intense ion signal corresponding to $C_{36}H_6$ was obvious, even in the separated sample. The Co-UFP matrix plays an effective role in the desorption and ionization of the $C_{36}H_6$ ion.

Figure 2.13(c) shows a mass spectrum of the C_{36} species, including C_{60}, in CS_2. The mixture of C_{36} species and C_{60} was prepared by one-step separation and collection of the C_{36} species and C_{60} HPLC fractions simultaneously. Although no Co-UFP matrix was used and the laser intensity was close to the threshold for detecting a signal, a $C_{36}H_6$ signal comparable to that obtained using Co-UFP is seen in this mass spectrum. C_{60} is known to be an effective matrix for LD TOF MS [2.37]. The existence of C_{60} molecules, which have an absorption band at 328 nm, and the N_2 laser wavelength of 337 nm, both significantly enhanced the intensity of the $C_{36}H_6$ signal.

Furthermore, the MALDI TOF mass spectrum of the purified $C_{36}H_6$ with a higher laser fluence also contained a series of peaks due to oligomers of C_{36} species (i.e., $C_{144} \sim C_{216}$) and others due to fragments (Fig. 2.14). Due to its very high reactivity, purified C_{36} forms oligomers or clusters immediately after the removal of solvent CS_2 molecules or concentration of the C_{36} species solution. Recent theoretical calculations

[2.22,2.24] also support such oligomer formation by C_{36}. On the contrary, the purified C_{36} species containing Co-UFP or C_{60} matrix remain as independent molecules and do not combine, even if the solvent molecule is removed. Zettl *et al.* reported the mass spectra of solid pure C_{36} and solid K-doped C_{36} [2.38]. In their experiments, solid C_{36} had a very broad mass distribution peaking at about 120 carbon atoms, and the solid K-doped C_{36} had a very sharp peak of C_{36} similar to the MALDI TOF mass spectrum with Co-UFP matrix obtained in our experiments.

Of particular interest in my experiment was that C_{60} molecules prevented C_{36} species from aggregating and that they dispersed C_{36} species as molecules in the solid state or concentrated solution. The "C_{60} mixing technique" should enable spectroscopic characterization of "molecular $C_{36}H_6$".

2.3.4 Characterization by ^{13}C NMR and T-EELS

As mentioned above, purified $C_{36}H_6$ is reactive and fragile. The molecules readily aggregate or decompose each other. Figure 2.15 shows the mass spectrum of purified $C_{36}H_6$ kept in air at room temperature for a month. The intensity of the purified $C_{36}H_6$ signal deceased, while those of purified $C_{18}H_3$ and 524 amu increased. Other signals were also detected near $C_{36}H_6$. This change in the mass spectrum suggests that a nanostructure formed by the aggregation of $C_{36}H_6$ preferentially decomposed into $C_{18}H_3$ and a species of 524 amu. Presumably, $C_{18}H_3$ is a magic fragment formed by halving $C_{36}H_6$.

A very important problem is the aggregation of purified $C_{36}H_6$ that occurs when a sample in a solvent is concentrated for analysis, such as in NMR. Mixing C_{60} with the purified $C_{36}H_6$ is one way to avoid this aggregation. Figure 2.16 shows the mass spectrum of 1:1 mixture of purified $C_{36}H_6$ and C_{60} kept in air at room temperature for one month. Signals of $C_{18}H_3$ and other species were detected in the range of $200 \sim 400$ amu. A very weak $C_{36}H_6$ signal was detected. It should be noted that no signal of the 524 amu species (a fragment of the $C_{36}H_6$-aggregated species) was detected in the $C_{36}H_6$ / C_{60} mixture. The results suggest that C_{60} molecules were interspersed among the $C_{36}H_6$ molecules and prevented $C_{36}H_6$ from aggregating.

Figure 2.17 shows the energy loss near edge structures (ELNES) of the C K-edge obtained by transmission electron energy loss spectrometry (T-EELS) of purified $C_{36}H_6$, C_{60} and graphite. Here, the $C_{36}H_6$ sample used for T-EELS contained traces

of C_{60} and graphite. A general trend for π^* splitting has been reported in ELNES [2.39,2.40] and NEXAFS [2.41,2.42] studies of empty fullerenes, such as C_{60} (as shown in Fig. 2.17), C_{70}, C_{76}, and C_{84}, although only one peak in π^* region is found at $\sim$ 285 eV for the purified $C_{36}H_6$ solid. A similar single prominent π^* peak has been reported for other endohedral metallofullerenes [2.43], such as $Ca@C_{82}$ and $Gd@C_{82}$.

Figures 2.18(a) and (b) show electron diffraction patterns of graphite and $C_{36}H_6$ solid, respectively. The electron diffraction pattern of graphite obtained in Fig. 2.18(a) is due to a trace of contamination, and indicates spots corresponding to the interlayer distance of graphite (0.34 nm). The diffraction pattern shown in Fig. 2.18(b) indicates a hollow pattern due to the amorphous $C_{36}H_6$ solid. The diffraction ring (Debye-Scherrer ring) corresponds to a periodic structure estimated at about 0.65 nm from the graphite layers. The result is consistent with *d*-spacing calculated by Fowler *et al.* [2.24] and obtained experimentally by Piskoti *et al.* [2.16].

Figure 2.19 shows a ^{13}C NMR spectrum of $C_{36}H_6$ mixed with C_{60} in CS_2 solution. Three strong signals correspond to ^{13}C chemical shifts of CS_2, C_{60}, and $CDCl_3$. There are several resonance peaks near 200 ppm and 30 ppm, and 14 congested signals in the range from 110 to 140 ppm ("fullerene region") (Fig. 2.20). Several theoretical studies have suggested that molecular $C_{36}H_6(D_{3h})$ has five resonance peaks; one resonance peak due to carbons in a pentagonal ring in a low field region ($\sim$ 200 ppm), one due to carbons connected with a hydrogen atom in a high field region ($\sim$ 70 ppm), and three peaks in the fullerene region. The trend for the ^{13}C NMR chemical shifts obtained for $C_{36}H_6$ is consistent with theoretical suggestions. However, approximately 20 more NMR peaks than the calculated chemical shifts were observed, concentrated in the fullerene region. They may be due to isomers with lower symmetry than D_{3h} and to oligomers with several types of carbon sites. The EELS and NMR measurements suggest that isolated $C_{36}H_6$ has a structure similar to fullerenes, and demonstrate the existence of isomers or oligomers.

Summary

I found that C_{36} species were effectively produced by the laser-furnace method and the DC arc-discharge method using metal-doped graphite composite rods containing Ni/Co or Ni/Y. In particular, large amounts of $C_{36}H_6$ were produced by arc-discharge, and this was purified by HPLC with CS_2. The conditions that significantly enhanced the production of C_{36} species were consistent with those used to produce SWNTs. These results suggest that C_{36} is closely related to SWNTs.

The obtained mass spectra suggest that purified $C_{36}H_6$ aggregates readily and forms oligomers in the solid state. However, an additional species, such as metal particles or fullerenes (e.g. C_{60}), prevents the formation of C_{36} oligomers. This method enables the characterization of the C_{36} molecule in the solid state or concentrated solutions. MALDI mass analysis revealed that molecular $C_{36}H_6$ gives $C_{18}H_3$ as a magic fragment upon desorption/ionization.

The existence of some $C_{36}H_6$ isomers and oligomers was predicted from the EELS and NMR measurements of isolated $C_{36}H_6$ or $C_{36}H_6$ mixed with C_{60}.

Appendix: Prediction of the Bulk Production of Other Fullerene-Like Carbon Clusters

C_{28} and $C_{28}H_4$

The C_{28} fullerene is predicted to be the smallest fullerene-like carbon cluster. Guo *et al.* [2.6] reported that it was the smallest fullerene found in abundance in mass spectra. Their *ab inito* quantum chemical calculations predicted that this cluster favors a tetrahedral cage structure. In addition, very stable U@C_{28} was generated using the combined carbon-arc laser vaporization method. These authors suggest that C_{28} with a tetrahedral cage structure should behave as a sort of hollow superatom, with an effective valence of 4. This tetravalence acts in chemical bonds both outside and inside the cage. This confirmed the theoretically predicted tetravalent nature of C_{28} with a $^5A_2$ ground state arising from an electron configuration with four open shells. Thus, stable close-shell derivatives of C_{28} with large highest occupied molecular orbital-lowest unoccupied molecular orbital gaps should be attainable, either by reacting at the four tetrahedral vertices outside the C_{28} cage to make, for example, $C_{28}H_4$, or by trapping a tetravalent atom inside the cage to make endohedral fullerenes such as Ti@C_{28}. In addition to $C_{28}H_4$ and Ti@C_{28}, these authors also suggest the possibility of very stable $C_{28}F_4$ and M@C_{28} (M = Mg, Al, Si, S, Ca, Sc, Ge, Zr and Sn) compounds [2.8].

The smallest fullerene, C_{28}, and related materials are stable in gas-phase cluster-beam experiments, and their structures were predicted theoretically [2.7–2.9]. However, bulk production and isolation of these materials have not been successful, and these clusters have not been extensively investigated.

In this section I discuss about the possible of bulk production of C_{28} and the hydride $C_{28}H_4$ by high-temperature laser-vaporization.

Figure 2.21(a) shows an *in situ* TOF mass spectrum of soot produced by high-temperature laser-vaporization with a pure graphite rod (Toyo Tanso Co.Ltd., 5 × 5 × 20 mm). The second-harmonic output of a Nd:YAG laser (532 nm, 10 Hz, 6-7 ns, 600 mJ/pulse, ca.1 mm diam.spot; Spectra-Physics GCR-250) was used to vaporize the graphite rod at a temperature of 1,000 °C in an Ar flow (500 Torr, 300 ml/min.) condition.

A positive TOF signal corresponding to C_{28} appears at 336 amu. The compounds is abundant, because the intensity of the signal is 60 % that of C_{60}. Figure 2.21(b) shows a TOF mass spectrum of C_{28} containing soot (corresponding to Fig. 2.21(a)) exposed to moist air for 4 days. The peak due to C_{28} shifted from 336 to 340 amu, suggesting that the intact C_{28} in the as-produced soot was converted entirely to $C_{28}H_4$.

Similarly, the as-produced soot containing intact C_{28} was exposed to the D_2O moisture for 4 days. Interestingly, the peak due to C_{28} shifted from 336 to 344 amu (Fig. 2.21(c)). The intact C_{28} in the as-produced soot was converted entirely to $C_{28}D_4$. It is evident that the TOF signals at 340 and 344 amu were due to four hydrogenated C_{28} ($C_{28}H_4$) and four deuterated C_{28} ($C_{28}D_4$), respectively.

Thus, the observed transformation from C_{28} to $C_{28}H_4$ (and from C_{28} to $C_{28}D_4$) suggests that the intact C_{28} has four reactive sites and forms four chemical bondings, which is consistent with previous theoretical predictions [2.8].

Smaller Heterofullerenes Containing Ti Atoms Related to Met-Cars

The new system that we developed, the laser-furnace-LD TOF mass spectrometer, is certain to produce various novel carbon clusters in addition to those mentioned above. One example is a Ti-C cluster. It has been predicted that fullerene-like carbon clusters containing titanium atoms, such as Met-Cars (metallocarbohedrenes) [2.44–2.52], have a unique structural and electronic nature. However, the bulk production has not been successful, so these clusters have not been investigated thoroughly. In this appendix, I describe the possible bulk production of novel Ti-C clusters by the laser-furnace method.

Figure 2.22 shows an *in situ* TOF mass spectrum of as-produced soot produced by the laser-furnace method with Ti-doped graphite (Ti = 10 at%, 5 × 5 × 20 mm, Toyo Tanso Co.Ltd.) at 1,000 °C in Ar flow (300 Torr, 300 ml/min.). The second-harmonic output of a Nd:YAG laser (532 nm, 10 Hz, 6-7 ns, 600 mJ/pulse, ca.1 mm diam. spot) was used to vaporize the composite graphite rod. Three weak signals are observed from 200 to 500 amu as shown in Fig. 2.22 (top). These signals were assigned as $TiC_{19}H_2$, $Ti_2C_{18}H_2$, and $TiC_{35}H_6$, respectively. The possible combination

of Ti and C in a Ti-C cluster cannot be decided only by the mass number, because the mass number of a Ti atom is nearly equal to that of four carbon atoms. However, this assignment can be made using the distribution of signal intensity, due to the natural isotope distribution of Ti atoms (^{46}Ti = 8.0%, ^{47}Ti = 7.3%, ^{48}Ti = 73.8%, ^{49}Ti = 5.5%, ^{46}Ti = 5.4%). Figure 2.22 (bottom) shows the mass spectrum in the top figure ,expanded around 280 amu. Clearly, a Ti atom is contained in this cluster. My explanation for this result is as follows. TiC_{19} and Ti_2C_{18} consist of 20 Ti and C atoms, and may have a pentagonal dodecahedron structure, like Met-Cars, Ti_8C_{12}. Intact TiC_{19} and Ti_2C_{18} were not observed in this experiments, but their hydrides were detected. These Ti-C clusters must be quite reactive, so that immediately after their formation TiC_{19} and Ti_2C_{18} incorporate two hydrogen atoms at the reactive sites, although only a trace amount of hydrogen is present in the entire laser-furnace TOF-MS system.

Of particular interest, $TiC_{35}H_6$ consisting of 36 Ti and C atoms and 6 hydrogenated species was detected. This result reminds us of the structure and character of $C_{36}H_6$, as described above. It appears likely that one carbon atom in $C_{36}H_6$ is replaced by one titanium atom.

The results suggest the possibile of production of novel carbon clusters and metal-carbon clusters by the laser-furnace method, and that *in situ* observation using the laser-furnace TOF-MS system enables their detection.

Bibliography

[2.1] W. Krätschmer, L. D. Lamb, K. Fostiropoulos, and D. R. Huffman, *Nature* **347**, 354 (1990).

[2.2] H. Shinohara, *Advances in Metal and semiconductor Clusters* **4**, 205 (1998).

[2.3] Z. C. Ying, R. L. Hettich, R. N. Compton, and R. E. Haufler, *J. Phys. B: At. Mol. Opt. Phys.* **29**, 4935 (1996).

[2.4] H. J. Muhr, R. Nesper, B. Schnyder, and R. Kötz, *Chem. Phys. Lett.* **249**, 399 (1996).

[2.5] H. W. Kroto, *Nature* **329**, 529 (1987).

[2.6] T. Guo, M. D. Diener, Y. Chai, M. J. Alford, R. E. Haufler, S. M. McClure, T. Ohno, J. H. Weaver, G. E. Scuseria, and R. E. Smalley, *Science* **257**, 1661 (1992).

[2.7] M. Feyereisen, M. Gutowski, J. Simons, and J. Almlöf, *J. Chem. Phys.* **96**, 2926 (1992).

[2.8] T. Guo, R. E. Smalley, and G. E. Scuseria, *J. Chem. Phys.* **99**, 352 (1993).

[2.9] E. J. Bylaska, P. R. Talor, R. Kawai, and J. H. Weare, *J. Phys. Chem.* **100**, 6966 (1996).

[2.10] S. Portmann, J. M. Galbraith, H. F. Schaefer, G. E. Scuseria, and H. P. Lüthi, *Chem. Phys. Lett.* **301**, 98 (1999).

[2.11] E. A. Rohlfing, D. M. Cox, and A. J. Kaldor, *J. Chem. Phys.* **81**, 3322 (1984).

[2.12] H. W. Kroto, J. R. Heath, S. C. O'Brien, R. F. Curl, and R. E. Smalley, *Nature* **318**, 162 (1985).

[2.13] J. Hunter, J. Fye, and M. F. Larrold, *Science* **260**, 784 (1993).

[2.14] G. von Helden, M. T. Hsu, N. Gotts, and M. T. Bowers, *J. Phys. Chem.* **97**, 8182 (1993).

[2.15] L. D. Book, C. Xu, and G. E. Scuseria, *Chem. Phys. Lett.* **222**, 281 (1994).

[2.16] C. Piskoti, J. Yarger, and A. Zettl, *Nature* **393**, 771 (1998).

[2.17] T. Heine, G. Seifert, P. W. Fowler, and F. Zerbetto, *J. Phys. Chem. A* **103**, 8738 (1999).

[2.18] J. C. Grossman, M. Côté, S. G. Louie, and M. L. Cohen, *Chem. Phys. Lett.* **284**, 344 (1998).

[2.19] Z. Slanina, X. Zhao, and E. Ōsawa, *Chem. Phys. Lett.* **290**, 311 (1998).

[2.20] P. G. Collins, J. C. Grossman, M. Côté, M. Ishigami, C. Piskoti, S. G. Louie, M. L. Cohen, and A. Zettl, *Phys. Rev. Lett.* **82**, 165 (1999).

[2.21] P. W. Fowler, D. Mitchell, and F. Zerbetto, *J. Am. Chem. Soc.* **121**, 3218 (1999).

[2.22] T. Heine, P. W. Fowler, and G. Seifert, *Solid State Commun.* **111**, 19 (1999).

[2.23] E. Halac, E. Burgos, and H. Bonadeo, *Chem. Phys. Lett.* **299**, 64 (1999).

[2.24] P. W. Fowler, T. Heine, K. M. Rogers, J. P. B. Sandall, G. Seifert, and F. Zerbetto, *Chem. Phys. Lett.* **300**, 369 (1999).

[2.25] R. A. Jishi and M. S. Dresselhaus, *Chem. Phys. Lett.* **302**, 533 (1999).

[2.26] M. N. Jagadeesh and J. Chandrasekhar, *Chem. Phys. Lett.* **305**, 298 (1999).

[2.27] M. Menon and E. Richter, *Phys. Rev. B* **60**, 13322 (1999).

[2.28] A. Ito, T. Monobe, T. Yoshii, and K. Tanaka, *Chem. Phys. Lett.* **315**, 348 (1999).

[2.29] M. Côté, J. C. Grossman, M. L. Cohen, and S. G. Louie, *Phys. Rev. Lett.* **81**, 697 (1998).

[2.30] J. C. Grossman, S. G. Louie, and M. L. Cohen, *Phys. Rev. B* **60**, 6941 (1999).

[2.31] A. Koshio, M. Inakuma, T. Sugai, and H. Shinohara, *J. Am. Chem. Soc.* **122**, 398 (2000).

[2.32] R. E. Haufler, Y. Chai, L. P. F. Chibante, J. Conceicao, C. Jin, L. S. Wang, S. Maruyama, and R. E. Smalley, *Mat. Res. Soc. Symp. Proc.* **206**, 627 (1990).

[2.33] A. Thess, R. Lee, P. Nikolaev, H. Dai, P. Petit, J. Robert, C. Xu, Y. H. Lee, S. G. Kim, A. G. Rinzler, D. T. Colbert, G. E. Scuseria, D. Tománek, J. E. Fischer, and R. E. Smalley, *Science* **273**, 483 (1996).

[2.34] C. Journet, W. K. Maser, P. Bernier, A. Loiseau, M. L. de la Chapelle, S. Lefrant, P. Deniard, R. Lee, and J. E. Fischer, *Nature* **388**, 756 (1997).

[2.35] C. R. Wang, M. Inakuma, and H. Shinohara, *Chem. Phys. Lett.* **300**, 379 (1999).

[2.36] K. Tanaka, H. Waki, Y. Ido, S. Akita, Y. Yoshida, and T. Yoshida, *Rapid Commun. Mass Spectrom.* **2**, 151 (1988).

[2.37] F. G. Hopwood, L. Michalak, D. S. Alderdice, K. J. Fisher, and G. D. Willett, *Rapid Commun. Mass Spectrom.* **8**, 881 (1994).

[2.38] A. Zettl, C. Piskoti, J. C. Grossman, M. L. Cohen, and S. G. Louie, in *Electronic Properties of Novel Materials- Science and Technology of Molecular Nanostructures*, edited by H. Kuzmany, J. Fink, M. Mehring, and S. Roth (PUBLISHER, ADDRESS, 1999), p. 183.

[2.39] R. Kuzuo, M. Terauchi, M. Tanaka, Y. Saito, and H. Shinohara, *Phys. Rev. B* **49**, 5054 (1994).

[2.40] R. Kuzuo, M. Terauchi, M. Tanaka, Y. Saito, and Y. Achiba, *Phys. Rev. B* **51**, 11018 (1995).

[2.41] L. J. Terminello, D. K. Shuh, F. J. Himpsel, D. A. Lapiano-Smith, J. Stöhr, S. D. S. Bethune, and G. Meijer, *Chem. Phys. Lett.* **191**, 491 (1991).

[2.42] P. L. Hansen, P. J. Fallon, and W. Krätschmer, *Chem. Phys. Lett.* **181**, 367 (1991).

[2.43] K. Suenaga, S. Iijima, H. Kato, and H. Shinohara, *Phys. Rev. B* (in press).

[2.44] B. C. Guo, K. P. Kerns, and A. W. Castleman, Jr., *Science* **255**, 1411 (1992).

[2.45] S. Wei, B. C. Guo, J. Purnell, S. Buzza, and A. W. Castleman, Jr., *J. Phys. Chem.* **96**, 4166 (1992).

[2.46] B. C. Guo, S. Wei, J. Purnell, S. Buzza, and A. W. Castleman, Jr., *Science* **256**, 515 (1992).

[2.47] S. F. Cartier, Z. Y. Chen, G. J. Walder, C. R. Sleppy, and A. W. Castleman, Jr., *Science* **260**, 195 (1993).

[2.48] S. Wei, B. C. Guo, J. Purnell, S. Buzza, and A. W. Castleman, Jr., *Science* **256**, 818 (1992).

[2.49] Z. Y. Chen, G. J. Walder, and A. W. Castleman, Jr., *J. Phys. Chem.* **96**, 9581 (1992).

[2.50] S. Wei, B. C. Guo, J. Purnell, S. A. Buzza, and A. W. Castleman, Jr., *J. Phys. Chem.* **97**, 9559 (1993).

[2.51] B. C. Guo, K. P. Kerns, and A. W. Castleman, Jr., *J. Am. Chem. Soc.* **115**, 7415 (1993).

[2.52] S. Wei, B. C. Guo, H. T. Deng, K. Kerns, J. Purnell, S. A. Buzza, and A. W. Castleman, Jr., *J. Am. Chem. Soc.* **116**, 4475 (1994).

List of Figures

the MS sample in Fig. 2.11). The shaded area shows the HPLC fraction containing C_{36} species.

Fig. 2.13 LD TOF mass spectra of (a) purified $C_{36}H_6$, (b) purified $C_{36}H_6$ with Co ultra fine particles (Co-UFP) matrix and (c) $C_{36}H_6$ with C_{60} matrix.

Fig. 2.14 A LD TOF mass spectrum of a dried $C_{36}H_6$ solid prepared by evaporating the purified CS_2 extract.

Fig. 2.15 LD TOF mass spectra of (a) the purified $C_{36}H_6$ with Co-UFP matrix in CS_2 and the sample kept at a room temperature in air for one month.

Fig. 2.16 LD TOF mass spectra of (a) the mixture, $C_{36}H_6$ containing C_{60}, in CS_2 and (b) the sample kept at a room temperature in air for one month.

Fig. 2.17 Energy loss near-edge structures of the C K-edge obtained by Transmission electron energy loss spectrometry (T-EELS) of $C_{36}H_6$, C_{60} and graphite.

Fig. 2.18 Electron-diffraction patterns of (a) graphite and (b) $C_{36}H_6$ crystal.

Fig. 2.19 A ^1H decoupled ^{13}C NMR spectrum of $C_{36}H_6$ in CS_2 solution.

Fig. 2.20 A ^1H decoupled ^{13}C NMR spectrum of $C_{36}H_6$ in CS_2 solution (expanded from 120 ppm to 142 ppm in Fig. 2.19).

Fig. 2.21 LD TOF mass spectra of (a) *in situ* as-produced soot produced by laser-furnace method with a pure graphite rod, (b) the soot kept in air (moisture: H_2O) for three days and the soot moisturized by D_2O for three days.

Fig. 2.22 An *in situ* LD TOF mass spectrum of as-produced soot prepared by laser-furnace method with a Ti/C composite target rod (top) and the expanded spectrum (bottom).

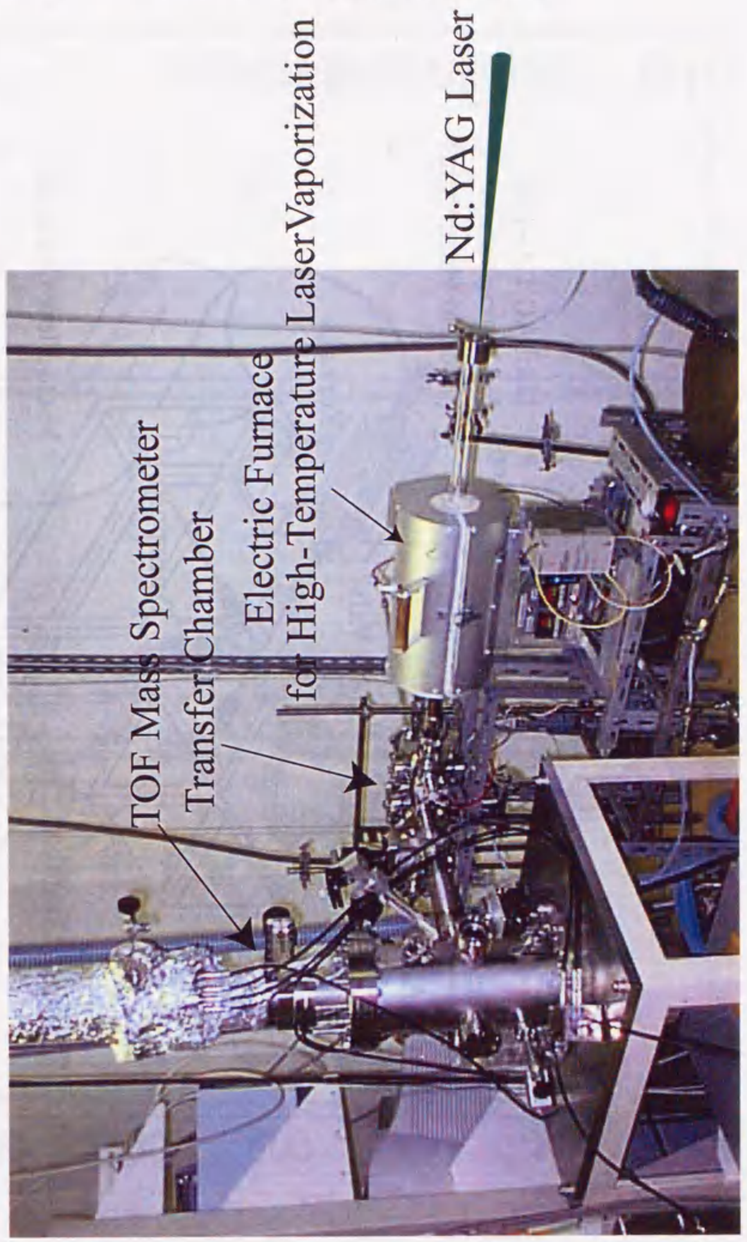

Fig. 2.1

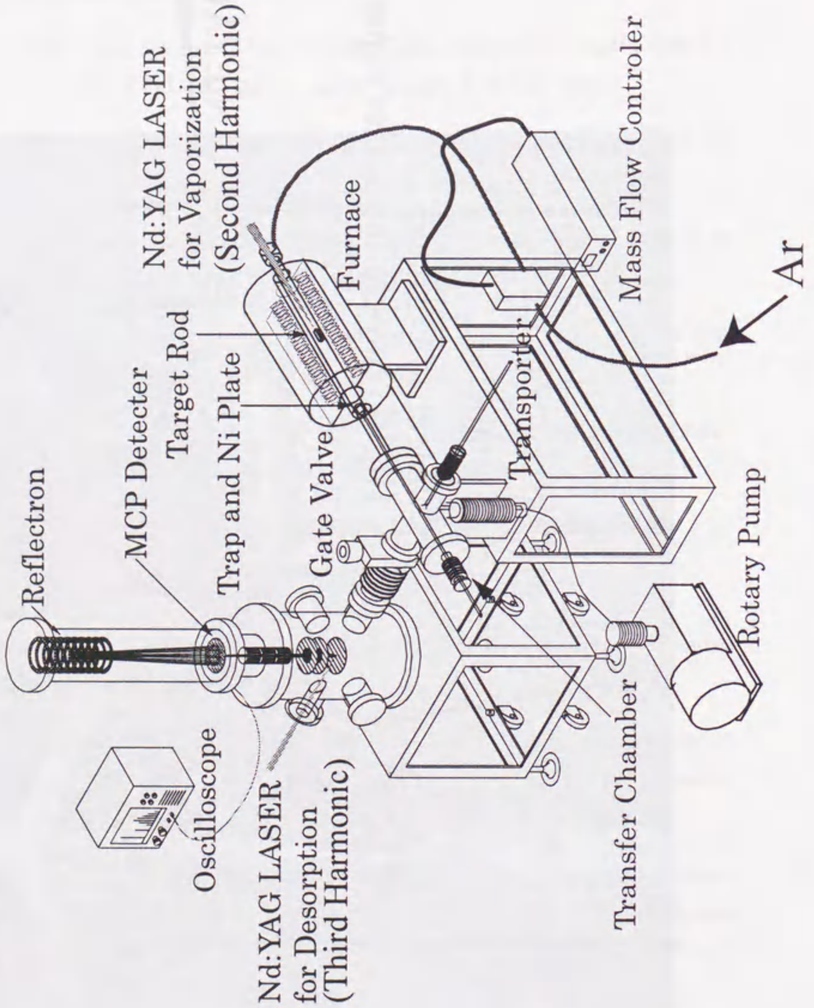
Nd:YAG LASER
for Vaporization
(Second Harmonic)
Furnace
Mass Flow Controler
Ar
Target Rod
and Ni Plate
Transporter
Gate Valve
Rotary Pump
Reflectron
MCP Detecter
Trap
Oscilloscope
Nd:YAG LASER
for Desorption
(Third Harmonic)
Transfer Chamber

Fig. 2.2

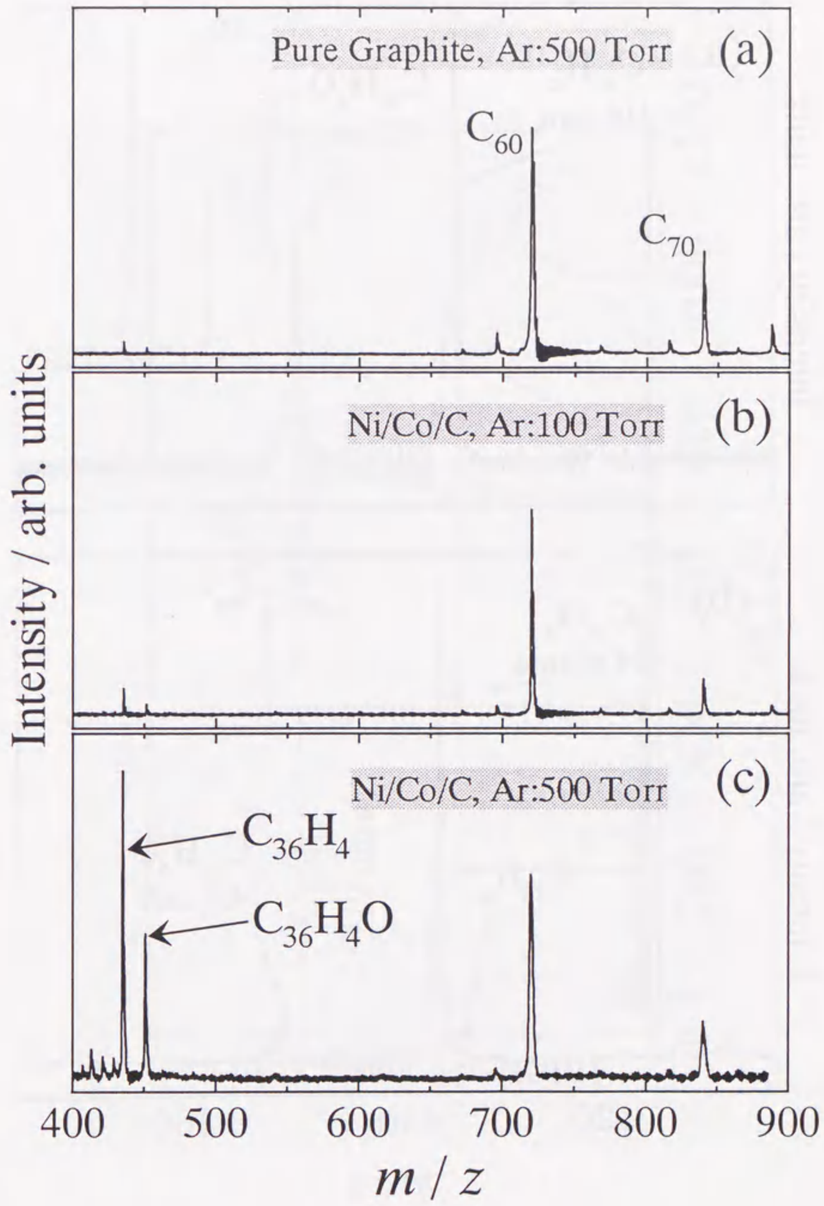
Pure Graphite, Ar:500 Torr
(a)
C_{60}
C_{70}
Ni/Co/C, Ar:100 Torr
(b)
Ni/Co/C, Ar:500 Torr
(c)
$C_{36}H_4$
$C_{36}H_4O$
Intensity / arb. units
400
500
600
700
800
900
m / z

Fig. 2.3

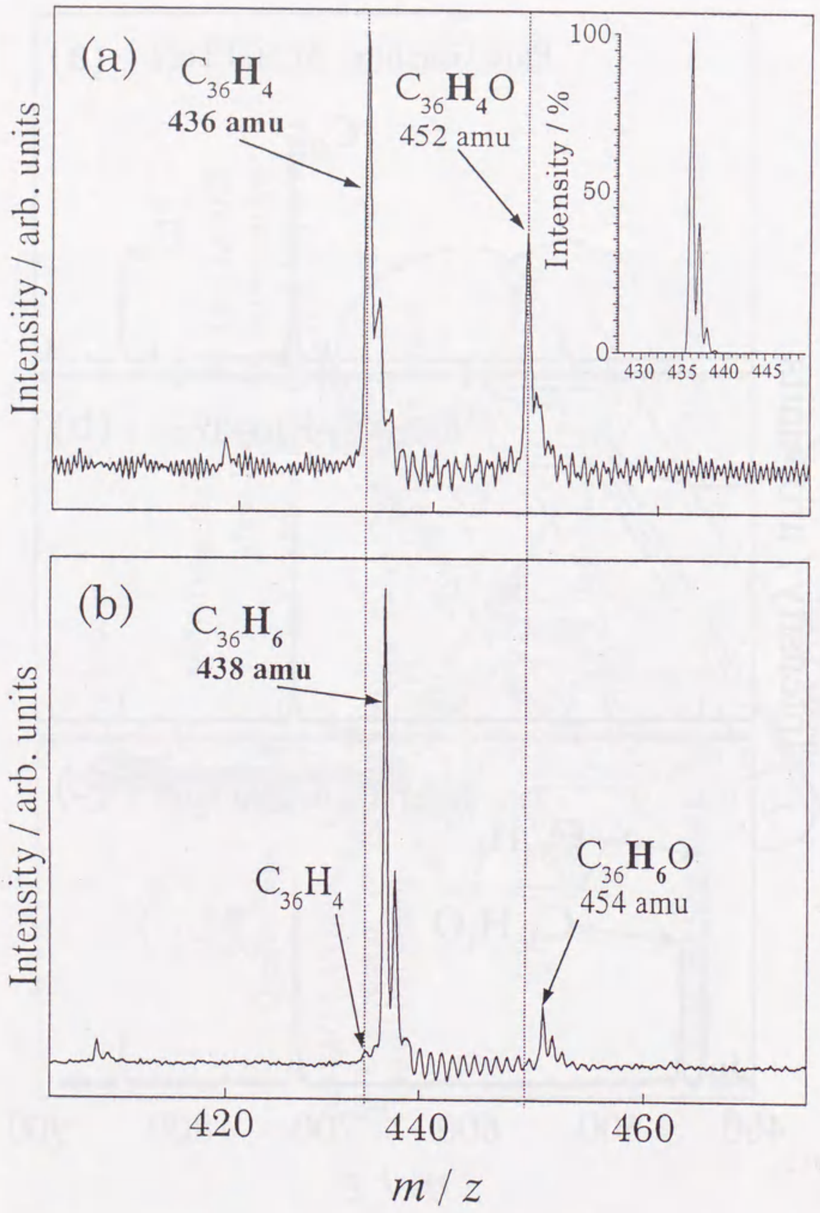
(a)
$C_{36}H_4$
436 amu
$C_{36}H_4O$
452 amu
Intensity / %
100
50
0
430 435 440 445
Intensity / arb. units
(b)
$C_{36}H_6$
438 amu
$C_{36}H_4$
$C_{36}H_6O$
454 amu
Intensity / arb. units
420
440
460
m / z

Fig. 2.4

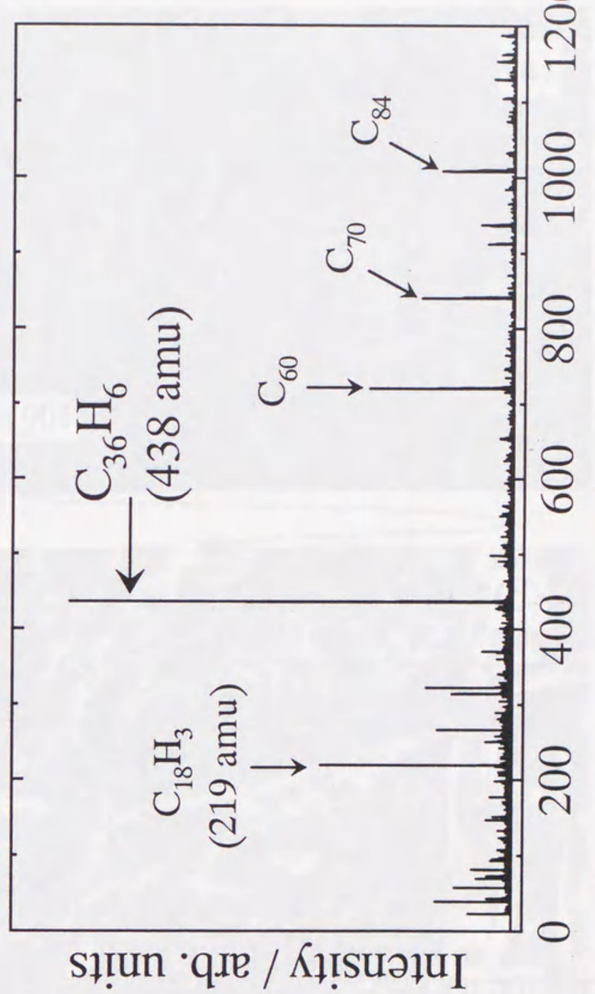
$C_{36}H_6$
(438 amu)
C_{60}
C_{70}
C_{84}
$C_{18}H_3$
(219 amu)
Intensity / arb. units
0
200
400
600
800
1000
1200
m / z

Fig. 2.5

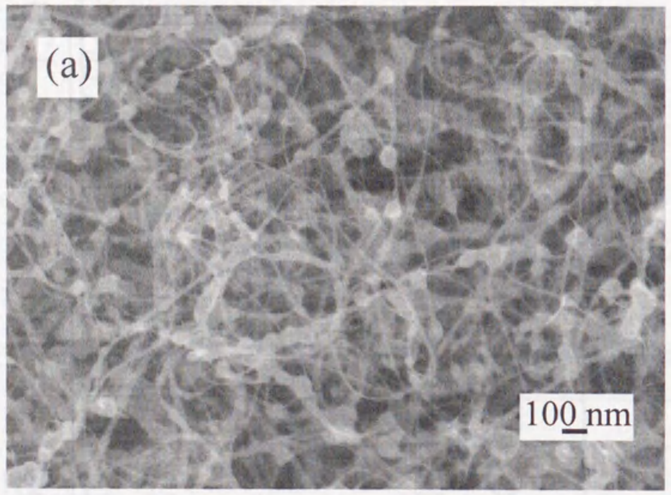
(a)
100 nm

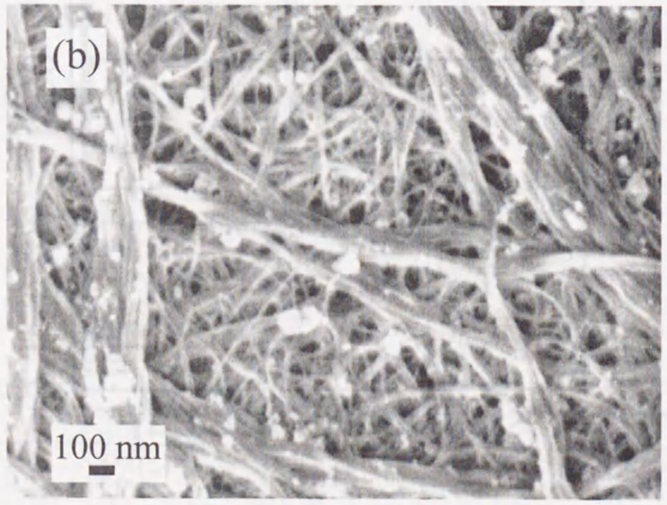
(b)
100 nm

Fig. 2.6

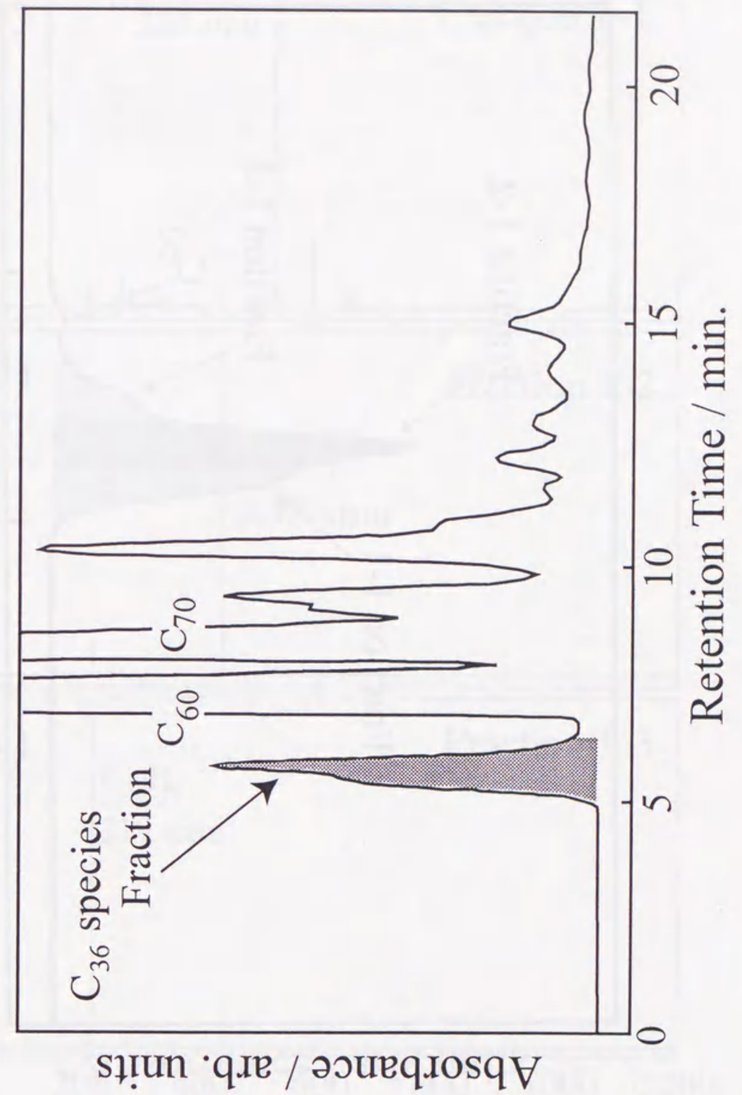
Absorbance / arb. units
0
5
10
15
20
Retention Time / min.
C_{36} species
Fraction
C_{60}
C_{70}

Fig. 2.7

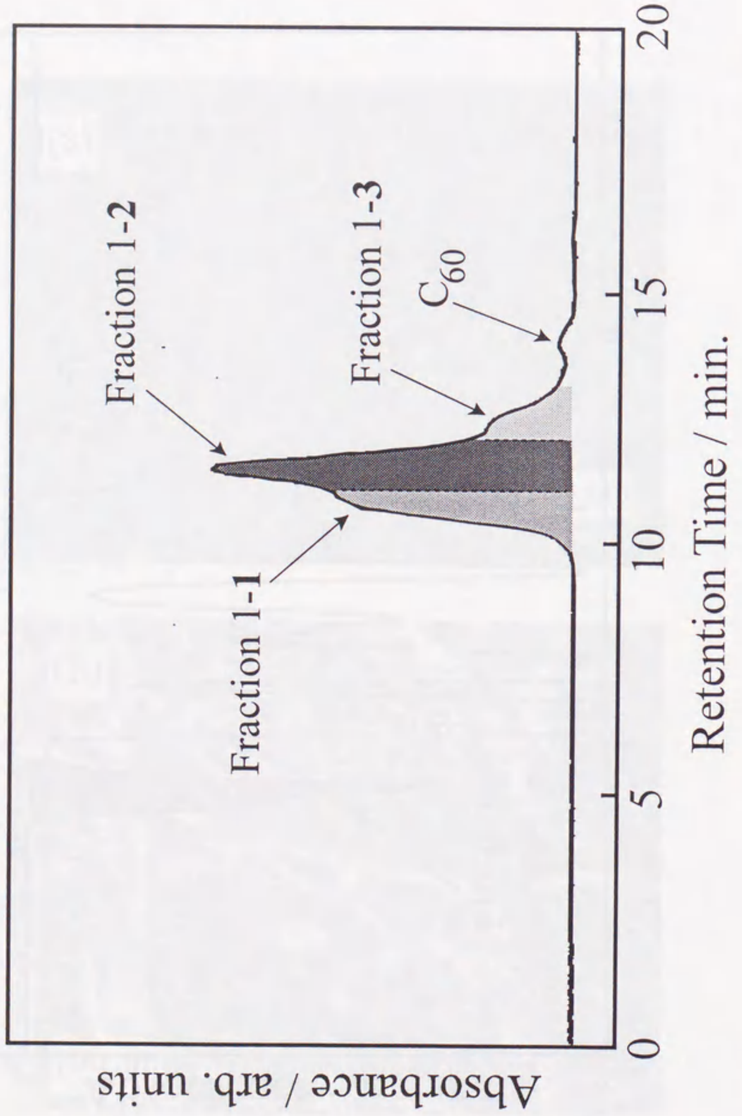
Fraction 1-2
Fraction 1-3
C_{60}
Fraction 1-1
Absorbance / arb. units
Retention Time / min.
0
5
10
15
20

Fig. 2.8

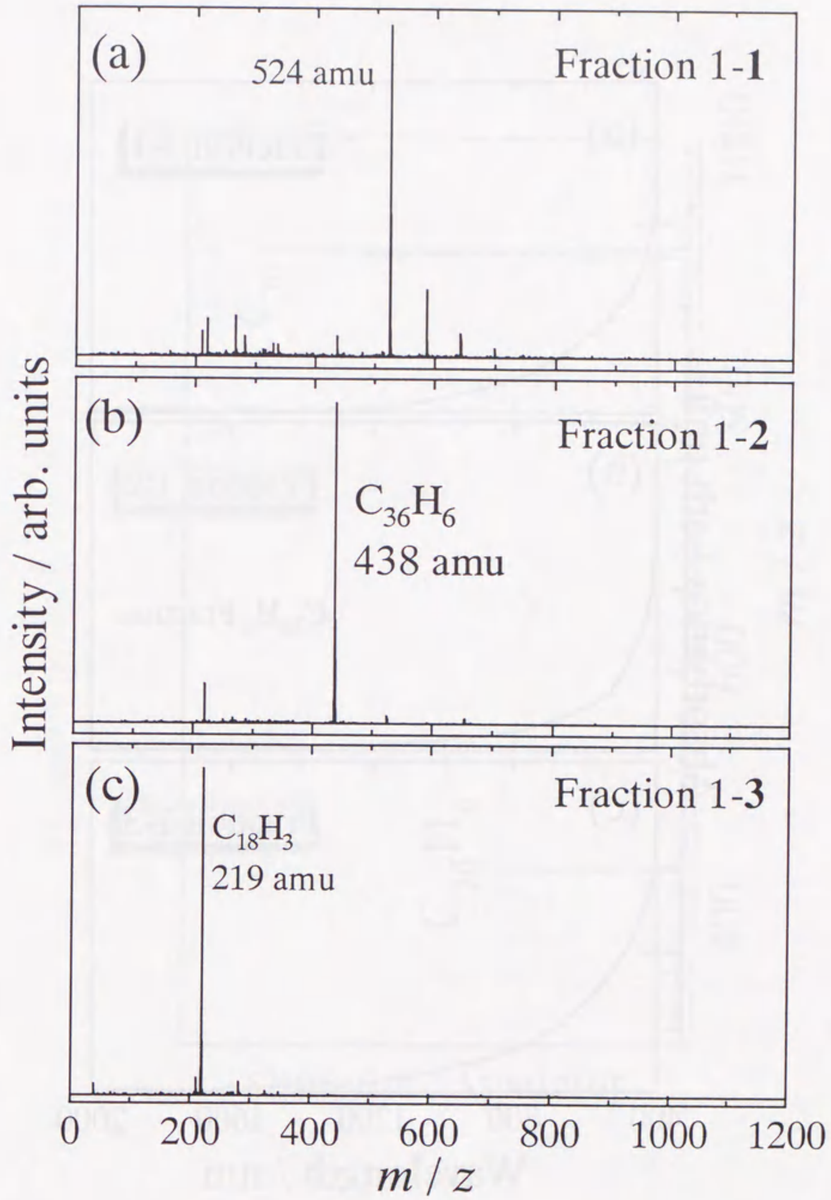
(a)
524 amu
Fraction 1-1
(b)
Fraction 1-2
$C_{36}H_6$
438 amu
(c)
Fraction 1-3
$C_{18}H_3$
219 amu
Intensity / arb. units
0
200
400
600
800
1000
1200
m / z

Fig. 2.9

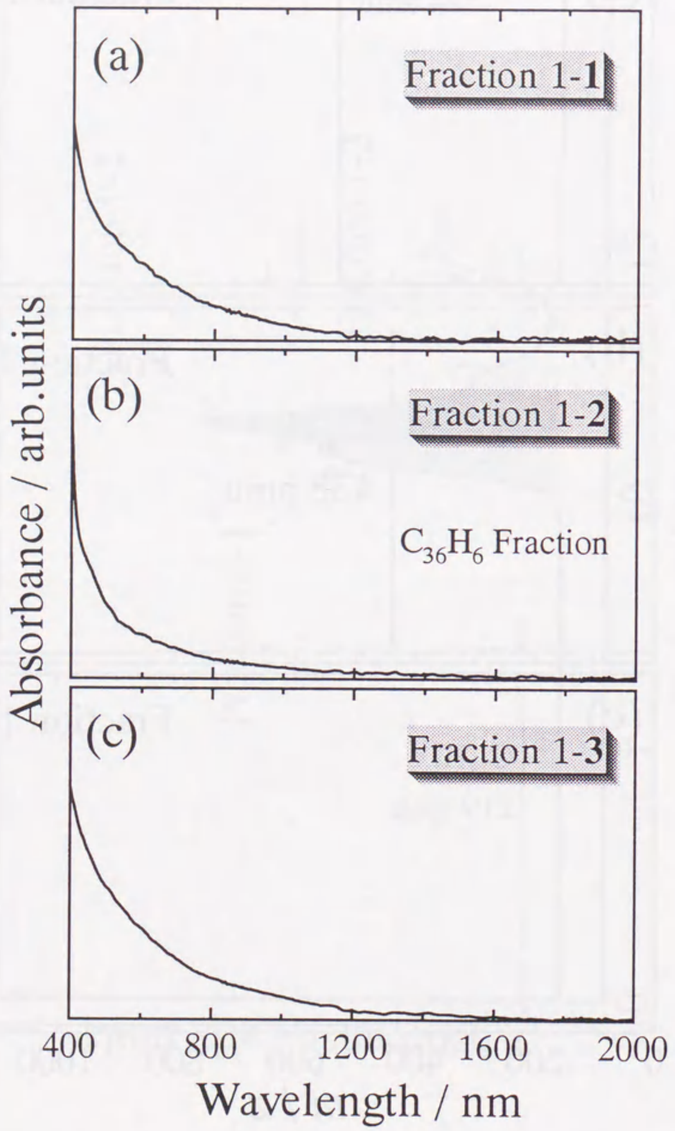

Fig. 2.10

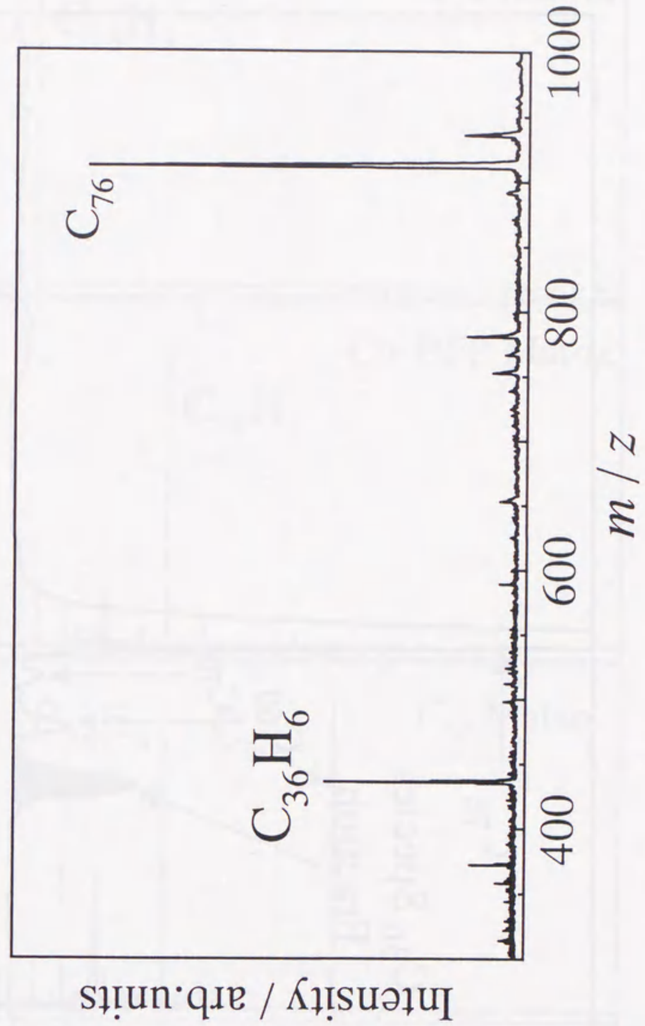

Fig. 2.11

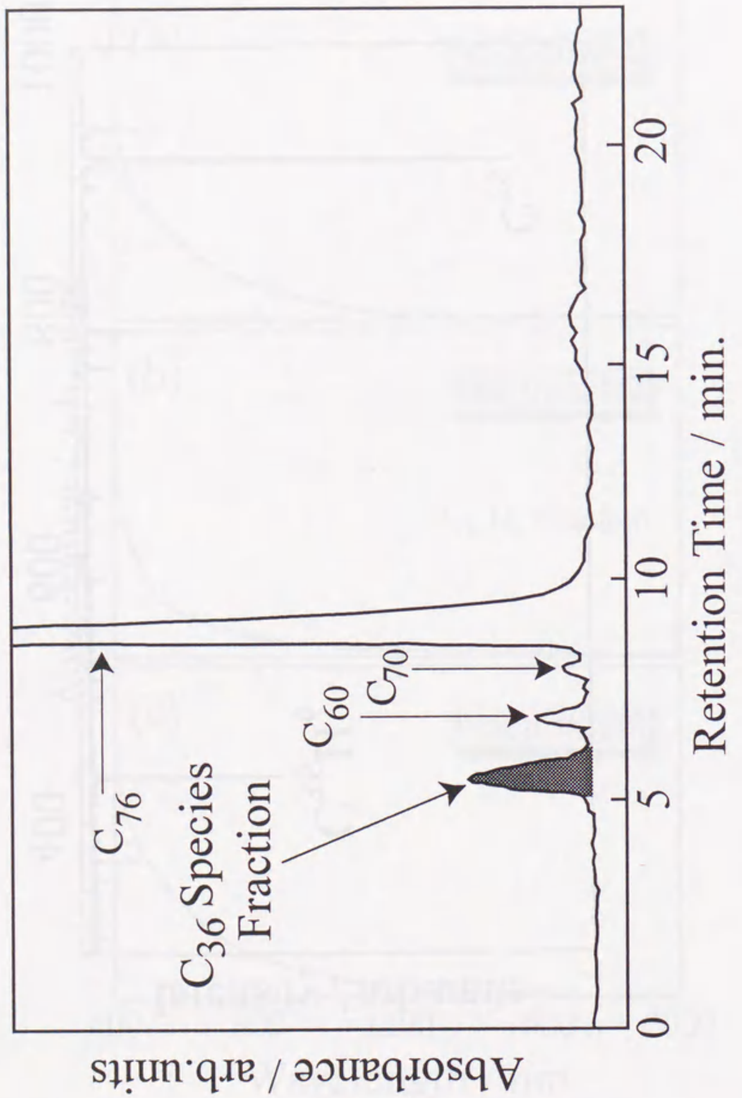

Fig. 2.12

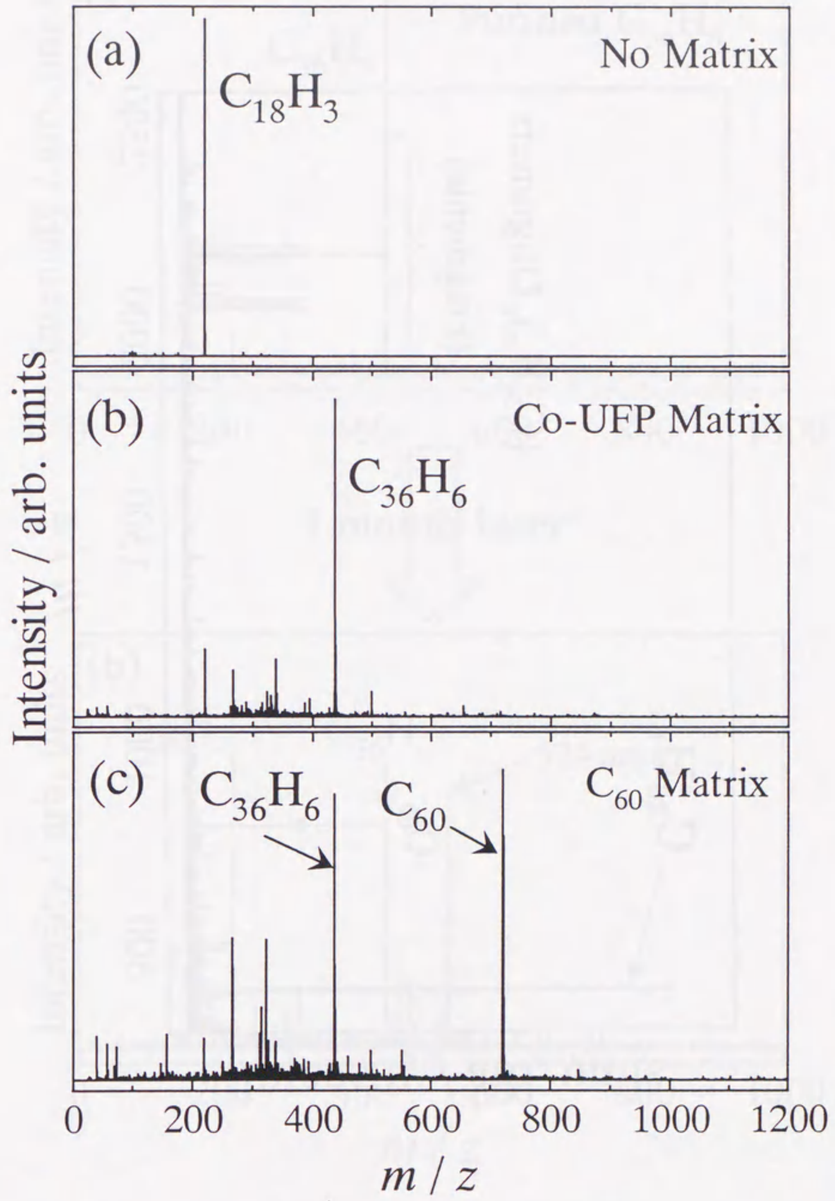

Fig. 2.13

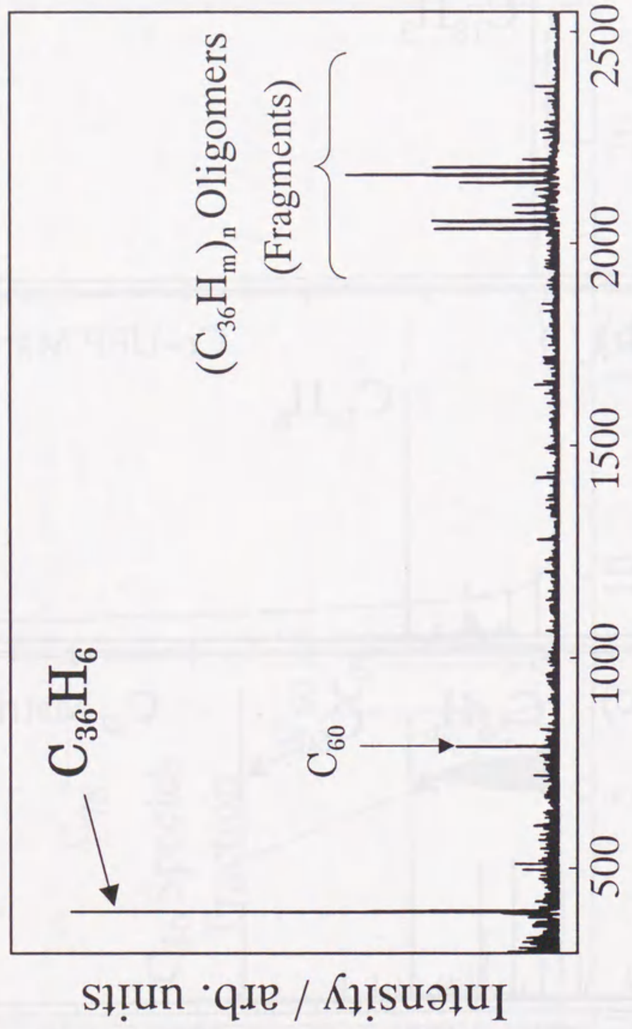

Fig. 2.14

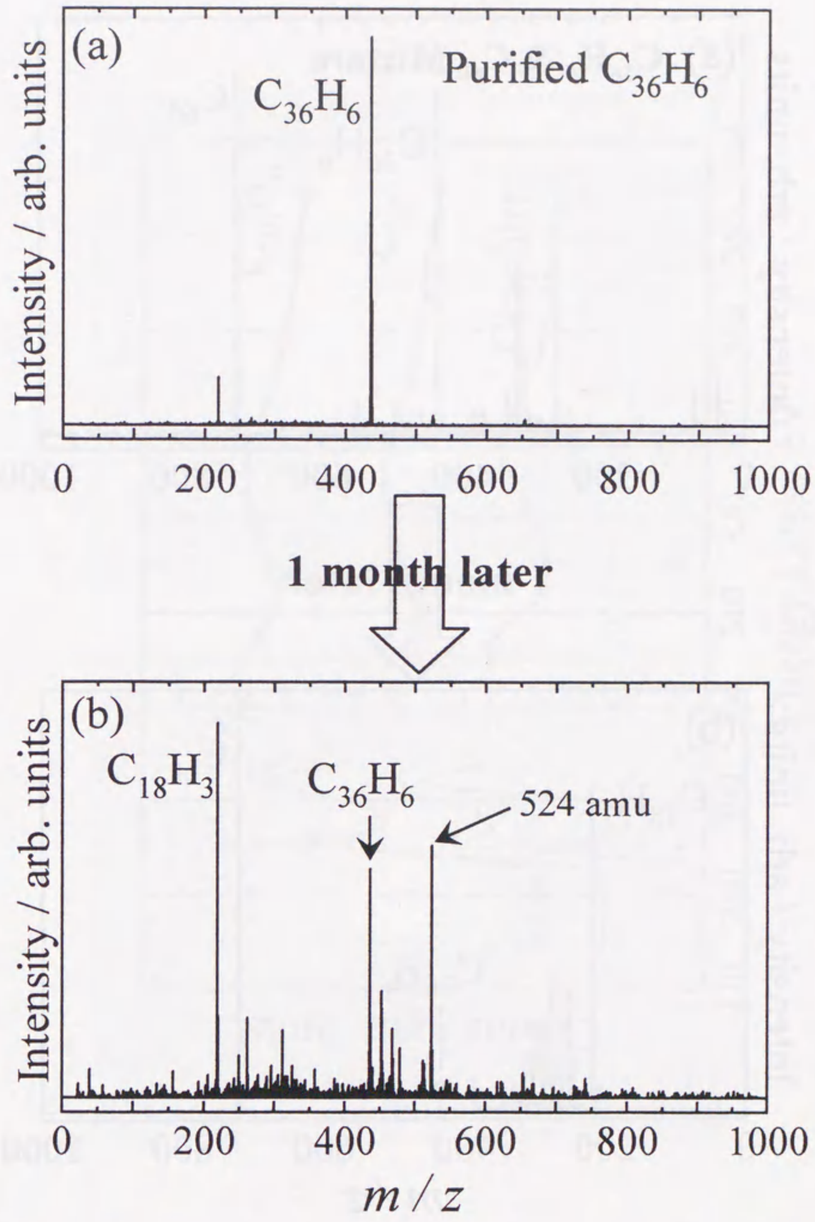

Fig. 2.15

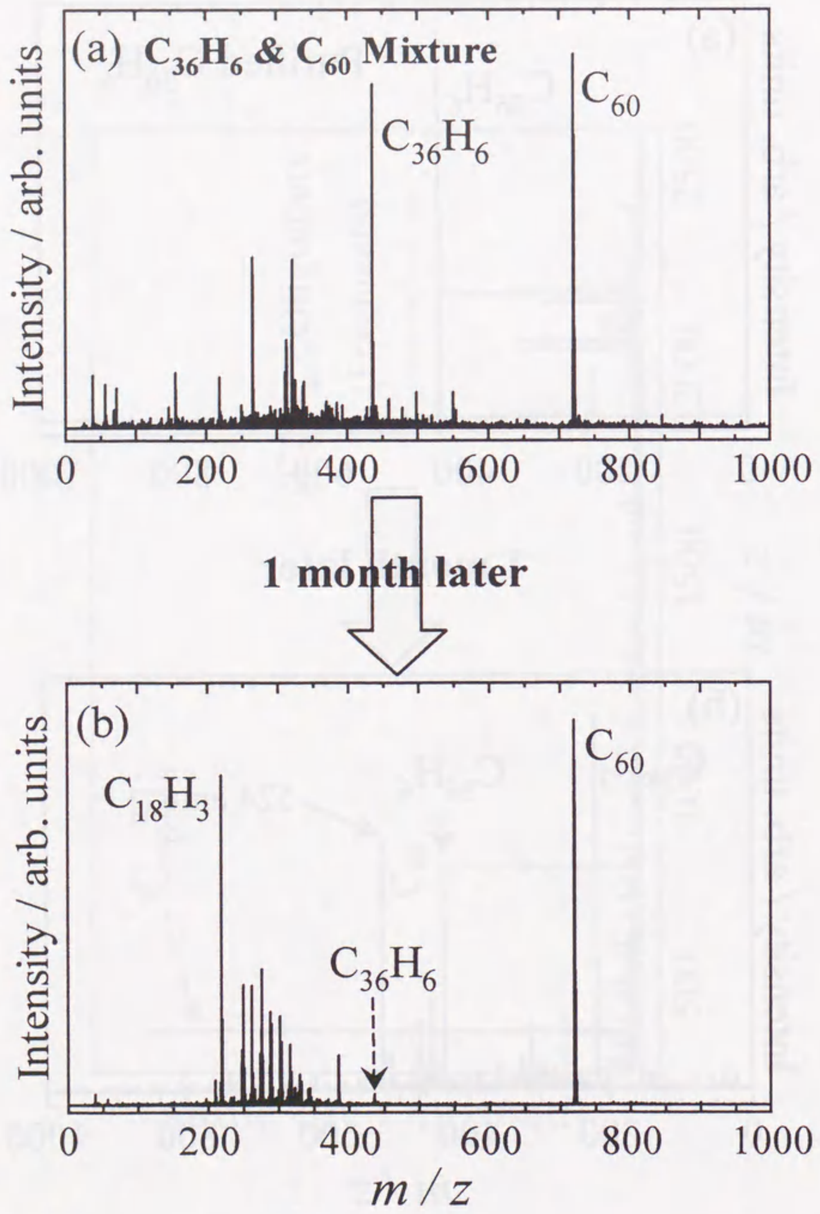

Fig. 2.16

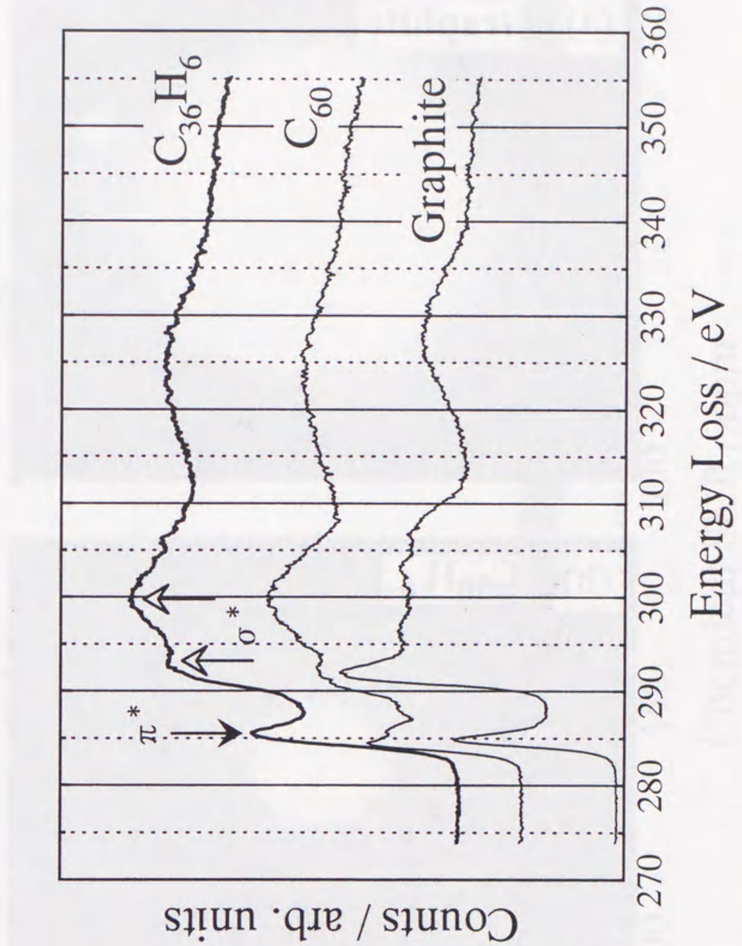

Fig. 2.17

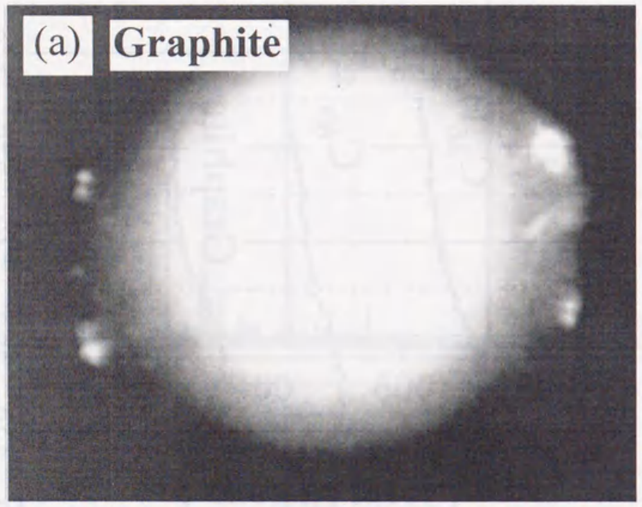

Fig. 2.18

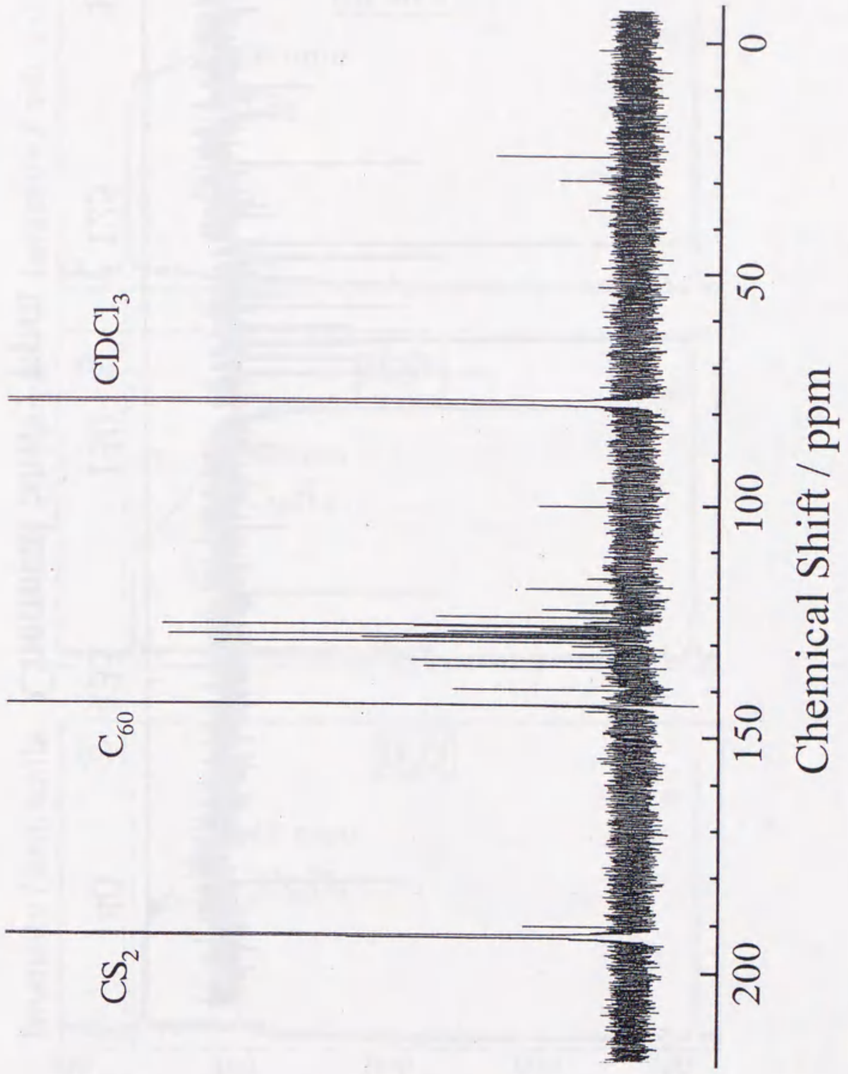

Fig. 2.19

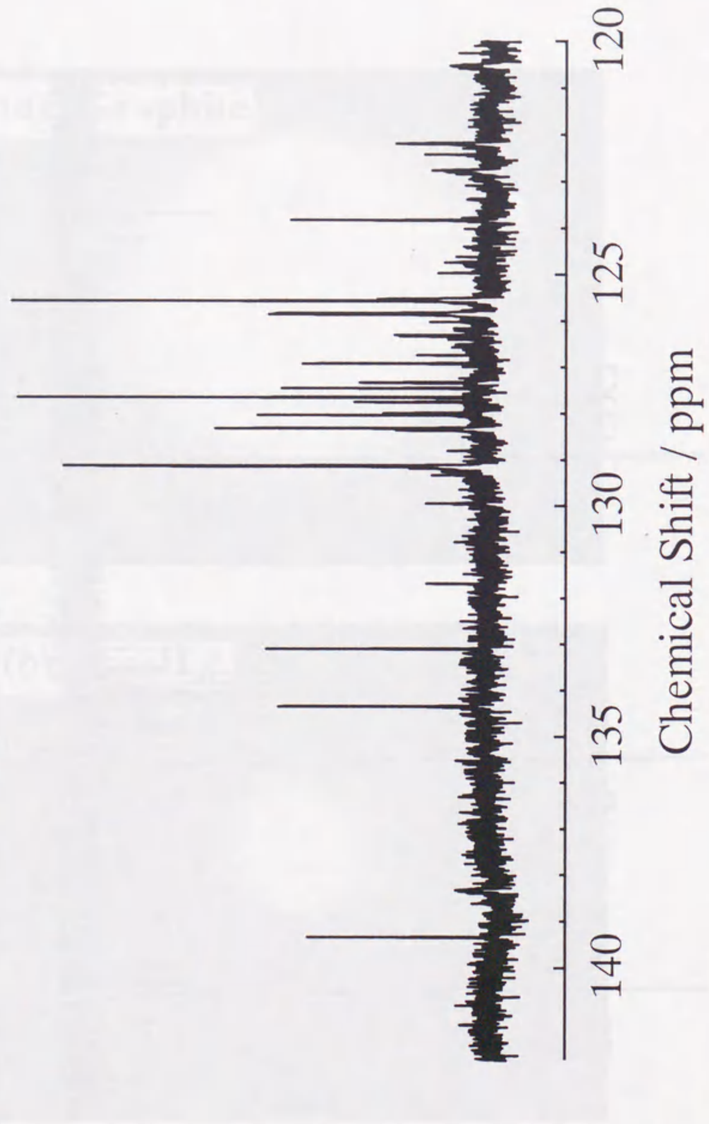

Fig. 2.20

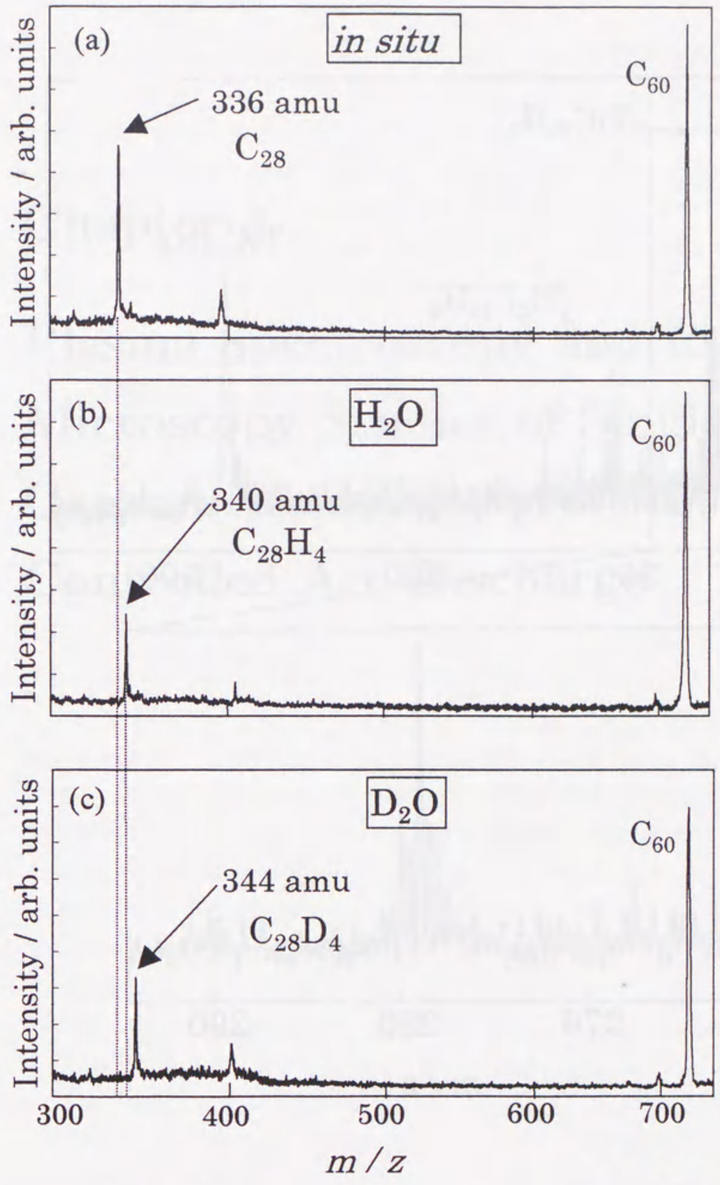

Fig. 2.21

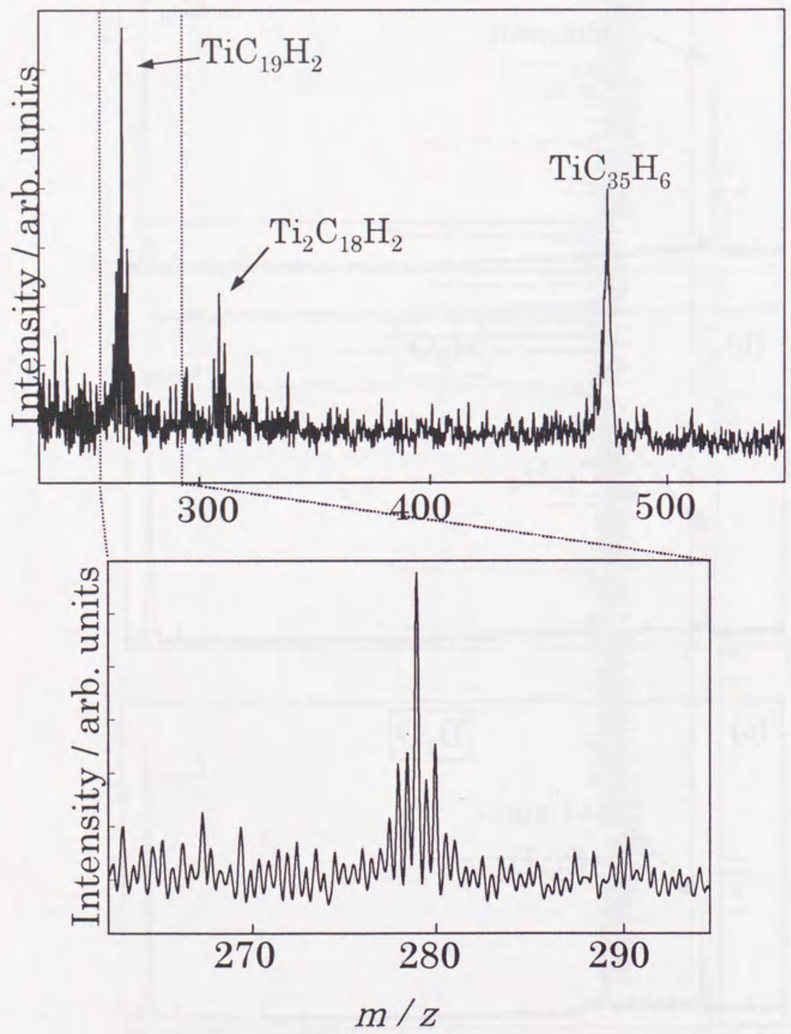

Fig. 2.22

Chapter 3

Plasma Spectroscopy and Electron Microscopy Studies of Single-Wall Carbon Nanotubes (SWNTs) via Controlled Arc-Discharge

3.1 Introduction

Since the rediscovery of carbon tubules [3.1, 3.2] much effort has been devoted to finding efficient methods for their manufacture [3.3–3.5]. However, there are relatively few publication on the elementary processes occurring in the carbon plasma where these structures grow.

Study of the carbon arc plasma is necessary for an understanding of the formation and decay of the reactive carbon species in a high-temperature zone, which can be related to carbon nanostructure synthesis. Optical emission spectroscopy seems to be well suited to such studies. Some rather qualitative results on carbon plasma characteristics during fullerene and nanotube formation have already been published [3.6–3.8].

It is known that carbon nanotube growth in a carbon electric arc occurs in a turbulent environment, which cannot be controlled on the microscopic scale. However, on the macroscopic scale one can envisage various means of influencing the arc discharge, e.g. by the buffer gas, its pressure, power input, electrode gap and electrode diameter, or by varying condensation rates by various methods of cathode cooling [3.4, 3.9, 3.10].

Previous experiments reported by Huczko and co-workers proved that fibrous cathode deposits containing nanotubes grow at a very specific arc current and buffer gas pressure [3.9, 3.11]. They connected this observation with the anisotropic crystallization of graphite at quasi-equilibrium conditions and proper gas concentration and temperature. Both parameters can be easily controlled by helium pressure and arc current.

It is well known that one of the most effective method of producing fullerenes and carbon nanotubes is the vaporization of carbon species via carbon arc plasma in an arc-discharge. In particular, the arc-discharge of graphite electrode doped with a binary metal, such as Ni/Y, is the most effective method for producing single-wall carbon nanotubes (SWNTs).

Arc plasma produced carbon vapors showed to be the source of novel fascinating carbon nanostructures such as fullerenes and nanotubes. The carbon arc co-evaporation of different elements and compounds is also known to produce other various interesting carbon nanomaterials. Some published results, regarding those

syntheses are, however, inconclusive and even contradictory, mostly due to the poor repeatability and flaws in experimental techniques applied. This is the case, for example, of the synthesis of tubules catalyzed by Cu. Also in the production of single-wall carbon nanotubes (SWNTs) different catalysts and/or process parameters are clamed to be the best. When Fe was used, SWNTs grew efficiently in He atmosphere. However, Bethune *et al.* argued that Fe/Ni and Ni/Cu mixture do not catalyze the process while Co does. Iijima and Ichihashi claimed that the synthesis using Fe is successful only when methane is present in the reactor.

This section describes the results of optical emission studies of Fe/C and Co/Ni/C arc plasma [3.12, 3.13] under conditions used to produce fullerenes and SWNTs. The composition of solid products, such as the web-like soot and cathode deposits, in relation to the process operating parameters, is discussed.

3.2 C_2 Emission Spectrometry in Carbon Arc-Discharge

3.2.1 Theory

The C_2 (0, 0) Swan band was simulated for various optical densities and rotational temperatures. Afterwards the integrated band intensity of the normalized intensity distribution was obtained in a function of the volume density, i.e. the product of C_2 (a $^3\Pi_u$, v=0) concentration and optical path length.

3.2.2 Spectrum Simulation

The method of calculation is based on the fundamental formula for the emission coefficient of the rotational components,

$$\varepsilon_{J'J''} = \frac{2\pi he^2}{m}\nu^4 S_{J'J''} f_{mn} g_n q_{v'v''} \exp(-\frac{E'_J}{kT'_r}) Q_r'^{-1} N_{nv'} [Wcm^{-3}sr^{-1}] \quad (3.1)$$

where T'_r is the rotational temperature of excited molecules, $S_{J'J'J'}$ are the calculated H-L factors, $E_{J'}$ are the energies of the rotational levels J' from which the transitions originate (calculated according to Budo [3.14]), ν is the wavenumber, f_{mn} is the electronic absorption oscillator strength equal to 0.033 for Swan system [3.15], $g_n = 6$, $q_{v'v''}$ are the F-C factors equal to 0.722 and 0.333 for 0-0 and 1-1 bands, respectively and $N_{mv'}$ is the population of the vibrational level v' (0 or 1) of the excited d $^3\Pi_g$ electronic state. The calculated spectrum of the individual rotational lines was convoluted with the apparatus function that in the case of the optical system was of Gaussian type with the width equal to 0.03 nm at half peak intensity.

For an optically non-thin plasma the self-absorption has to be taken into account. This effect obviously depends on the absorption coefficient. The coefficient at a given frequency is a function of the volume density of absorbing molecules, real spectral line profile and the degree of overlapping of lines within their profiles. When plasma is non-uniform at high temperature gradients, transition from the observed intensity distributions to the local emission coefficients of the molecular bands is rather a complex task. In this study the calculations were done only for the case of a uniform system. The basic formula connecting the intensity of a rotational line with its emission coefficient for radiation emitted from a uniform plasma column of length L is as follows [3.16],

$$I_{J'J''} = \int \frac{\varepsilon_{J'J''}(\nu)L}{\kappa(\nu)L}(1 - e^{-\kappa(\nu)L})d\nu [Wcm^{-2}sr^{-1}] \quad (3.2)$$

where $\varepsilon_{J'J''}(\nu)$ and $\kappa(\nu)$ are the spectral line emission and absorption coefficients, respectively. The total spectral absorption coefficient includes contributions from all possible transitions,

$$\kappa(\nu) = \sum \kappa_{J'J''}(\nu) \quad (3.3)$$

Because of high gas temperature and moderate carbon species pressure, the calculations were performed assuming the Doppler broadening of the emission and absorption lines according to

$$\varepsilon(\text{or } \kappa)_{J'J''}(\nu) = \varepsilon(\text{or } \kappa)^0_{J'J''} e^{-4\ln 2(\frac{\nu - \nu_{J'J''}}{\Delta\nu_D})^2} \quad (3.4)$$

where $\varepsilon(\text{or } \kappa)^0_{J'J''}$ is the peak emission (absorption) coefficient and $\Delta\nu_D$ is the Doppler width at half peak intensity. Assuming a statistical equilibrium between the rotational and translational degrees of freedom the Doppler width can be expressed by T'_r and T''_r for the emission and absorption lines, respectively. Two different rotational temperatures reflect the situation when radiation from hot plasma zone is self-absorbed in the cooler region surrounding the emitting zone. The absorption coefficients equation 3.2 are expressed by the concentration of C_2 radicals in the ground $d^3\Pi_u$ electronic state ($N_{mv''}$),

$$\kappa_{J'J''} = \frac{\pi e^2}{mc^2} f_{mn} q_{v'v''} S_{J'J''} \exp\left(-\frac{E''_J}{kT''_r}\right) Q_r''^{-1} N_{mv''} [cm^{-2}] \quad (3.5)$$

The equations from equations 3.1 $\sim$ 3.5 were used for the calculation of the spectra of individual rotational lines in a function of the volume density, $N(a^3\Pi_u) \times L$, and rotational temperatures T'_r and T''_r. The examples of the spectral intensity distributions (normalized relatively to the P(0,0) head band) are shown in Fig. 3.3.

3.2.3 Method of $C_2(a\ ^3\Pi_u,\ v=0)$ Concentration Determination

The P(0,0) head band is the most sensitive part of the spectrum to the self-absorption because it contains many lines overlapping within their real profiles. As a result, with the volume density increasing there is a significant increase in the intensities of the resolved rotational components relative to the P(0,0) head band. This is clearly seen comparing the traces (a) and (b) in Fig. 3.3. It can be quantitatively expressed by the integrated intensity of the normalized (0,0) band in a function of the volume density. The integration was made between P(0,0) and P(1,1) head bands. Such dependence is illustrated as curves (called growth curves) [3.17]. The integrated band intensities were expressed in arbitrary units related to the bands not disturbed by self-absorption at given rotational temperatures. Thus, the proposed method of the determination of density can be directly obtained from the growth curves after the experimental determinations of the integrated emission intensities from normalized band intensity distributions. The knowledge of the absorbing column length (L) leads directly to the average radical concentration value; in the case of the axial symmetry it is also possible to obtain radial concentration distributions. It follows that self-absorption becomes significant at volume densities 10^{15}cm^{-2}. Hence, the intensity distribution in Fig. 3.3 corresponds to the optically thin plasma and resembles the spectrum computed directly from the emission coefficients (equation 3.1).When the integrated intensity in absolute units is considered (non-normalized spectrum), then one can see the opposite dependence on the volume density.

As the intensity distributions had already been obtained, it was of interest to inquire whether the rotational temperature could be directly determined from the Boltzmann plots $\ln(\frac{I}{S\nu^4})$ vs. E. Such a procedure was applied to the simulated spectra using lines with J' between 26 and 30, and 39 and 45 of the P(0,0) branch [3.18]. We consider that the errors of the temperature calculations as a function of the volume density. The T_r'(calc) denotes the temperature calculated from the Boltzmann plots. As expected at low volume densities T_r'(calc) is close to T_r'. The temperature errors are also small when $T_r' \approx T_r''$ (around 5,000 K) for low and high volume densities. Significant errors can be made when $T_r' > T_r''$ when the calculated values can even be 2,000 K overestimated.

3.3 Experimental

3.3.1 The Controlled Arc-Discharge System

The arc-discharge was performed by the conventional Krätschmer-Huffman technique. A schematic diagram of the controlled arc-discharge system, including the carbon arc plasma generator, the optical emission diagnostic instrumentation and electrode gap stabilization system, is presented in Fig. 3.2.

In the present experiment, the metal-doped graphite composite rods (Fe/C (0.6 atomic %, ϕ 5 mm $\times$ 150 mm) and Ni/Co/C (0.6 at.%/0.6 at.%, 5 $\times$ 5 $\times$ 150 mm): Toyo Tanso Co. Ltd.) were used for the anode, and a graphite 6 mm in diameter for the cathode was used. The electrodes are attached to linear, feedthrough, stainless-steel drives using copper holders, and connected to the leads from a DC power supply. The drives themselves are coupled to $x-y-z$ translation stages. The electrode assemblies were driven in a horizontal (z) direction by variable-speed screw drives. The feed rate of the translation stages was controlled so the desired electrode gap was maintained. A bellow stage provided for the fine adjustment of electrodes in the vertical ($x-y$) plane. The mutual configuration of electrodes was also monitored through the viewport with a charge coupled device image camera and displayed onto the calibrated monitor screen so that the gap distance could be accurately determined.

The gap and space position of the electrodes was controlled by the side branch of the diagnostic optical system by means of a semitransparent mirror. The set of lens projects the magnified images of the electrodes onto the linear photodetector array in front of which a cyrindical lens was placed to compress the image perpendicularly to the array. A magnification of between two and four timed, along the electrodes, could be fixed prior to the start of the experiment.

The linear photodetector array was made of 11 silicon epiplanar PIN photodiodes with a 0.9 mm element pitch. Photodetector currents are amplified and converted to voltage signals. These signals are compared with the regulated reference voltage level. At the output of the comparators the digital transistor-transistor logic (TTL) level, signals inform whether particular photodiodes are illuminated by the light coming from the electrodes. One should mention that the total electrode radiation exceeds several times the plasma radiation. Thus the plasma radiation is considered as the background.

The monitoring block includes 11 light emitting diodes coupled with drivers. It allows for a preliminary positioning of the electrodes, sensitivity adjustment of the photodetector amplifier, and direct observation oh the electrode position during the process.

The block of logic control is composed of TTL integrated circuits and programmable logic device. It maintains the direction and speed motion of the electrodes. The control unit enables the setting of the array switches. The real distance between the electrode results from the optical magnification of the electrode image in the plane of the photodetector array.

The applied system ensured maintenance of a desired distance with the accuracy of $\pm$ 0.2 mm.

3.3.2 The Arcing Procedure

The arc power supply consisted of a 150 V rotor welding machine and a suitable ballast resister. The plasma id usually ignited by the contact-arc technique. When the anode is advanced until it touches the cathode, the temperature of the electrode material at the location is elevated to the point of instantaneous evaporation that ignites the plasma. Thus the arc is struck and electrodes are separated to maintain a desired gap. However, the overheating of the contact point often results uneven erosion of the electrodes and that can cause prolonged plasma instabilities. Also, the initial growth of the cathode deposit can be disturbed. In a more elaborate method, a wire is inserted through the reactor shell and through the cathode until it touches the anode and the arc is ignited. To overcome those drawbacks we initiated the arc discharge by superimposing the high voltage (600 V), glow discharge on the electrodes at a preadjusted gap.

During the burn-out process the anode was steadily consumed. Carbon deposit containing multi-wall carbon nanotubes (MWNTs) grew on the cathode while the resulting soot containing fullerenes and single-wall carbon nanotubes (SWNTs) was condensed on the reactor's walls.

3.4 Results and Discussion

3.4.1 Spectral Diagnostic of the Interelectrode Gap

Table 1 contains the parameters of the performed tests and the final content of fullerene in the collect soot. In the both case ((a)Fe/C and (b)Ni/Co/C), the sublimation rate of the anode generally increases at lower pressures, and it decreases at higher pressures. It is seen that the presence of the metals in the anode changes increases required power for the effective sublimation process. At higher pressures in order to have approximately similar sublimation rate the input power should be much higher in respect to the anode made of pure graphite [3.19]. It is probably connected with higher electrical conductivity of the graphite mixed with the metals and decreased diffusion of the vaporized carbon under higher buffer gas pressure. At lower pressure the presence of Fe or Co/Ni significantly decreases yield of C_{60} formation process, while at higher pressures the C_{60} yield does not depend on metal content.

The radial temperature and column density of C_2 (a $^3\Pi_u$, v=0) distribution obtained for the case of using a Ni/Co/C composite electrode are shown in Figs. 3.4 and 3.5, respectively. In the both figures three vertical dotted line indicate the center of electrode gap (0 mm), the position of the anode edge (+ 0.5 mm) and the cathode edge (- 0.5 mm). The temperature curve represent the values obtained from the Boltzman plot method applied to the sufficiently well resolved rotational component of the C_2 (516.5 nm, 0-0) band. As shown in Fig. 3.4 the feature of temperature curves of a high input power (117 A) and a low input-power (85 A) almost shows the same tendency to have a minimum at -1.5 mm and a maximum at 1.0 mm. Taking into account some errors due to the self-absorption effects [3.17] one can say that the temperatures for different conditions (gas pressure and anode composition) are very close each other (Figs. 3.4 and 3.6).

In Figs. 3.5 and 3.7 there are also the temperature values that characterize excitation degree of the Fe atoms. They were calculated on the basis of the relative intensities of a group of the UV atomic lines located in the spectral range between 323 and 328 nm. These values are very close to the rotational temperatures suggesting existence of a partial local thermodynamic equilibrium.

The column densities were derived from the fitting method of calculated to the

experimental spectra [3.13]. The C_2 column density decreases rapidly towards the arc edge that may suggest that the coalescence process occurs so close to the arc.

Despite of the similar sublimation rates there is a distinct difference in column density distributions. In the case of Fe/C electrode always a trend of lower C_2 density was observed, in the range of Fe concentration used. One has to admit, however, that because of a small arc gap ($\approx$ 1 mm), the positioning of the plasma cross-section of the optical axis could not be achieved with accuracy better than $\pm$ 0.2 mm. It was shown earlier [3.13] that C_2 density rapidly decreases from the anode to cathode surface, therefore, even a small horizontal displacement (tenths of millimeter) may return plasma column density belong to different arc cross-sections. The spectroscopic measurements performed under conditions of lower pressure discharge resulted in similar radial temperature distributions but a few times lower C_2 column densities.

Obviously, partial pressures of He in the chamber and of the carbon species in the arc plasma influence the mechanism and kinetics of the carbon vapor nucleation process. It is worth noting that minima in the temperature distributions (a few hundred degrees) (Figs. 3.4 and 3.6) on the axis are observed. This may be related to movement of the arc spot around the cathode edge. It is also expected that the minima in temperature distribution are related to the effective production of high density SWNTs, since minima were not observed in experiments using pure graphite [3.19, 3.20] and B-doped graphite [3.21].

3.4.2 SEM Analyses

The use of the homogeneous graphite/metal anode changes mechanistic properties and a structure of produced soot. At presence of Fe or Ni/Co the soot seems to be more compact and much less dusty than the one resulting from the pure graphite. Beside, under conditions of the high pressure arc discharge, a part of products appears in a form of a web-like material, especially in the case of Ni/Co/C anode. The soot collected from the arc chamber walls and the web-like product were analyzed using scanning electron microscope (SEM; Hitachi S-900).

Figures 3.8 (a) and (b) show SEM images of "sheet-like soot" deposited on the chamber wall and "web-like soot" in the chamber produced by low current arc-discharge (500 Torr, 85 A) with a Ni/Co-doped graphite anode. The production condition corresponds to the 85 A curve in Fig. 3.4 and in Fig. 3.5. It is clear that

the web-like soot contains many bundles of SWNTs, and a few byproducts, such as metal and carbon nanoparticles (Fig. 3.8(b)). The sheet-like soot also contains many bundles of SWNTs; however, there are many other particles in the soot, which would make it difficult to purify the SWNTs (Fig. 3.8(a)). Low current conditions using controlled arc-discharge produced a much higher density of SWNTs than a conventional arc-discharge. This suggests that the stability of the carbon arc plasma affects the effective growth of high density and high purity SWNTs.

Figures 3.9 show a SEM image of the soot produced by high current arc-discharge (500 Torr, 117 A) with a Ni/Co-doped graphite anode (Fig. 3.9(a)); the area in the white rectangle in (a) is magnified in Fig. 3.9(b). With high currents, web-like soot was not produced and sheet-like soot was deposited on the chamber wall. In the sheet-like soot, more thick carbon tubular materials were produced than SWNTs, and the soot contained carbon nanoparticles. The tubular materials were about 80 nm thick. It is likely that during the formation of SWNTs, an excess supply of carbon species halted the growth of SWNTs and preferentially formed thicker tubulites. The column density distribution curve (Fig. 3.5) shows that 117 A supplied many more carbon species to the arc plasma than 85 A.

Figure 3.10 shows an SEM image of the "web-like soot" produced by arc-discharge (280 Torr, 70 A) with a Ni/Co-doped graphite anode. With low current and low pressure, a trace of web-like soot was produced in the chamber. Traces of SWNTs and thicker tubulites were observed in the soot. The arc plasma contain excess carbon species at high currents and pressures, because the sublimation rate of the anode generally increases as the pressure decreases.

Figure 3.11 shows an SEM image of "web-like soot" produced by arc-discharge (600 Torr, 76 A) with a Fe-doped graphite anode. It is clear that a trace of SWNTs are contained among carbon nanoparticles. As mentioned in the section of *general introduction* it has been reported that in the case of using Fe/C anode SWNTs were produced only under the condition of Ar/CH_4 mixture working gas [3.22]. In the present experiment, SWNTs were produced in the web-like soot in spite of using only He gas. The result also suggests that the stability of the carbon arc plasma effects on the effective production of SWNTs with Fe-doped graphite more than with Co/Ni-doped graphite..

In this experiment it is worth mentioning here that the soot produced in the case

of high current of Fe-doped graphite seemed to be similar to that of pure graphite. The most interesting feature of the soot is connected with the presence of elongated carbon nanostructures. The nanotubes are among them. In the case of pure carbon electrodes the nanostructures could not be spot in the chamber soot. In the case of Fe/C carbon nanotubules were contained mostly in the webs formed on the cathode (Fig. 3.11). In the case of Co/Ni/C electrodes the nanotubes were found both in the chamber soot as well as in the web-like soot. However, significant amount of the bundles of 6 nm nanotubes thick were found in the webs only Fig. 3.8. The chamber soot contained high density of thin nanotubes together with amorphous carbon and catalyst particles (Fig. 3.9).

Summary

Optical emission studies and electron microscopy studies of Fe/C and Co/Ni/C arc plasma during the formation of fullerenes or SWNTs were performed with the controlled arc-discharge system .

The composition of solid products such as web-like soot and cathode deposits, was found to depend on operating parameters such as working gas pressure and input power (current). Though it has been known that SWNTs were produced only under the condition of Ar/CH_4 mixture working gas in the case of Fe/C carbon, SWNTs were contained in the webs formed on the cathode . In the case of Co/Ni/C electrodes the nanotubes were found both in the chamber soot as well as in the web-like soot.

It is worth to note that minima in temperature distributions (a few hundred degrees) on the axis are observed. It is expected that the minima in temperature distribution is related to the effective production of high density SWNTs.

Bibliography

[3.1] R. Bacon, *J. Appl. Phys.* **31**, 283 (1960).

[3.2] S. Iijima, *Nature* **354**, 56 (1991).

[3.3] L. Lou, P. Nordlander, and R. E. Smalley, *Phys. Rev. B* **52**, 1429 (1995).

[3.4] T. W. Ebbesen, in *Progress in Fullerene Research*, edited by H. Kuzmany (World Scientific, , 1994), p. 116.

[3.5] P. Byszewski, E. Kowalska, K. Ukalski, R. Diduszko, E. Czerwosz, and E. Mizera, *Mol. Phys. Rep.* **12**, 65 (1995).

[3.6] D. V. Afanas'ev, I. O. Blinov, A. A. Bogdanov, G. A. Dyuzhev, V. I. Karataev, and A. A. Kruglikov, *Mol. Mat.* **5**, 105 (1994).

[3.7] T. Belz, H. Wrener, F. Zemlin, U. Klengler, M. Wesemman, B. Tesche, B. Zeitler, A. Reller, and R. Schlögl, *Angew. Chem. Ed. Eng.* **33**, 1866 (1994).

[3.8] A. Wkisaka, J. J. Gaumet, Y. Shimizu, H. Sato, and K. Tokumaru, *J. Chem. Soc. Faraday Trans.* **89**, 1001 (1993).

[3.9] P. Byszewski, K. Ukalski, M. Baran, P. Dłużewski, and M. Kozłowski, *Acta Phys. Pol.* **A87**, 885 (1995).

[3.10] X. K. Wang, R. P. H. Chang, A. Patashinski, and J. B. Keterson, *J. Mater. Res.* **9**, 1578 (1994).

[3.11] A. Huczko, H. Lange, and P. Byszewski, *XXII Int. Conf. Phenom. Ion. Gas.* **1**, 77 (1995).

[3.12] A. Huczko, H. Lange, P. Byszewski, A. Koshio, and H. Shinohara, in *Electronic Properties of Novel Materials-Science and Technology of Molecular Nanostructures: Proceedings of the XIIIth International Winterschool on Electric Properties of Novel Materials*, edited by M. Mehring H. Kuzmany, J. Fink and S. Roth (World Scientific, Kirchberg, 1999), p. 258.

[3.13] H. Lange, A. Huczko, H. Shinohara, A. Koshio, and P. Byszewski, in *Symposium Proceedings of 14th International Symposium on Plasma Chemistry*, edited by M. Konrád M. Hrabovský and V. Kopecký (Institute of Plasma Physics AS CR, Prague, 1999), Vol. IV, p. 2241.

[3.14] A. Budo, *Z. Physik* **96**, 219 (1935).

[3.15] L. L. Danylewych and R. W. Nicholls, *Proc. R. Soc. Lond.* **339**, 197 (1974).

[3.16] H. Lange, *Pol. J. Chem* **55**, 897 (1981).

[3.17] H. Lange, A. Huczko, and P. Byszewski, *Spectrosc. Lett.* **29**, 1215 (1996).

[3.18] A. Huczko, H. Lange, A. Resztak, and P. Byszewski, *High Temp. Chem. Processes* **4**, 125 (1995).

[3.19] A. Huczko, H. Lange, P. Byszewski, M. Poplawska, and A. Starski, *J. Phys. Chem. A* **101**, 1267 (1997).

[3.20] P. Byszewski, H. Lange, A. Huczko, and J. F. Behnke, *J. Phys. Chem. Solids* **58**, 1679 (1997).

[3.21] H. Lange, A. Huczko, P. Byszewski, E. Mizera, and H. Shinohara, *Chem. Phys. Lett.* **289**, 174 (1998).

[3.22] S. Iijima and T. Ichihashi, *Nature* **363**, 603 (1993).

List of Figures

Fig. 3.11 An SEM image of "web-like soot" produced by arc discharge (600 Torr, 76 A) with a Fe-doped graphite electrode.

Table 1

(a) Fe/C

Expt. No.	Current (A)	Voltage (V)	Duration Time (min.)	Sublimation Rate (mg/s)	Initial Pressure (Torr)	Experimental Pressure (Torr)	Fullerene Content (wt.%)
1	78.8	24.5	11	4.0	34	62.5	4.4
2	70.6	28.0	14	2.9	200	295	4.5
3	65.0	30.5	20	2.2	406	590	6.4
4	76.3	32.0	16	2.6	390	600	7.1
5	66.3	23.5	12	3.5	35	60	5.5
6	72.5	24.5	7	5.6	110	180	1.8
7	78.8	31.5	16	3.0	280	470	6.7
8	68.8	23.0	8	3.9	388	520	-

(b) Ni/Co/C

Expt. No.	Current (A)	Voltage (V)	Duration Time (min.)	Sublimation Rate (mg/s)	Initial Pressure (Torr)	Experimental Pressure (Torr)	Fullerene Content (wt.%)
11	65	21.0	7.5	8.1	35	60	4.2
22	70	28.5	13	3.6	190	280	1.0
33	95	34.0	16	3.3	290	500	3.7
314	64	22.5	-	4.2	-	70	13.5
315	96	28.5	-	6.1	-	380	6.0
316	116	36.5	-	4.8	-	740	2.6

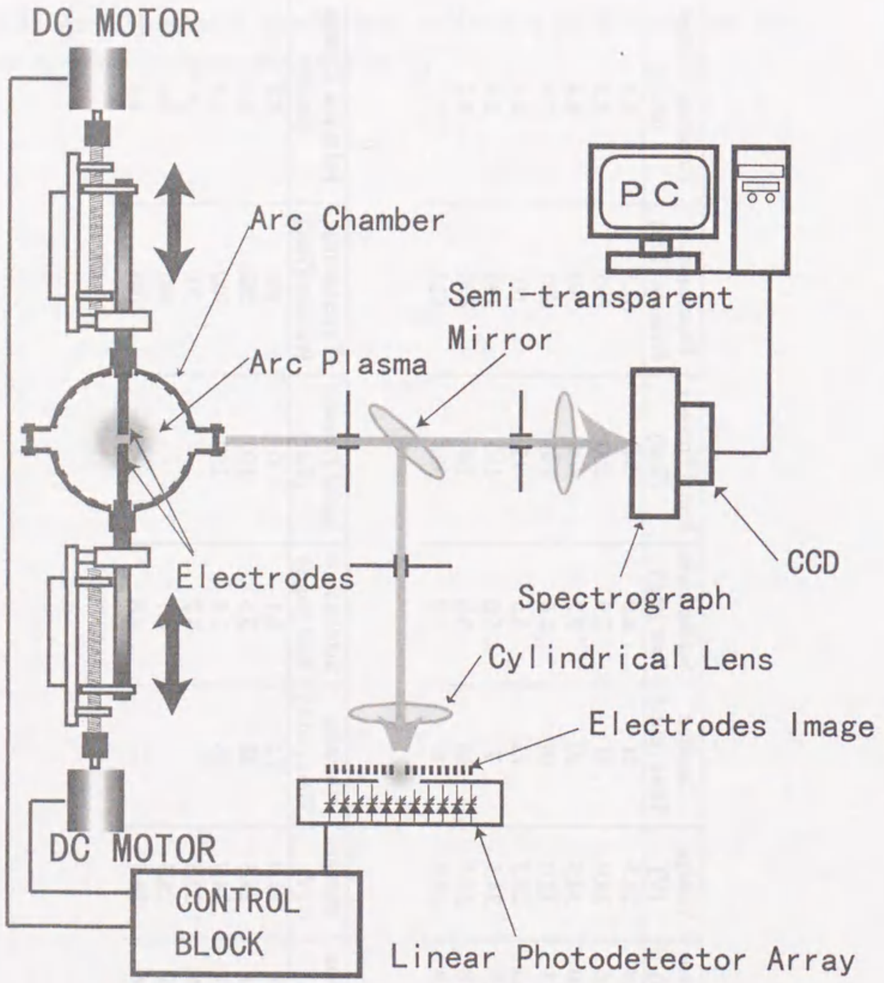
DC MOTOR
PC
Arc Chamber
Semi-transparent
Mirror
Arc Plasma
Electrodes
Spectrograph
CCD
Cylindrical Lens
Electrodes Image
DC MOTOR
CONTROL
BLOCK
Linear Photodetector Array

Fig. 3.2

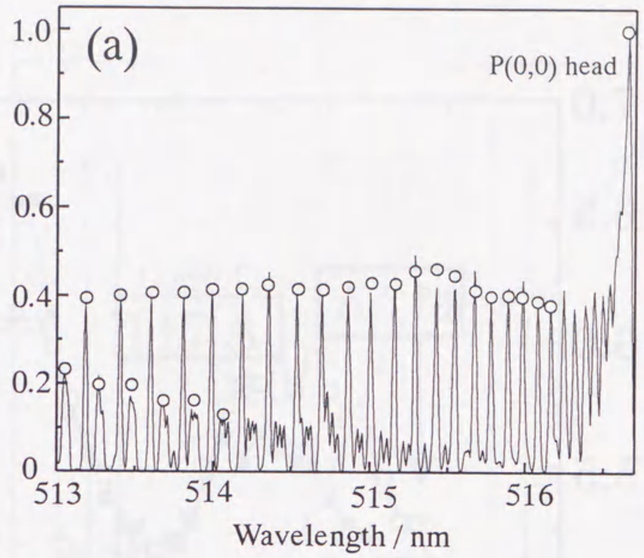
(a)
P(0,0) head
1.0
0.8
0.6
0.4
0.2
0
513
514
515
516
Wavelength / nm

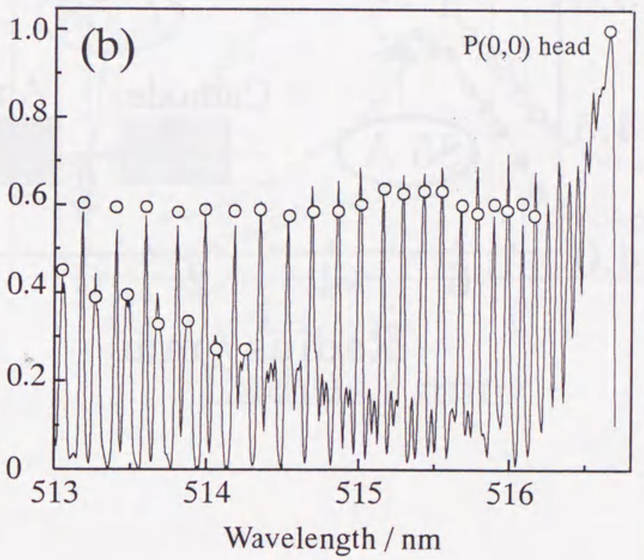
(b)
P(0,0) head
1.0
0.8
0.6
0.4
0.2
0
513
514
515
516
Wavelength / nm

Fig. 3.3

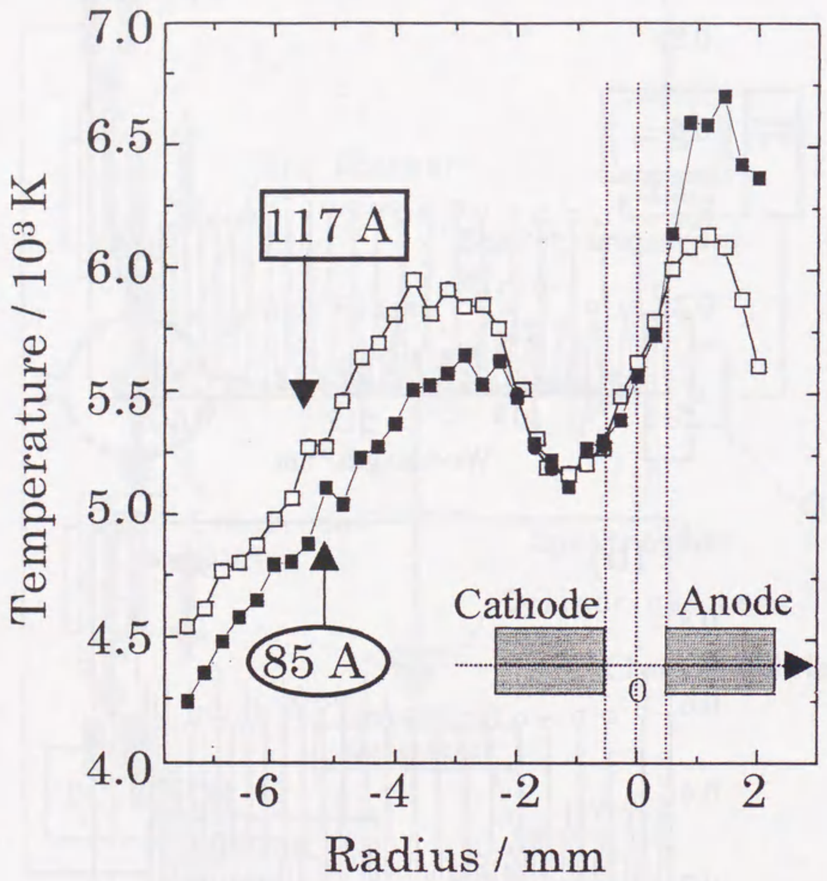
Temperature / 10³ K
7.0
6.5
6.0
5.5
5.0
4.5
4.0
117 A
85 A
Cathode
Anode
0
-6
-4
-2
0
2
Radius / mm

Fig. 3.4

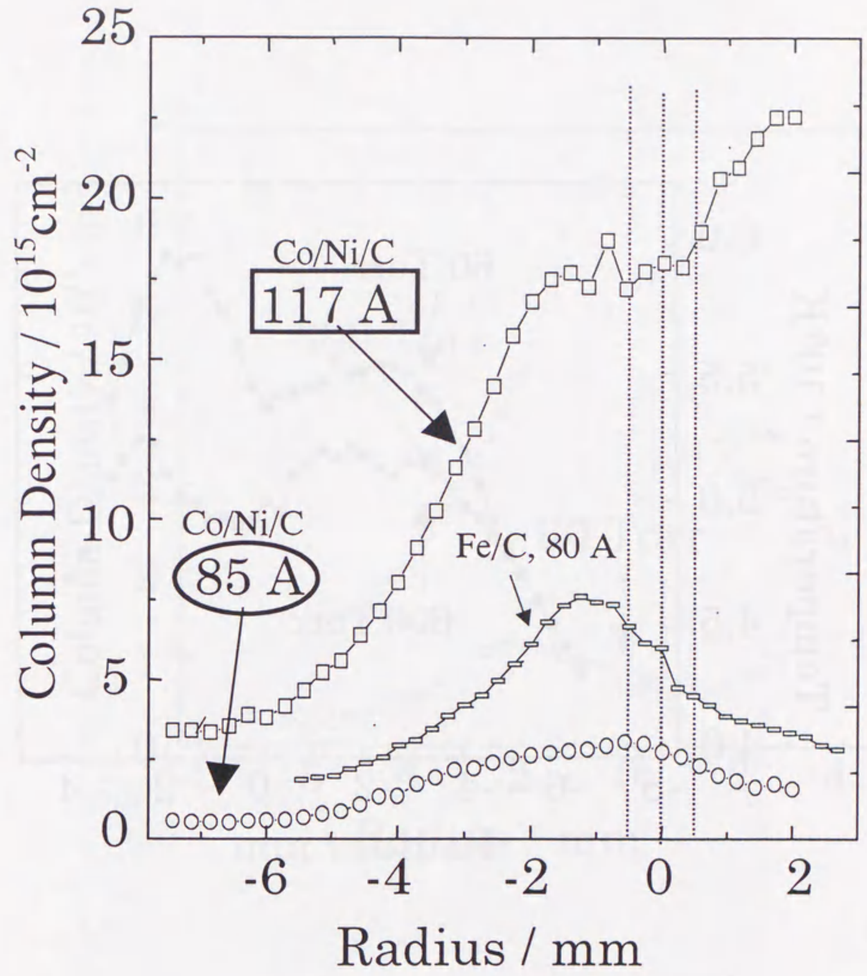
Column Density / 10¹⁵cm⁻²
25
20
15
10
5
0
Co/Ni/C
117 A
Co/Ni/C
85 A
Fe/C, 80 A
-6
-4
-2
0
2
Radius / mm

Fig. 3.5

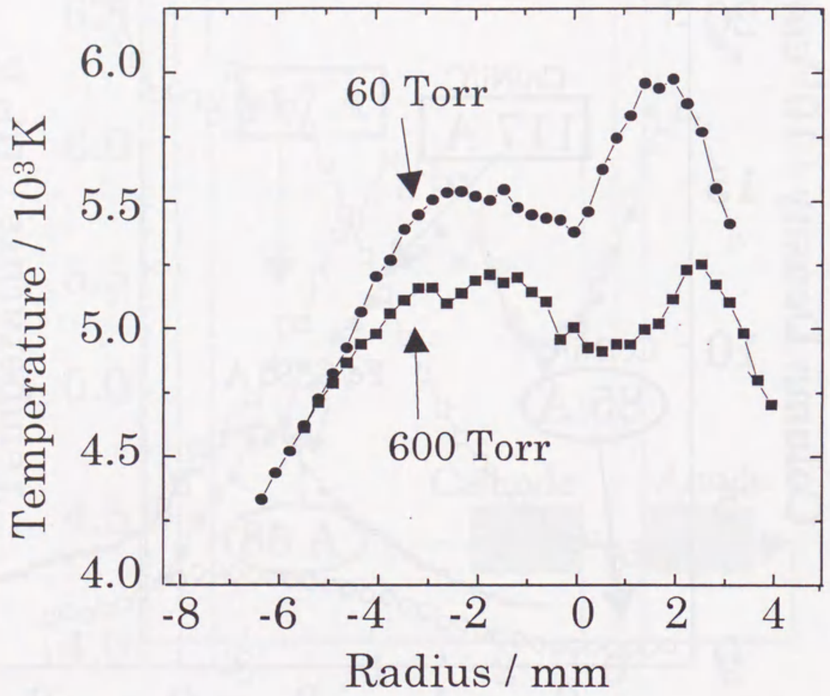
Temperature / 10^3 K
6.0
5.5
5.0
4.5
4.0
60 Torr
600 Torr
-8
-6
-4
-2
0
2
4
Radius / mm

Fig. 3.6

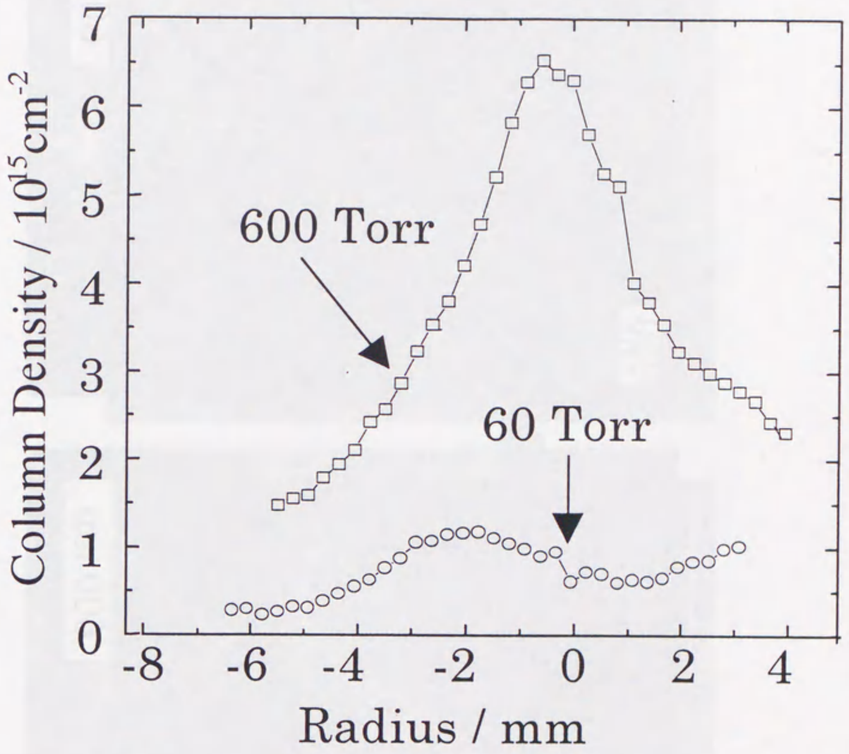
Column Density / 10^{15}cm^{-2}
7
6
5
4
3
2
1
0
600 Torr
60 Torr
-8
-6
-4
-2
0
2
4
Radius / mm

Fig. 3.7

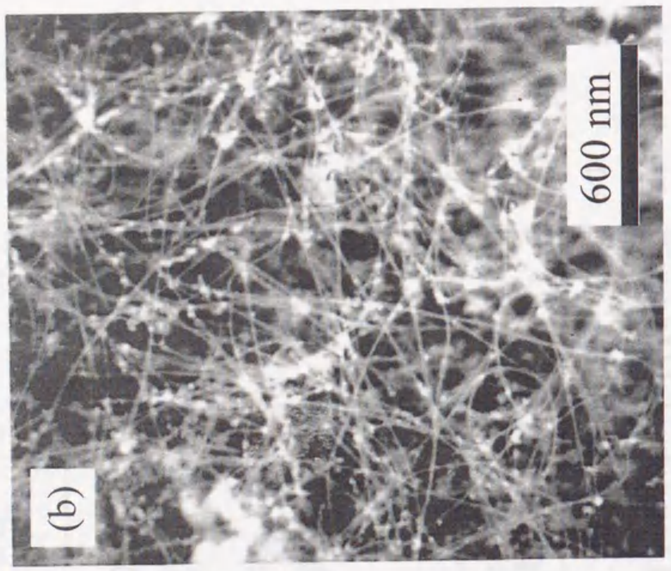

Fig. 3.8

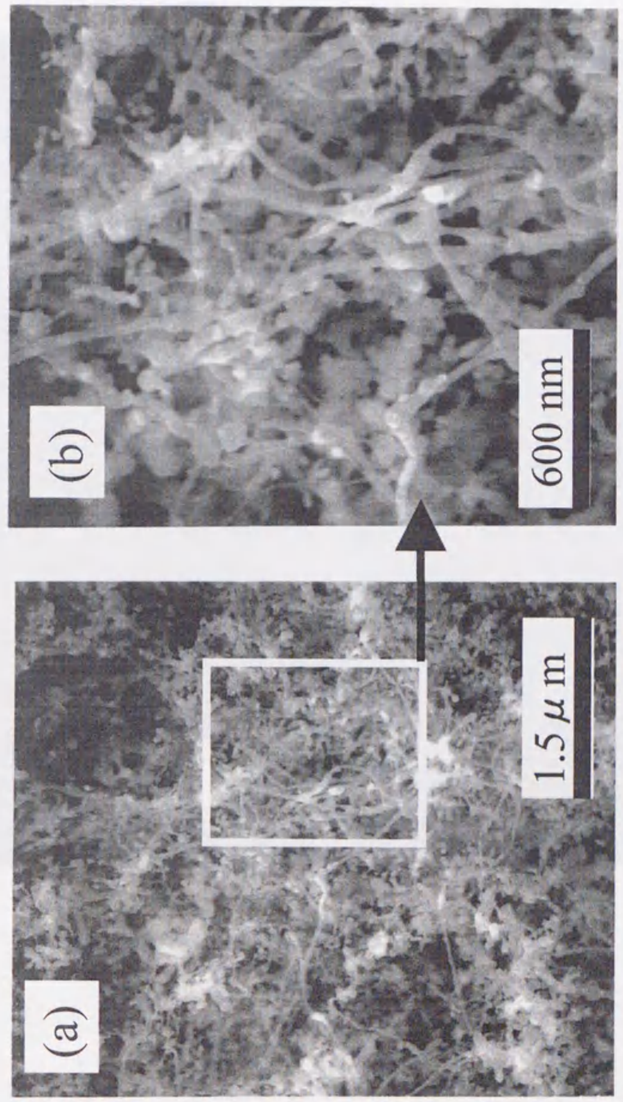

Fig. 3.9

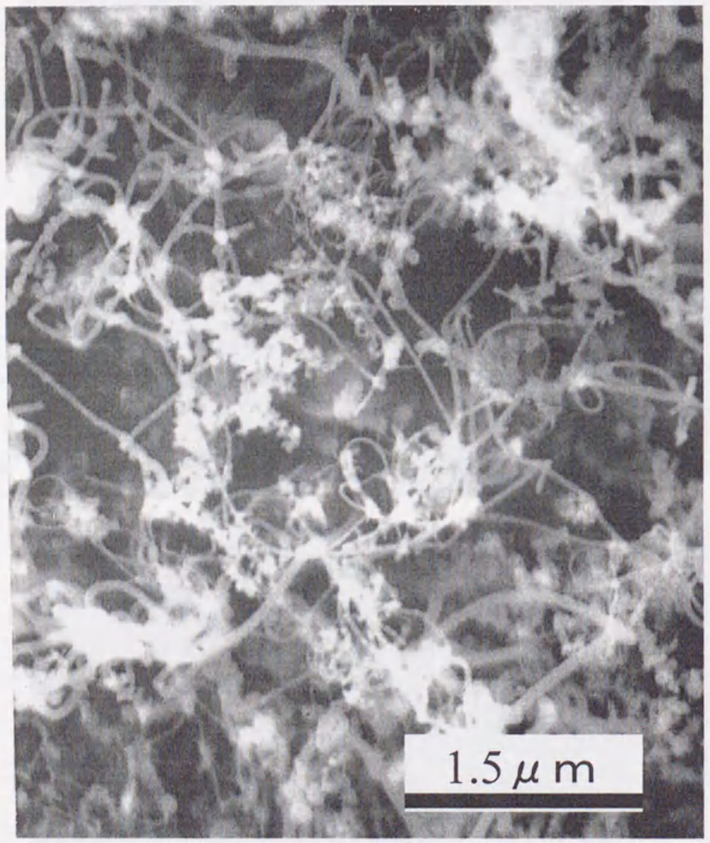

Fig. 3.10

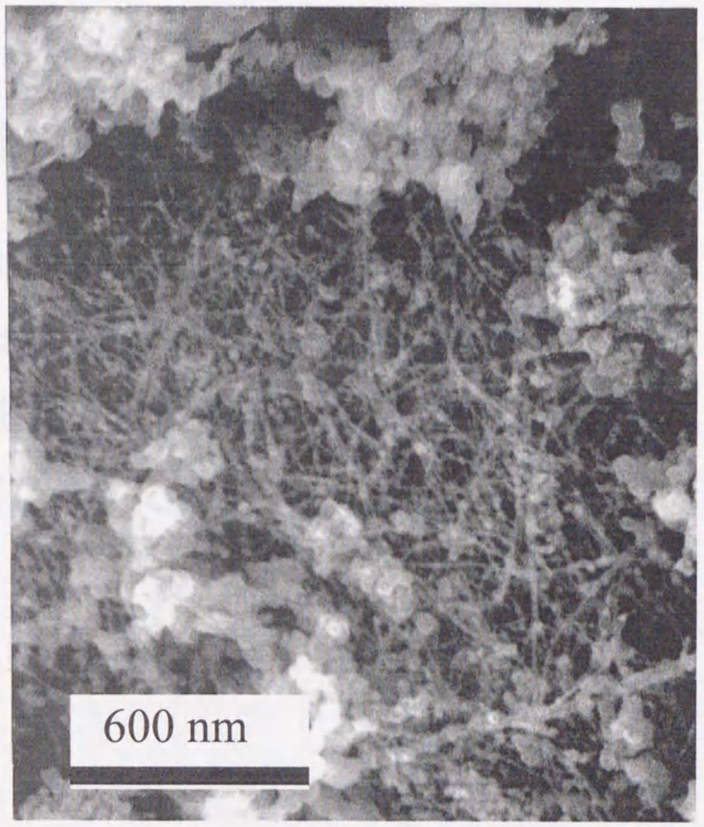

Fig. 3.11

Chapter 4

Production of Carbon Nanotubulites and the Characterization by Electron Microscopy

4.1 Introduction

Arc-discharge and high-temperature laser-vaporization are classified in the gas vaporization method [4.1]. The gas vaporization method, which was vaporization of raw starting materials in an atmosphere of a novel gas, has been employed as one of methods to produce ultrafine particles for a long time. The methods include various types of vaporization such as resistance heating, plasma flame heating and arc discharge heating. In particular, since the bulk-production method of fullerenes was reported by Krätschmer *et al.* [4.2], the DC arc-discharge method has been well known as one of the most effective production methods of fullerenes (and recently carbon nanotubes) in large quantities. We know that the DC arc-discharge of a graphite anode containing various metals is a production method of metallofullerenes [4.3] and single-wall carbon nanotubes (SWNTs) [4.4]. In particular SWNTs are effectively produced by DC arc-discharge of graphite anode containing binary metals, such as cobalt/nickel (Co/Ni) and yttrium/nickel (Y/Ni).

Carbon nanotubes are produced by vaporization of pure graphite rods or graphite rods containing metals. In particular, SWNTs are produced by DC arc-discharge or laser-vaporization of composite graphite rods containing transition metals in an atmosphere of He or Ar. However, many impurities, such as amorphous carbon particles, metal particles, and carbon nanocapsules, are produced together with the carbon nanotubes. Although some methods for purifying SWNTs have been reported [4.5–4.9], high-quality carbon nanotubes have to be produced to study the detailed bulk properties of carbon nanotubes and to develop applications for their use.

In general, fullerenes and SWNTs grow in an atmosphere of Novel gases, such as helium or argon. That is to say, only the graphite rods supply carbon species. It has been reported when hydrocarbon gases, such as methane and acetylene, are mixed with the buffer gases, the production of fullerenes drastically reduced. There is one exception; SWNTs can be produced by the DC arc-discharge of a graphite anode containing iron using a mixture of methane and argon [4.10, 4.11]. It has been also reported that hydrogen gas enhances the production of multi-wall carbon nanotubes (MWNTs), in which "walls" are stuffed into the center of the tube [4.12]. Nagatsu *et al.* reported producing carbon clusters using plasma chemical vapor deposition in He/CH_4 glow discharge [4.13], although they have not examined carbon nanotubulites

or nanotubes. Thus far, the effects of hydrocarbons or hydrogen on the mechanism of nanotube growth have not been investigated satisfactorily. The mechanisms for growing carbon nanotubes have also not been elucidated experimentally, and MWNTs and SWNTs could be produced by different methods.

The enhancement of production of high-quality carbon nanotubes due to existence of hydrocarbons was not observed. However, I have found that carbon tubular materials (carbon nanotubulites) were produced during production of carbon nanotubes by arc-discharge or laser-vaporization of a metal-doped graphite rod (or 100% metal rod) in an atmosphere of hydrocarbon gases such as methane. In this section the observation and the characterization of novel carbon nanotubulites by electron microscopes are described.

4.2 Experimental

The production of carbon nanotubulites was carried out by a home-made DC arc-discharge chamber with a fixed cathode made of a pure graphite rod (ϕ15 mm) and an anode rod burned and vaporized by the high temperature of the arc plasma. The edges of two electrodes and the arc plasma were observed through a view port (with a filter) centered at the chamber, and the gap between two electrodes was controlled by using the feed-through anode to be set at approximately 1 mm. In the present experiment, two kinds of the anode were tested, the one was a metal-doped graphite composite rod (Co/Ni-doped graphite rod; 5 mm $\times$ 5 mm $\times$ 150 mm: Toyo Tanso Co.Ltd.), and the other was an alloy rod of cobalt and nickel. The former consisted of a graphite rod containing cobalt of 0.6% and nickel of 0.6% at atomic ratio. The latter was alloy rod that consisted of nickel and cobalt of ca. 80%, and iron of ca.20% (78permalloy; ϕ5 mm $\times$ 150mm: Nilaco Co.Ltd.).

Two methods were used to produce carbon nanotubulites using the two types of electrodes described. In this experiment, carbon nanotubulites were produced by the DC arc-discharge method in an atmosphere of methane. When using a composite graphite rod, the arc-discharge current was 50 A and the pressure of methane gas was 500 Torr. Different ratios of methane and helium were also used. When using an alloy anode, the arc-discharge current was 20 A and the pressure of methane gas was set at 100$\sim$500 Torr. With the alloy anode, 20 A was the maximum current, because the anode melted before vaporizing when the current was larger than 20 A, since its melting and boiling point were approximately 1,800 °C and 3,200 °C, respectively.

The production of carbon nanotubulites by the high-temperature laser-vaporization (laser-furnace) method was carried out by the a part of the laser-furnace LD-TOF mass spectrometer (Section 2.2, P. 30). The same Ni/Co-doped graphite rod and the alloy rod as those used for the DC arc-discharge experiment was used as the target rod. The second-harmonic output of a Nd:YAG laser (wavelength, 532 nm; frequency, 10 Hz; pulse width, 6-7 ns; power, 600 mJ/pulse; diameter of the laser spot, ca. 1 mm; GCR-250, Spectra-Physics Laser, Inc.) was used to vaporize the target rods at a temperature, which set between a room temperature and 1000°C, in an Ar flow.

In this study, in order to compare Ti-doped graphite rods with Co/Ni-doped graphite or Co-Ni alloy rods, the production of carbon nanotubulites was investigated

using the same two methods: DC arc-discharge and a laser-furnace.

The resulting products, such as the soot on the inner wall of the chamber and the materials deposited on the electrodes, were observed by scanning electron microscopy (SEM: Hitachi S-900) and transmission electron microscopy (TEM: Hitachi H-800 and JEOL JEM-2010).

4.3 Results and Discussion

4.3.1 Nanostructures Produced using Ti-doped Graphite

This first subsection describes the nanostructures produced using Ti-doped graphite as a starting material for DC arc-discharge or high-temperature laser-vaporization. The Ti atom produced few endohedral metallofullerenes, and Ti did not catalyze the production of SWNTs at all. Cluster-beam experiments and theoretical calculations suggest that some fullerene-like clusters, such as $Ti@C_{28}$ [4.14] and Ti_8C_{12}(Metallo-carbohedrenes; Met-Cars) [4.15–4.23] are stable. Thus, the properties of fullerenes and nanotubes using group IV elements, such as Ti, are very different from those using other atoms, such as Sc and Y. It is also expected that Ti behaves differently toward carbon species during the formation of carbon nanostructures than other metal atoms.

Nanostructures produced using Ti-doped composite graphite were observed and characterized by SEM and TEM to compare with the soot produced using graphite containing metals (Co/Ni) which produce metallofullerenes, or which catalyzed a growth of SWNTs.

Figures 4.1 (a) and (b) show SEM images of raw soot (as-produced soot) produced by vaporization of high-temperature laser-vaporization (laser-furnace) of a Ti-doped graphite rod (Ti/C = 10% atomic ratio, Toyo Tanso Co.Ltd.) and DC arc-discharge of a 100% metal Ti anode (ϕ4 mm; Nilaco Co.Ltd.) in methane gas (the partial pressure: ca. 1 Torr, without He buffer gas), respectively.

The soot of the laser-furnace was produced under the SWNTs production condition (Ar pressure: 500 Torr, the flow rate: 300 ml/min., furnace temperature: 1,000 °C) for the laser-furnace method. The second-harmonic output of the Nd:YAG laser (532 nm, fluence: 600 mJ/pulse, frequency: 10 Hz, pulse width: 6-7 ns, spot size: ϕ1 mm) was irradiated on the surface of the Ti-doped graphite rod (5 mm × 5 mm × 20 mm) in a heated quartz tube. In this experiments No SWNTs (carbon nanotubulites) was observed in the soot, however, many specific ultra fine particles (UFPs) were observed (Fig. 4.1 (a)). The diameters of the spherical UFPs are distributed about 30 nm. The UFPs continuously connect with each other (the beads-like structure) and form a fibrous nanostructure with "necks".

The fibrous nanostructure was also observed in the soot of the DC arc-discharge method with the metal Ti anode (Fig. 4.1 (b)). The size of a spherical UFP is smaller than that of laser-furnace, ca. 10 nm. Thus the beads-like fibrous carbon nanostructures were produced by the both methods. They have same fibrous structure, however, the particle size in both nanostructures is very different.

Arc discharge supplies fewer carbon species to the arc plasma during the production of fibrous nanostructures than a laser-furnace. The composite graphite target rod supplies carbon species to the plasma directly in laser-furnace production, while in arc-discharge production using a Ti alloy, the carbon source is indirect, since it is the methane near the arc plasma area. The hydrogen atoms in methane terminate the growth of UFPs in arc-discharge with methane. The drastic temperature decrease seen around the vaporizing area might cool the UFPs in the arc-discharge method, whereas the high temperatures in the laser-furnace method keep UFPs growing into larger particles, until they are deposited on the trap surface. Thus, the carbon nanostructures grown in a laser-furnace form larger particles than those grown in an arc-discharge.

Spherical UFPs (diameter; 50 nm $\sim$ 150 nm) were produced in the arc-discharge using Ti alloy in methane (Fig. 4.1(b)). The spherical particles appear much brighter than the other particles in images of the arc-discharge method. They are likely metal Ti particles. The arc-discharge method contains more Ti species in the arc plasma than are seen in the laser-furnace, due to the direct vaporization of the metal Ti anode. Thus, UFPs formed just from Ti species could be observed by SEM.

Figure 4.2 shows a high resolution TEM image of the cathode deposit produced by arc-discharge with a Ti-doped graphite anode (Ti/C = 10% atomic ratio, 12.5 mm × 12.5mm × 300 mm; Toyo Tanso Co.Ltd.) in He (50 Torr). Apparently, many MWNTs are included in the cathode deposit, and they have about 10 graphite layers. The concentric circles in the center are a vertical image of a MWNT. Vertical image of MWNTs are much rarer than vertical images of SWNTs [4.4, 4.24].

The graphite layers in the MWNTs produced by Ti-doped graphite are damaged. The layers in the case of the Ti-doped anode are clearly wavy, and not straight like those formed with a pure graphite anode, shown in Fig. 4.3. The TEM observations suggest that the existence of reactive Ti atoms (or Ti UFPs) causes defects, such as bending, bucking and dislocations in the walls of MWNTs.

4.3.2 Carbon Nanotubulites Produced in Methane

Figure 4.4(a) and (b) show SEM images of a cathode deposit produced by the DC arc-discharge method with Co/Ni alloy anode in an atmosphere of methane at 500 Torr. The SEM images show long, thin tubular material (carbon nanotubulites) about 30 nm thick. The thickness and length are similar to those of SWNT bundles; however, carbon nanotubulites have a large curvature and are wavier than SWNTs, which are typically straight with a small curvature. The cathode deposit contained a very small quantity of carbon nanotubulites (the product ratio was less than ca. 1%).

Figures 4.5 show high-resolution TEM images of the carbon nanotubulites in Fig. 4.4 (the thinnest tubular carbon material). The carbon nonotubulites were classified into three types of structure, shown in Fig. 4.5(a), (b), and (c), respectively. Figure 4.5(a) shows carbon nanoparticles connected to each other to form fibrous carbon particles. The hollow carbon nanoparticles are composed of ca. 10 carbon layers, with defects in the outer layer. They look like a string of beads, forming so called bead-like nanostructures. Figure 4.5(b) shows a similar structure; however, each carbon nanoparticle is collapsed and folded to form a U-shape. Figure 4.5(c) clearly reveals a structure with continuous carbon layers, which is similar to the structure of multi-wall carbon nanotubes; however, its construction is defective. It is clear from these TEM images that carbon nanotubulites are wavy and can become entangled.

When using a composite graphite rod containing Co/Ni and methane as the buffer gas, the soot deposited on the inner wall of the chamber was normal powdery soot like that containing fullerenes. In general, chamber soot containing SWNTs produced in a Novel gas, such as helium, tends to form a soft sheet. In this experiment using methane gas, the soot of the inner chamber was powdery, and no SWNTs were observed. This suggests that the hydrogen atoms of methane terminated the growth of SWNTs.

On the other hand, the appearance of the soot deposited on the part of the anode near the graphite composite anode and the electrode connector was different from that of the chamber soot. The materials deposited on the anode formed a thin, very stiff sheet. Figures 4.6 shows SEM images of the anode deposit produced by the DC arc-discharge of a Co/Ni-doped composite graphite anode in helium and methane gas (partial pressure ratio, $He:CH_4 = 1:1$) at 500 Torr. The Figure 4.6 clearly reveals

that the carbon nanotubulites are uniformly distributed and stuffed within the stiff sheet. Hence, the sheet containing the carbon nanotubulites is highly homogeneous.

The carbon nanotubulites shown in Fig. 4.6(b) are very thick, long, curved, and spiral in comparison to a bundle of SWNTs. They were classified into three types by thickness: types I, II, and III, as shown in Fig. 4.7. Type I carbon nanotubulites are the thinnest fibrous particles, and are ca. 30 nm thick. The size and shape of the type I fibrous particles in Fig. 4.7 show that they are the same as the tubules in the deposit produced by the alloy electrode (Fig. 4.4). The type II carbon nanotubulites are medium-sized tubules less than 100 nm thick. The type II carbon nanotubulites are wavy and are tangled in the two SEM images. Some of the type II carbon nanotubulites were several μ m long, making type II longer than type I and III. The thickest carbon nanotubulites are classified as type III, and are ca. 100 nm thick. It is clear from the SEM image in Fig. 4.6 that the stiff sheet contains mainly type III carbon nanotubulites.

Figures 4.8 and 4.9 show TEM images of the carbon nanotubulites in the stiff sheet shown in SEM images (Figs. 4.6 and 4.7). It can be seen three types of carbon nanotubulites of distinct thickness, which are labeled as the same labels using in Fig. 4.7. Type I and II have bead-like structures which are formed by capsular carbon nanoparticles connecting with each other. Figure. 4.9 shows the magnified view of one of type III carbon nanotubulites. We ca see two layers which have distinct contrasts. It was observed that the surface of the thickest type III carbon nanotubulites have not had the structure of perfect carbon layers and had that of amorphous carbons. Thus they had the structure which is tubular covered by amorphous carbons around the beads-like thin tubules.

Figure 4.10 shows an EDX (Energy Dispersive X-ray analysis) spectrum of the thickest carbon nanotubulites (type III) in Fig. 4.9. The 0.3 keV corresponds to carbon and the $5 \sim 8$ keV signals correspond to Cr, Fe, and Ni. These signals are likely due to impurities in the stainless steel cathode connector. No signal corresponding to Co in the composite anode rod was observed. This suggests that the carbon nanotubulites did not contain any Co or Ni from the Co/Ni-doped graphite, only carbon (and hydrogen). Perhaps the Co/Ni acts as a catalyst to increase the yield of carbon nanotubulites.

In the case of DC arc-discharge with the Co/Ni-doped graphite anode, SWNTs

are produced most effectively under He of ca. 500 Torr (Fig. 4.11(a)), while in the case of He slightly containing methane (less than 1 Torr) no SWNTs are produced in the soot (Fig. 4.11(b)). It is evidence that hydrogen in methane terminates to grow SWNTs. It should be noted that carbon nanotubulites were observed as shown in Fig. 4.11(c) after heating (1,600 °C, 1 hour) the soot containing no SWNTs in Fig. 4.11(b) in vacuum of 10^{-4}. No SWNTs were observed in the obtained soot after the same treatment of the soot produced with a pure graphite anode. It is expected that high temperature(more than 1,000 °C), a metal catalyst such as Co/Ni and hydrogen enhance the growth of carbon nanotubulites.

Figure 4.12 shows a SEM image of a trace of carbon nanotubulite bundle in th e stiff sheet of the cathode deposit. A lot of carbon nanotubulites ($\sim$ 100 nm) aligned like a "brush" (diameter of 2 μ m, length of 3 μ m). Though the detail growth mechanism and conditions of the carbon nanotubulites bundle have not been confirmed, it is likely that a Co/Ni catalyst and hydrogen play an important role in the growth of carbon nanotubulite bundles (carbon nanobrush).

It has been reported that carbon tubular materials had also produced by pyrolysis from a hydrocarbon such as kerosene and camphor [4.25] and by heat-treatment of products made by DC arc-discharge of a graphite electrode in methane [4.26]. Thus so far, in the former pyrolysis experiment the carbon tubular materials have been produced in spite of not using metal catalyst. On the contrary, the stiff sheet deposit containing various carbon nanotubulites on the electrode has not observed in the case of DC arc-discharge of a pure graphite electrode in methane. Thus it can be said that when the carbon nanotubulites are produced by DC arc-discharge, a metal catalyst are always needed, and it should affect producing a large number of carbon nanotubulites.

The mechanism of carbon nanotubulite growth using the arc-discharge method may be similar to that of pyrolysis. One piece of evidence is the various hydrocarbons observed by mass spectrometry in the soot produced by DC arc-discharge in methane. Carbon nanotubulites are produced from species of heated hydrocarbons. In addition, metal catalysts in the DC arc-discharge method help to produce carbon nanotubulites.

Summary

I found that various tubular carbon materials (carbon nanotubulites) were effectively produced by DC arc-discharge with a Co/Ni-doped graphite anode in methane, and characterized the products by SEM and TEM. SEM observation revealed three types of carbon nanotubulites classified by thickness. High-resolution TEM observation revealed that the thinnest carbon nanotubulites consisted of three types of carbon nanoparticles. The results suggest that Co/Ni acts as a catalyst in the high yield synthesis of carbon nanotubulites. It is thought that high temperature, metal catalysts such as Co/Ni, and hydrogen enhance the growth of carbon nanotubulites.

Ti can not catalyze the growth of SWNTs, although Ti-doped graphite can produce MWNTs, even when there is a large proportion of Ti. The graphite layers in the MWNTs produced by Ti-doped graphite are much damaged. TEM observation suggests that the existence of reactive Ti atoms (or Ti UFPs) causes defects such as bending, bucking, and dislocation on the wall of MWNTs.

Bibliography

[4.1] R. Ueda, *Prog. Mater. Sci.* **35**, 1 (1991).

[4.2] W. Krätschmer, L. D. Lamb, K. Fostiropoulos, and D. R. Huffman, *Nature* **347**, 354 (1990).

[4.3] H. Shinohara, *Advances in Metal and semiconductor Clusters* **4**, 205 (1998).

[4.4] C. Journet, W. K. Maser, P. Bernier, A. Loiseau, M. L. de la Chapelle, S. Lefrant, P. Deniard, R. Lee, and J. E. Fischer, *Nature* **388**, 756 (1997).

[4.5] K. Tohji, T. Goto, H. Takahashi, Y. Shinoda, N. Shimizu, B. Jeyadevan, I. Matsuoka, Y. Saito, A. Kasuya, T. Ohsuna, K. Hiraga, and Y. Nishina, *Nature* **383**, 679 (1996).

[4.6] S. Bandow, A. M. Rao, K. A. Williams, A. Thess, R. E. Smalley, and P. C. Eklund, *J. Phys. Chem. B* **101**, 8839 (1997).

[4.7] K. B. Shelimov, R. O. Esenaliev, A. G. Rinzler, C. B. Huffman, and R. E. Smalley, *Chem. Phys. Lett.* **282**, 429 (1998).

[4.8] B. W. Smith and D. E. Luzzi, *Chem. Phys. Lett.* **321**, 169 (2000).

[4.9] E. Mizoguti, F. Nihey, M. Yudasaka, S. Iijima, T. Ichihashi, and K. Nakamura, *Chem. Phys. Lett.* **321**, 297 (2000).

[4.10] S. Iijima and T. Ichihashi, *Nature* **363**, 603 (1993).

[4.11] D. S. Bethune, C. H. Kiang, M. S. de Vries, G. Gorman, R. Savoy, J. Vazquez, and R. Beyers, *Nature* **363**, 605 (1993).

[4.12] X. Zhao, M. Ohkochi, H. Shimoyama, and Y. Ando, *J. Cryst. Growth* **198/199**, 934 (1999).

[4.13] S. Sasaki, N. Kitagawa, N. Takada, and M. Nagatsu, *Jpn. J. Appl. Phys.* **36**, 7399 (1997).

[4.14] T. Guo, M. D. Diener, Y. Chai, M. J. Alford, R. E. Haufler, S. M. McClure, T. Ohno, J. H. Weaver, G. E. Scuseria, and R. E. Smalley, *Science* **257**, 1661 (1992).

[4.15] B. C. Guo, K. P. Kerns, and A. W. Castleman, Jr., *Science* **255**, 1411 (1992).

[4.16] S. Wei, B. C. Guo, J. Purnell, S. Buzza, and A. W. Castleman, Jr., *J. Phys. Chem.* **96**, 4166 (1992).

[4.17] B. C. Guo, S. Wei, J. Purnell, S. Buzza, and A. W. Castleman, Jr., *Science* **256**, 515 (1992).

[4.18] S. F. Cartier, Z. Y. Chen, G. J. Walder, C. R. Sleppy, and A. W. Castleman, Jr., *Science* **260**, 195 (1993).

[4.19] S. Wei, B. C. Guo, J. Purnell, S. Buzza, and A. W. Castleman, Jr., *Science* **256**, 818 (1992).

[4.20] Z. Y. Chen, G. J. Walder, and A. W. Castleman, Jr., *J. Phys. Chem.* **96**, 9581 (1992).

[4.21] S. Wei, B. C. Guo, J. Purnell, S. A. Buzza, and A. W. Castleman, Jr., *J. Phys. Chem.* **97**, 9559 (1993).

[4.22] B. C. Guo, K. P. Kerns, and A. W. Castleman, Jr., *J. Am. Chem. Soc.* **115**, 7415 (1993).

[4.23] S. Wei, B. C. Guo, H. T. Deng, K. Kerns, J. Purnell, S. A. Buzza, and A. W. Castleman, Jr., *J. Am. Chem. Soc.* **116**, 4475 (1994).

[4.24] A. Thess, R. Lee, P. Nikolaev, H. Dai, P. Petit, J. Robert, C. Xu, Y. H. Lee, S. G. Kim, A. G. Rinzler, D. T. Colbert, G. E. Scuseria, D. Tománek, J. E. Fischer, and R. E. Smalley, *Science* **273**, 483 (1996).

[4.25] Y. Ando, X. Zhao, M. Sharon, P. D. Kichambare, and M. Kumar, *J. Cryst. Growth* (submitted).

[4.26] Y. Ando and M. Ohkohchi, *Fullerenes Science & Technplogy* **3**, 359 (1995).

List of Figures

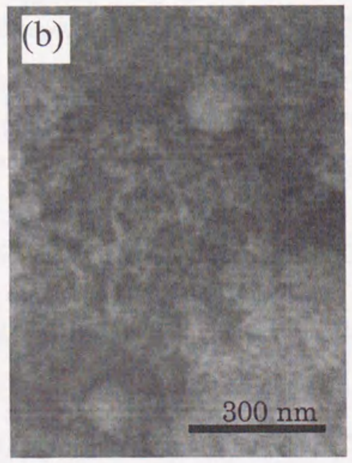

Fig. 4.1

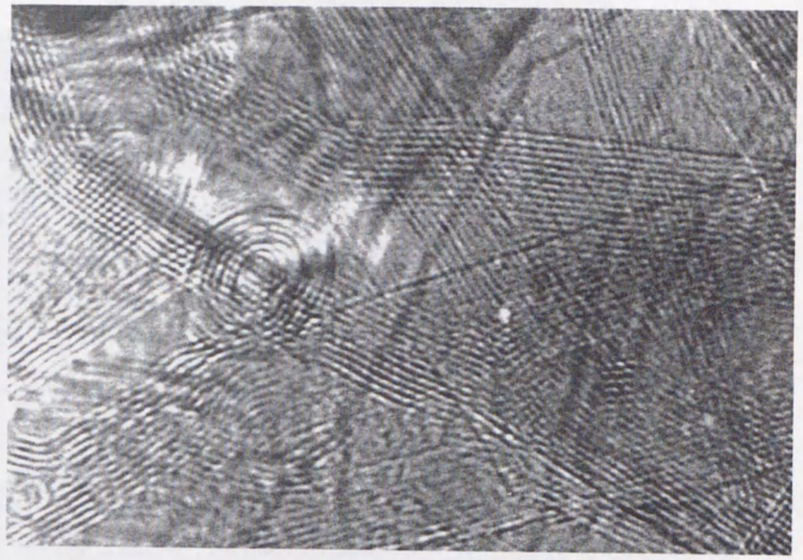

Fig. 4.2

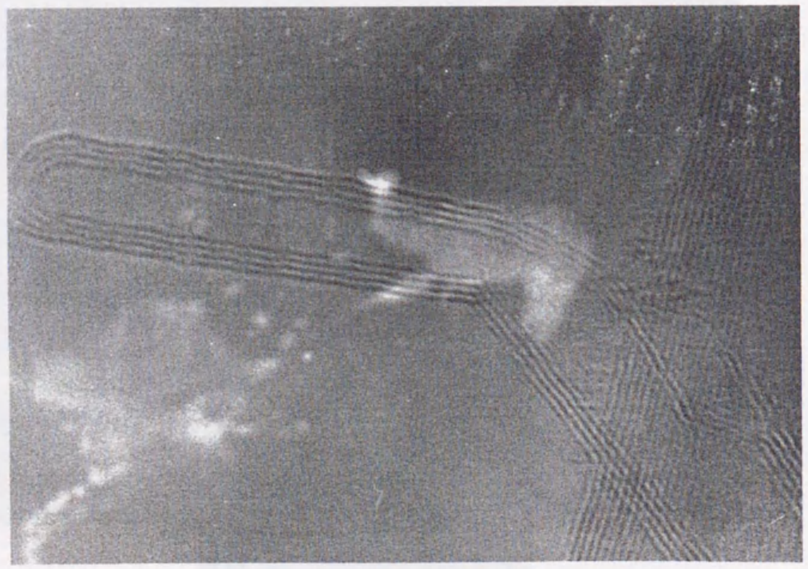

Fig. 4.3

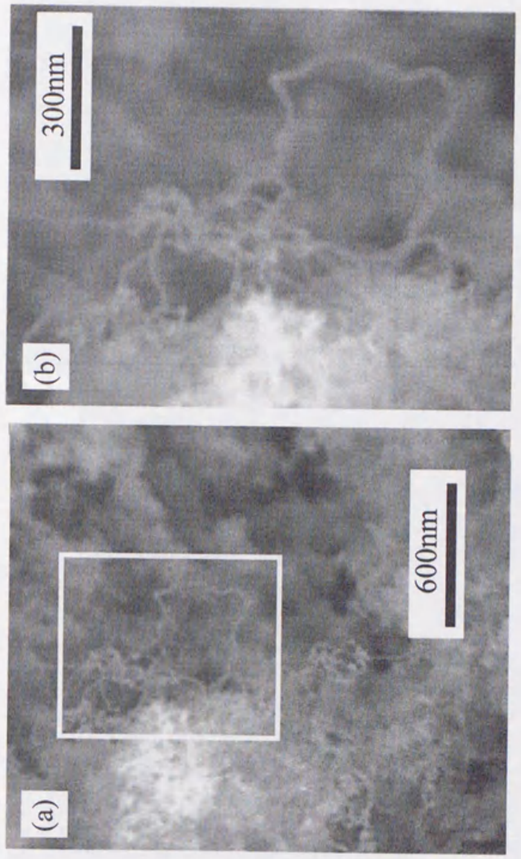

Fig. 4.4

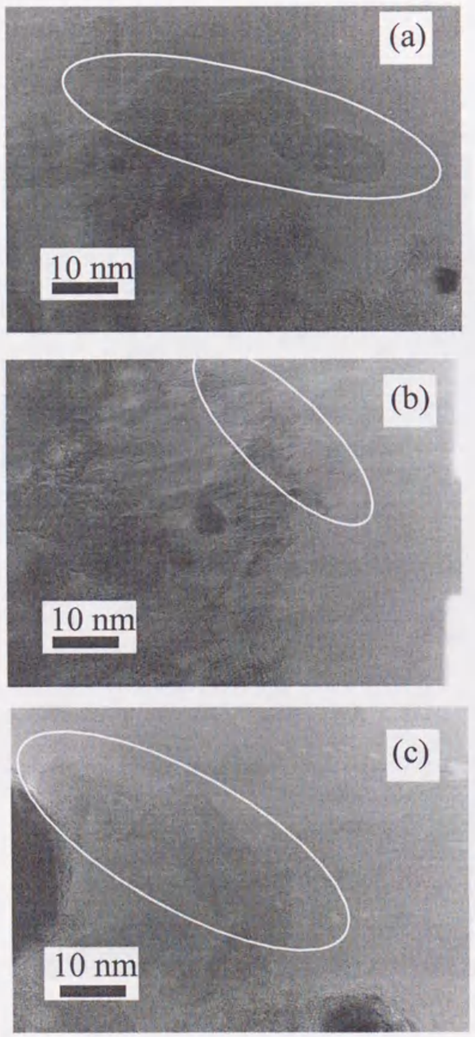

Fig. 4.5

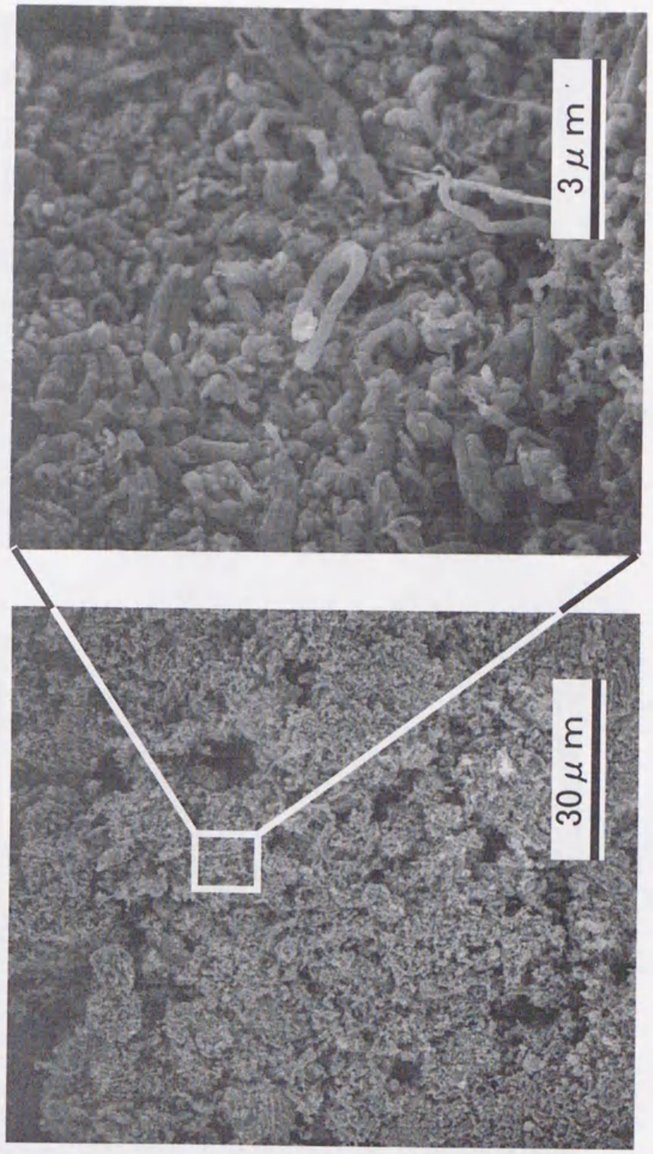

Fig. 4.6

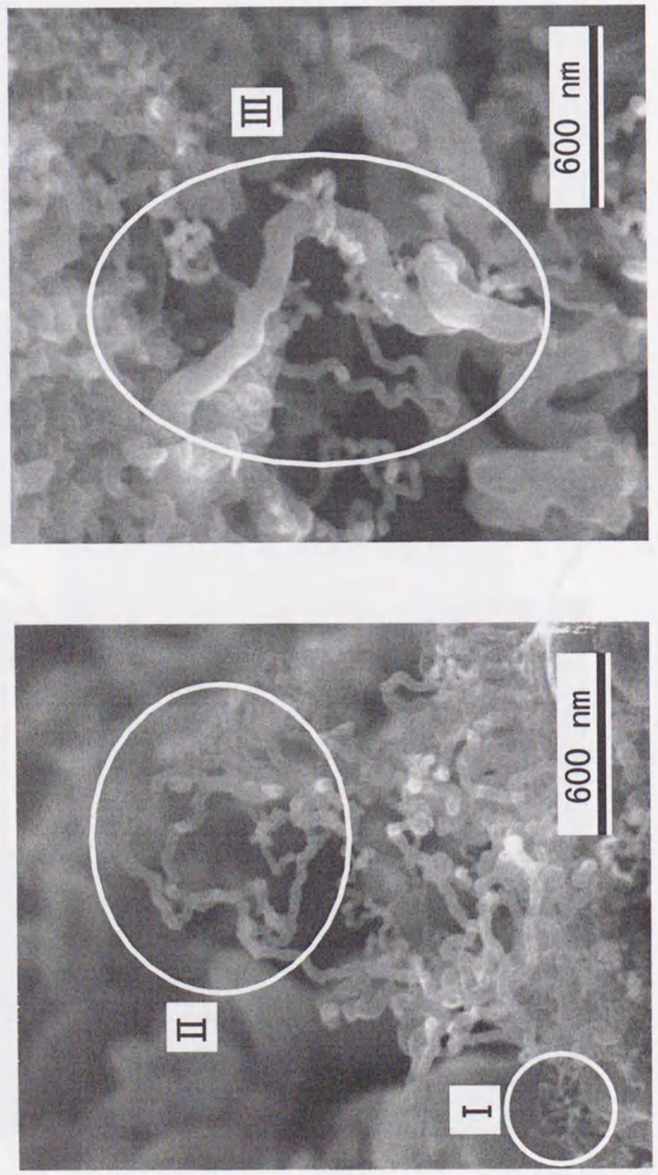

Fig. 4.7

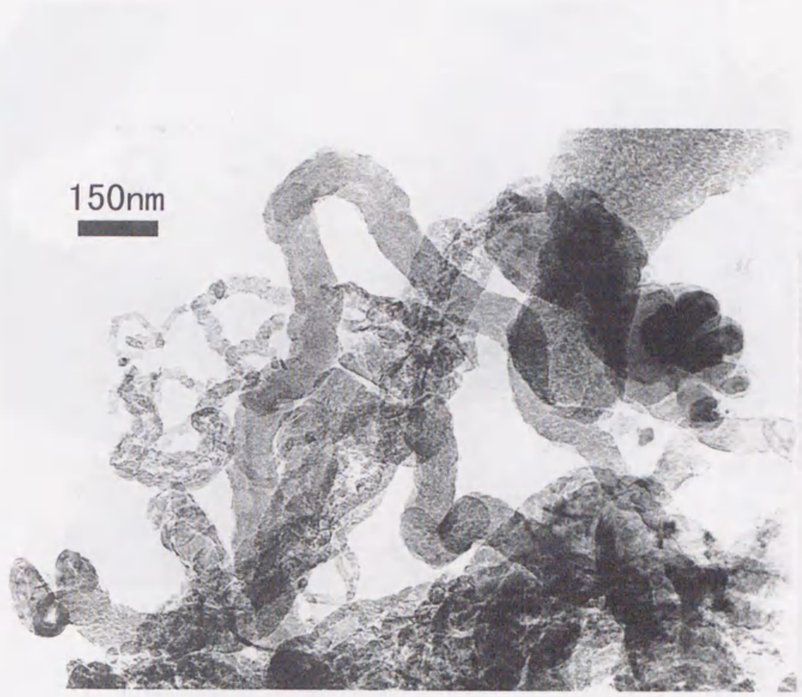

Fig. 4.8

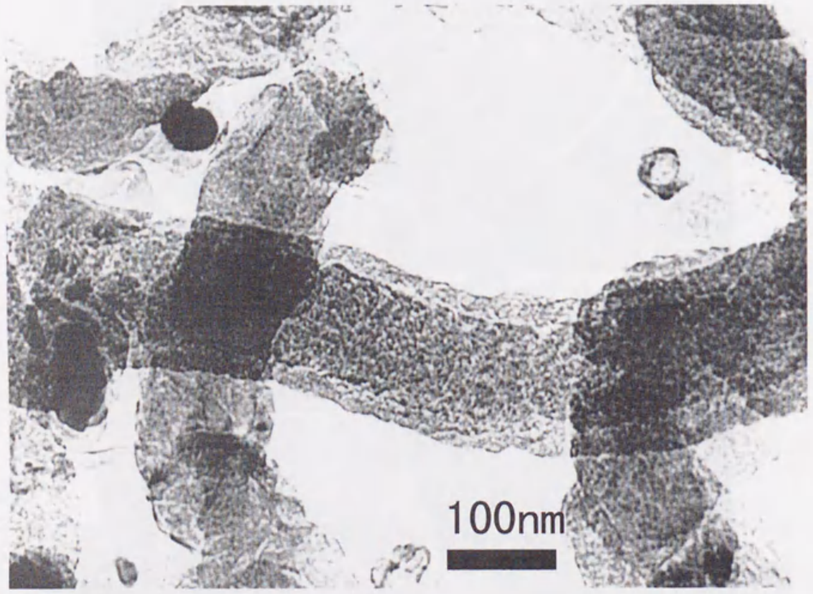

Fig. 4.9

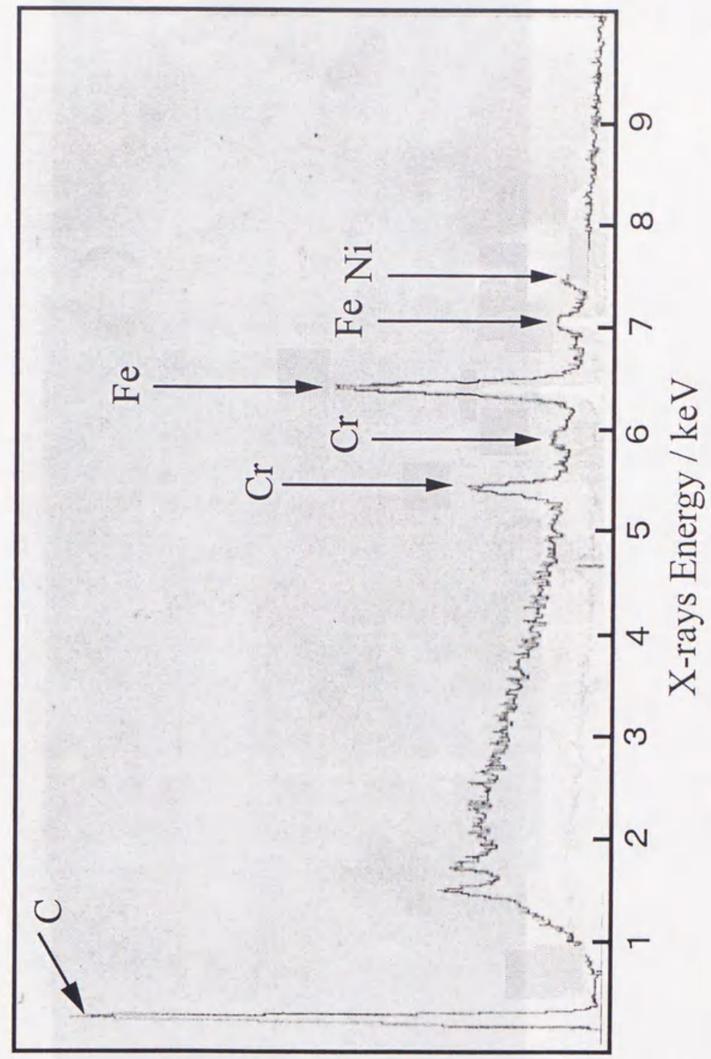

Fig. 4.10

Fig. 4.11

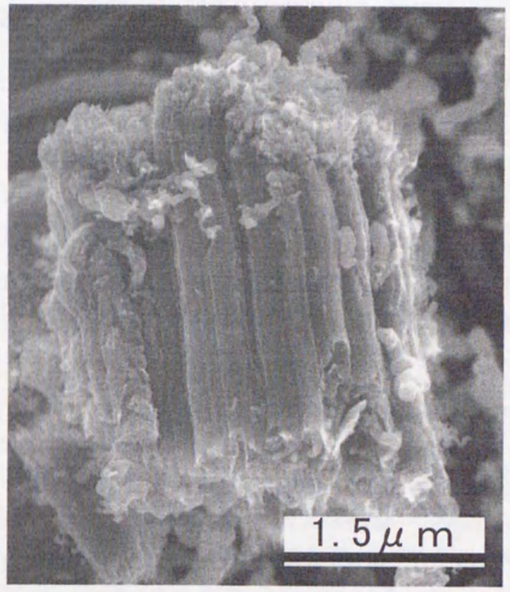

Fig. 4.12

List of Publications

I. 副論文

1. "*In situ* laser-furnace TOF mass spectrometry of C_{36} and the large scale production by arc-discharge"
   A. Koshio, M. Inakuma, Z. W. Wang, T. Sugai and H. Shinohara
   J. Phys. Chem. B, in press.

2. "A preparative scale synthesis of C_{36} by high-temperature laser-vaporization: Purification and identification of $C_{36}H_6$ and $C_{36}H_6O$"
   A. Koshio, M. Inakuma, T. Sugai and H. Shinohara
   J. Am. Chem. Soc. **122**, 398(2000).

3. "Carbon arc plasma doped with Fe and Co/Ni: spectroscopy and formation of carbon nanostructures"
   A. Huczko, H. Lange, P. Byszewski, A. Koshio and H. Shinohara
   Electronic properties of novel materials - Science and technology of molecular nanostructures: Proceedings of the XIII international winterschool on Electronic properties of novel materials,
   Eds. H. Kuzmany, J. Fink, M. Mehring and S. Roth, World Scientific, 258(1999).

4. "A simple and novel way to synthesize aligned nanotube bundles at low temperature"
   K. Mukhopadhyay, A. Koshio, N. Tanaka and H. Shinohara
   Jpn. J. Appl. Phys. **37**, 1257(1998).

II. 参考論文

1. "A high yield synthesis and isolation of C_{36} materials(C_{36}化合物の高収率生成と単離)"
   A. Koshio and H. Shinohara
   NEW DIAMOND **57**, 30(2000).
2. "Production of carbon nanotubes via catalytic chemical vapor deposition (CCVD) technique"
   K. Mukhopadhyay, M. Kanai, A. Koshio, T. Sugai, S. Bandow, N. Tanaka, and H. Shinohara
   Advanced materials 2000: Proceedings of the 7th national institute for research in inorganic materials (NIRIM) international symposium on advanced materials (ISAM 2000),
   Eds. Y. Bando, Y. Matsui, M. Mitome, K. Kimoto, K. Tajima and N. Aida, 11(2000).
3. "Bulk production of quasi-aligned carbon nanotube bundles by the catalytic chemical vapor deposition (CCVD) method"
   K. Mukhopadhyay, A. Koshio, T. Sugai, N. Tanaka, Z. Konya, J. B. Nagy and H. Shinohara
   Chem. Phys. Lett. **303**, 1170(1999).
4. "Studies of carbon arc plasma doped with Fe and Co/Ni during the formation of carbon nanostructures"
   A. Huczko, H. Lange, P. Byszewski, A. Koshio and H. Shinohara
   Symposium proceedings of 14th international symposium on plasma chemistry (ISPC),
   Eds. M. Hrabovsky, M. Konrad and V. Kopecky, **Vol. 4**, 2241(1999).
5. "On the effective growth of quasi-aligned carbon nanotube bundles by catalytic chemical vapor deposition (CCVD) technique"
   K. Mukhopadhyay, A. Koshio, N. Tanaka and H. Shinohara
   Chem. Phys. Lett., in press.

III. その他出版物

1. *Nikkankogyo-Shinbun*(日刊工業新聞), Dec.15,1999(1999年12月15日).
2. *Ceramics* (セラミックス), **35**, 210(2000).
3. "A high yield synthesis, isolation and characterization of C_{36} ralated materials"
   A. Koshio, M. Inakuma, T. Kai, K. Suenaga, Z. W. Wang, T. Sugai and H. Shinohara
   4th conference on ultrafine particles and clusters (超微粒子とクラスター懇談会第4回研究会講演論文集), Sendai, Japan, May 11~12, 2000, p.129(12p-9).

Acknowledgements

The studies presented in this thesis have been performed under the direction of Professor Hisanori Shinohara, Graduate School of Science, Nagoya University. The author is indebted to my teachers, colleagues and co-workers, who have provided his inspiration, criticism and enlightenment for my work. The author would like to express my sincere gratitude to Professor Hisanori Shinohara for his cordial guidance and helpful criticism and encouragement.

In the development of instruments (DC arc-discharge chamber and laser-furnace LD TOF mass spectrometer) the author has greatly benefited from the advice of Dr. Toshiki Sugai and Dr. Masayasu Inakuma, Graduate School of Science, Nagoya University.

The author wishes to thank Professor Andrzej Huczko and Dr. Hubert Lange (Department of Chemistry, Warsaw University) for providing me the controlled arc-discharge system, the precise plasma analysis and valuable advice. The author also wishes to express my gratitude to Dr. Shunji Bandow (Nanotubulites Projects, Japan Science and Technology Corporation) for providing me SEM and EDX (Institute of Molecular Science) and valuable advice. Thanks are due to Professor Nobuo Tanaka and Kaori Hirahara (Department of Applied Physics, Faculty of Engineering, Nagoya University) for high-resolution TEM observation and valuable advice. Thanks are also due to Dr. Kazutomo Suenaga (Nanotubulites Projects, Japan Science and Technology Corporation) for TEM and EELS analysis and helpful discussion. The author gratefully acknowledges Tsutomu Kai (Graduate School of Science, Nagoya University) with NMR analysis and his expert advice. Thanks are also due to Professor Toyoko Imae, Dr. Tetsuo Tomiyama and Dr. Toshiya Okazaki (Graduate School of Science, Nagoya University) for their encouragement. Finally, thanks are due to all members of the laboratory of Nano-structured Materials (Physical Chemistry Lab.).

Lastly, I wish to thank my parents for their care and support during the course of this work. And I wish to thank H.S. for her encouragement.

All words were processed by LaTeX.

副 論 文

副 論 文

4 冊

題 目

1.. *In situ* laser-furnace TOF mass spectrometry of C_{36} and the large scale production by arc-discharge
A. Koshio, M. Inakuma, Z. W. Wang, T. Sugai and H. Shinohara
J. Phys. Chem. B, in press.
（C_{36}の *in situ* TOF 質量分析とアーク放電による大量合成）

2. A preparative scale synthesis of C_{36} by high-temperature laser-vaporization: Purification and identification of $C_{36}H_6$ and $C_{36}H_6O$
A. Koshio, M. Inakuma, T. Sugai and H. Shinohara
J. Am. Chem. Soc. 122, 398(2000).
（高温レーザー蒸発による C_{36} 生成の予備的反応：$C_{36}H_6$ と $C_{36}H_6O$ の精製と同定）

3. Carbon arc plasma doped with Fe and Co/Ni: spectroscopy and formation of carbon nanostructures
A. Huczko, H. Lange, P. Byszewski, A. Koshio and H. Shinohara
Electronic properties of novel materials – Science and technology of molecular nanostructures:
Proceedings of the XIII international winterschool on Electronic properties of novel materials,
Eds. H. Kuzmany, J. Fink, M. Mehring and S. Roth, World Scientific, 258(1999).
（Fe および Co/Ni を添加した炭素アークプラズマ分光と炭素ナノ集合体の生成）

4. A simple and novel way to synthesize aligned nanotube bundles at low temperature
K. Mukhopadhyay, A. Koshio, N. Tanaka and H. Shinohara
Jpn. J. Appl. Phys. 37, 1257(1998).
（低温における配向ナノチューブバンドルの簡易かつ新規生成法）

参 考 論 文

5 冊

題 目

1. 小塩明, 篠原久典
   C_{36} 化合物の高収率生成と単離
   NEW DIAMOND 57, 30(2000).

2. Production of carbon nanotubes via catalytic chemical vapor deposition (CCVD) technique
   K. Mukhopadhyay, M. Kanai, A. Koshio, T. Sugai, S. Bandow, N. Tanaka, and H. Shinohara
   Advanced materials 2000:
   Proceedings of the 7th national institute for research in inorganic materials (NIRIM) international symposium on advanced materials (ISAM 2000),
   Eds. Y. Bando, Y. Matsui, M. Mitome, K. Kimoto, K. Tajima and N. Aida, 11(2000).
   (触媒を用いた化学気相成長法によるカーボンナノチューブの生成)

3. Bulk production of quasi-aligned carbon nanotube bundles by the catalytic chemical vapor deposition (CCVD) method
   K. Mukhopadhyay, A. Koshio, T. Sugai, N. Tanaka, Z. Konya, J. B. Nagy and H. Shinohara
   Chem. Phys. Lett. 303, 1170(1999).
   (触媒を用いた化学気相成長法による準配向カーボンナノチューブバンドルの大量合成)

4. Studies of carbon arc plasma doped with Fe and Co/Ni during the formation of carbon nanostructures

A. Huczko, H. Lange, P. Byszewski, A. Koshio and H. Shinohara

Symposium proceedings of 14th international symposium on plasma chemistry (ISPC),

Eds. M. Hrabovsky, M. Konrad and V. Kopecky, Vol. 4, 2241(1999).

（炭素ナノ集合体生成時における Fe および Co/Ni をドープした炭素アークプラズマの研究）

5. On the effective growth of quasi-aligned carbon nanotube bundles by catalytic chemical vapor deposition (CCVD) technique

K. Mukhopadhyay, A. Koshio, N. Tanaka and H. Shinohara

Chem. Phys. Lett., in press.

（触媒を用いた化学気相成長法による準配向カーボンナノチューブバンドルの効果的成長）